

**PRELIMINARY DESIGN AND ANALYSIS
FOR AN IMMERSSED TUBE TUNNEL
ACROSS THE İZMİR BAY**

**A Thesis Submitted to
The Graduate School of Engineering and Sciences of
İzmir Institute of Technology
in Partial Fulfillment of the Requirements for the Degree of**

MASTER SCIENCE

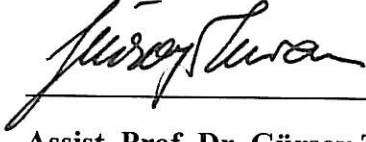
in Civil Engineering

**by
Nisa KARTALTEPE**

October 2008

İZMİR

We approve the thesis of Nisa KARTALTEPE



Assist. Prof. Dr. Gürsoy TURAN
Supervisor



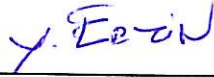
Assoc. Prof. Dr. İsfendiyar EGELİ
Co-Supervisor



Assist. Prof. Dr. Engin AKTAŞ
Committee Member

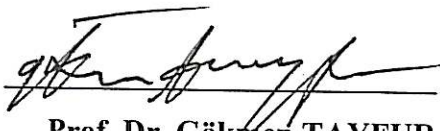


Assist. Prof. Dr. Şebnem ELÇİ
Committee Member



Assist Prof. Dr. Yusuf ERZİN
Committee Member

17 October 2008
Date



Prof. Dr. Gökmen TAYFUR
Head of the Department of
Civil Engineering

Prof. Dr. Hasan BÖKE
Head of the Graduate School

ACKNOWLEDGEMENTS

I would like to express my sincere gratitude to my supervisor Assist. Prof. Dr. Gürsoy TURAN and my co-supervisor Assoc. Prof. Dr. İsfendiyar EGELİ for their guidance, supervisions, and support throughout this study.

I also would like to special thanks to Asst. Prof. Dr. Engin AKTAŞ, who is the member of thesis committee, for their contributions to this thesis.

I also would like to thanks to other members of the thesis committee, Asst. Prof. Dr. Şebnem ELÇİ and Asst. Prof. Dr. Yusuf ERZİN.

I would like to thank to DLH (The State Railways, Ports, Airports Authority) and KGM (Republic of Turkey General Directorate of Highways) for providing us technical reports and data.

Thanks to research assistances at IYTE Department of Civil Engineering who helped me in anyway along this study. Also special thanks to Anıl ÇALIŞKAN and Aslı BOR for their good friendships and love.

I offer sincere thanks to my husband Barbaros KARTALTEPE for all his boundless love, continuous support, understanding, and patience. Finally, I would like to thank my father, my mother and my sisters for all their love, support, and encouragement.

ABSTRACT

PRELIMINARY DESIGN AND ANALYSIS FOR AN IMMERSED TUBE TUNNEL ACROSS THE İZMİR BAY

In this study, a preliminary design and analysis of an immersed tube tunnel is presented. The tube tunnel will connect the two coasts of the İzmir Bay and whereby will ease the transportation of the city. The reason to suggest an immersed tube tunnel is due to the shallow water depth (<25 m) and that the soil profile of the İzmir Bay is made up of silty-sand. Hence, the Bay is appropriate for an immersed tube tunnel.

First, a possible alignment was assigned for the tunnel. The technical, geometric properties of the tubes were determined, and the detailed drawings of them were made.

The allowable bearing capacity of the seabed was calculated and it was determined that the soil has not enough capacity to withstand the design load. The liquefaction risk of the soil was investigated as well, and it was shown that the soil has high liquefaction potential.

A static analysis of the tunnel was made in Calculix, a finite element program. The vertical displacement of the tube unit under static loads was calculated to be above the permissible settlement value. Afterwards, the seismic analysis was made to investigate stresses developed due to both racking and axial deformation of the tunnel during an earthquake. It was found that, the max stress due to the racking effect is less than the compressive strength of the concrete, and max stress due to the axial deformation is larger than compressive strength of the concrete. The high in the tube occur, because of the tubes high stiffness. This problem was solved by releasing the rigid connections in between two tube units. If these connections are made by using same form of elastomer joints, the deformation will occur in these joints, releasing the tubes internal stresses.

Considering these drawbacks, ground improvement was recommended for the seabed and an increased value of the standard penetration of the soil was estimated. Then, the analyses were repeated and it was found that all drawbacks were eliminated.

As a conclusion, it was decided that if suggested improvements are made in the seabed soil, the immersed tube tunnel can be constructed across the İzmir Bay.

ÖZET

İZMİR KÖRFEZİ İÇİN BATIRMA TÜP TÜNELİN ÖN TASARIMI VE ANALİZİ

Bu çalışmada, İzmir Körfezi'nin iki yakası arasında ulaşımı rahatlatmak için önerilen batırma tünelin ön tasarımı ve analizi yapılmıştır. Batırma tünelin seçilmesinin nedenleri; İzmir Körfezi'nin oldukça sığ su derinliğine(<25m) sahip olması, zeminin çoğunlukla yumuşak siltli-kum ihtiva etmesi nedeniyle bu geçiş sistemi için uygun olmasıdır.

Bu sebeple, öncelikle batırma tünelin güzergahı belirlenmiş, ardından tünelin teknik ve geometrik özellikleri sunularak en-kesit ve boy-kesit çizimleri yapılmıştır.

Zeminin maksimum ve izin verilebilir taşıma gücü hesaplanmış, bunun tünelin yerleştirilmesi sonrasında zeminde oluşacak basınç değerinin altında olduğu gösterilmiştir. Mevcut deney neticeleri kullanılarak zeminin sıvılaşma potansiyeli incelenmiş ve bu riskin yüksek olduğu saptanmıştır.

Tünelin statik analizi sonlu elemanlar programı olan Calculix yardımıyla yapılmıştır. Tünelin statik yükler altında düşey yer değiştirmesi hesaplanmış ve meydana gelen oturma değerinin izin verilen sınır değerinin üstünde olduğu belirlenmiştir.

Ardından, tünelin deprem esnasındaki yanal ve eksensel deformasyonundan dolayı oluşan gerilmeler hesaplanmıştır. Tünelin yanal ötelenmesi nedeniyle oluşan gerilmeler betonun basınç dayanımının altında olmasına rağmen, eksensel deformasyon nedeniyle meydana gelen gerilmelerin betonun basınç dayanımının oldukça üstünde olduğu tespit edilmiştir. Bu sonucun tünel elemanlarının birbirleriyle rijit olarak bağlanmasından dolayı olduğu anlaşılmıştır. Bu sorun her bir tüp ünitesinin arasına düşük rijitliğe sahip elastomer malzeme yerleştirilerek büyük gerilmelerin elastomer bağlantı elemanında oluşması sağlanmış, tüplerin üzerindeki gerilmelerin betonun basınç dayanımının altında kalması sağlanmıştır.

Bütün bu sakıncaları gidermek için tünel zemininde zemin iyileştirme yapılması gerekliliği belirtilmiş ve önerilen standart penetrasyon değeri hesaplanmıştır. Yeni standart penetrasyon değerine göre analizler yinelenmiş ve bütün değerlerin kabul edilebilir seviyelere indiği gösterilmiştir. Çalışmanın sonucunda, gerekli iyileştirmeler yapıldığı takdirde İzmir Körfezi'nin batırma tüp tünel için uygun olduğu saptanmıştır.

TABLE OF CONTENTS

LIST OF FIGURES	ix
LIST OF TABLES.....	xii
CHAPTER 1. INTRODUCTION	1
1.1. Purpose.....	1
1.2. Advantages of the Immersed Tube Tunnel.....	2
1.2.1. Contribution to the Environment and Economy	2
1.2.2. Regional Contributions	2
1.3. Scope of This Study	5
1.4. Possible Crossing Alternatives	6
1.4.1. Bridges	6
1.4.2. Underwater Tunnels	7
1.5. Soil Profile of the İzmir Bay Bottom.....	8
1.6. Application History of the Immersed Tube Tunnel.....	8
CHAPTER 2. PROPERTIES OF PROPOSED İZMİR BAY IMMERSSED TUBE TUNNEL	10
2.1. Possible Route of the Immersed Tube Tunnel.....	10
2.2. Geometric Properties of the Tube.....	12
CHAPTER 3. CURRENT SEABED –SOIL PROPERTIES.....	16
3.1. Allowable Bearing Capacity	16
3.1.1. SPT Results of the İzmir Bay	19
3.1.2. Allowable Bearing Capacity of the Seabed Soil of the İzmir Bay.....	22
3.2. Liquefaction Potential of the Seabed Soil.....	25
3.2.1. Liquefaction Analysis by using Depth and SPT Data Relationship.....	26
3.2.2. Liquefaction Analysis by using Simplified Procedure.....	27
3.2.2.1. Earthquake Induced Shear Stress Ratio (CSR).....	28
3.2.2.2. Depth Reduction Factor	29

3.2.2.3. Cyclic Resistance Ratio (CRR).....	30
CHAPTER 4. STATIC ANALYSIS FOR PRELIMINARY DESIGN	37
4.1. Estimation of the Modulus Of Subgrade Reaction	37
4.1.1. Finding the Modulus of Subgrade Reaction from Stress Strain Modulus, E_s (First method)	38
4.1.2. Finding the Modulus of Subgrade Reaction from Allowable Soil Pressure, q_a (Second method)	39
4.1.3. Application of the First and Second Methods in this Study.....	41
4.1.4. Calculation of the Spring Constants.....	43
4.2. Static Analysis of the Tunnel for Worst Case Scenario.....	47
4.2.1. Total Pressure Transferred to the Seabed Soil	49
CHAPTER 5. SEISMIC ANALYSIS OF THE IMMERSED TUBE TUNNEL	54
5.1. Types of Deformations	55
5.2. Seismic Analysis Procedures	55
5.2.1. Free-Field Deformation Approaches.....	57
5.2.1.1. Closed Form Solution Method (Simplified Procedure)	57
5.2.2. Soil-Structure Interaction Approaches	59
5.2.2.1. Dynamic Earth Pressure	59
5.2.2.2. Closed Form Solution Method to Calculate Axial and Bending Stresses.....	59
5.2.2.3. Numerical Analysis Method to Calculate Axial and Bending Stresses.....	62
5.2.2.4. Closed Form Solution Method to Calculate Racking Deformations	62
5.3. Application of Seismic Design Procedures in This Study	70
5.3.1. Calculation of the Axial and Curvature Deformations of the Immersed Tube Tunnel due to an Expected Seismic Wave Action.....	70
5.3.1.1. Closed Form Solution Method.....	72
5.3.1.2. Numerical Analysis Method (Finite Element Method)	76

5.3.2. Calculation of Racking Deformations and Stresses of the Immersed Tube Unit due to an Expected Seismic Wave Action.....	82
5.3.2.1. Simple Frame Analysis Model	82
5.3.2.2. Soil-Structure Interaction Approach.....	86
5.4. Seismic Design Issues.....	88
5.5. Calculation of Longitudinal Movement between Two Immersed Tube Units During an Earthquake	90
CHAPTER 6. GROUND IMPROVEMENT ALONG THE TUNNEL ALIGNMENT.....	94
6.1. Ground Improvement.....	94
6.1.1. Grouting Types.....	95
6.2. Encountered Soil Issues of the İzmir Bay	99
6.2.1. Which Method should be used?	99
6.3. New Situation of the Seabed Soil after Ground Improvement	100
6.3.1. Allowable Bearing Capacity of the Soil after Ground Improvement.....	101
6.3.2. Liquefaction Potential of the Soil after Ground Improvement	102
6.3.2.1. Liquefaction Analysis by using depth and SPT Data Relationship	102
6.3.2.2. Liquefaction Analysis by using Simplified Procedure.....	103
6.3.3. Static Analysis after Ground Improvement.....	103
6.4. Analysis Results after the Ground Improvement.....	104
CHAPTER 7. CONCLUSIONS	106
REFERENCES	109

LIST OF FIGURES

<u>Figure</u>	<u>Page</u>
Figure 2.1. The possible route of the tunnel	11
Figure 2.2. The water depths on the possible route of tunnel	11
Figure 2.3. The technical properties of the IBITT	13
Figure 2.4. The cross-section section of the IBITT	14
Figure 2.5. The longitudinal section of the IBITT	15
Figure3.1. Correction factor for position of water level: (a) depth of water level with respect to dimension of footing; (b)water level above base of footing (c): water level below base of footing	19
Figure 3.2. The locations of the 3 existing SPT boreholes nearest the IBITT route	20
Figure 3.3. Liquefaction process of the soil.....	26
Figure 3.4. Relationship between the possibility of liquefaction and N values.....	27
Figure 3.5. Stress ratio and penetration resistance.....	36
Figure 4.1. Influence factor I_f for a footing at a depth D	39
Figure 4.2. The modeling of the tube unit and the elastic foundation in Calculix	44
Figure 4.3. The weights for vertical spring constants corresponding to each node of a hexahedral element face.....	45
Figure 4.4. The modeling of the elastic foundation of the tube unit.....	45
Figure 4.5. Twenty-noded brick element (C3D20) in Calculix.....	48
Figure 4.6. The foundation pressure on the seabed soil before and after construction of the IBITT	49
Figure 4.7. S (1950) load train.....	51
Figure 4.8. Maximum vertical displacement of the tunnel.....	53
Figure 5.1. Axial and curvature deformations along a tunnel	56
Figure 5.2. Racking deformation of a rectangular tunnel.....	56
Figure 5.3. The propagation of the S wave along the tunnel axis.....	58
Figure 5.4. The racking deflection of the tunnel when applying unit displacement	67
Figure 5.5. Normalized structure deflections, circular versus rectangular tunnels tunnels.....	69

Figure 5.6. Simplified frame analysis model.....	69
Figure 5.7. The deformation of the tube unit during earthquake.....	78
Figure 5.8. Max compressive stress on the tube in longitudinal direction (before ground improvement)	79
Figure 5.9. Max compressive stress on the tube in lateral direction (before ground improvement)	80
Figure 5.10. Max stress on the tube in longitudinal direction (after ground improvement)	80
Figure 5.11. Max stress on the tube in lateral direction (after ground improvement)	81
Figure 5.12. The deformation of the tube unit after applying unit-racking deflection	83
Figure 5.13. Force averaging on the tube unit after applying unit deflection in lateral direction	84
Figure 5.14. Maximum racking deflection of the tube unit according to the simple frame analysis model	85
Figure 5.15. Maximum Von Misses stress of the tube unit according to simple frame analysis model	85
Figure 5.16. Fifteenth noded wedge element in Calculix.....	86
Figure 5.17. Racking deflection of the tube unit according to soil-structure interaction approach.....	87
Figure 5.18. Von misses stress of the tube unit according to simple frame analysis model	88
Figure 5.19. Conventional type flexible joint.....	89
Figure 5.20. Crown seal flexible joint	89
Figure 5.21. The shape of the immersed tube unit during an earthquake.....	91
Figure 6.1. Chemical grouting process	95
Figure 6.2. Chemical grouting applications.....	96
Figure 6.3. Slurry grouting process	97
Figure 6.4. Jet grouting process	98
Figure 6.5. Compaction grouting process.....	98
Figure 6.6. Maximum vertical displacement of the immersed tube unit before ground improvement.....	104

LIST OF TABLES

<u>Table</u>	<u>Page</u>
Table 3.1. The SPT results obtained from DLH İzmir	21
Table 3.2. The correction factor values for corrected SPT values.....	31
Table 3.3 Ground acceleration coefficients and peak ground acceleration	33
Table 4.1. Values of I_1 and I_2 to compute the Steinbrenner influence factor I_s	40
Table 4.2. The modulus of subgrade reaction (k_s) values obtained from 2 different approach	43
Table 5.1. Ratios of peak ground velocity to peak ground acceleration at the surface in rock and soil.....	64
Table 5.2. Ratios of ground motion at the tunnel depth to the motion at ground surface the ground surface	65
Table 5.3. Racking analysis results.....	87
Table 6.1. The situation of soil before and after ground improvement	105

CHAPTER 1

INTRODUCTION

1.1. Purpose

The purpose of this study was to make the preliminary design and analysis an immersed tube tunnel proposed to ease the İzmir Bay area traffic congestion problem by providing a shortcut circulation of traffic. The preferred analysis method is finite element method. To be able to apply the finite element analysis a three-dimensional finite element program Calculix and structural program SAP 2000 were used.

The reason why we focused on this topic is that the population of the İzmir city has been increase due to industry, university, and tourism presence, according to the State Institute of Statistics. Parallel to the population growth, the traffic congestion is also rising. Especially, people who live on the either side of the İzmir Bay are obliged to make use of either the ferry service or drive through the highway enclosing the Bay. Because of the fact that transportation capacity of the ferry is limited, people mostly use highways surrounding the Bay, although these highways do not meet the current traffic demand.

Considering all of these, it is apparent that there is a need for a shortcut solution across the İzmir Bay. Therefore, the immersed tube tunnel considered for the İzmir Bay so that it is both economic and more appropriate than any other crossing types of structures. Moreover, according to the State Railways, Ports, Airports Authority (DLH) estimates, the soil profile of the İzmir Bay bottom consists of mostly very loose to loose silty-sand layer. Therefore, the ultimate bearing capacity of the soil is very low. In order to take the advantage of natural buoyancy of water, total load transferred to the soil is considerably diminished. In addition, the existing maximum seawater depth is very shallow (<25 m). Hence, the immersed tube tunnel is the most suitable crossing structures for this type of soils.

1.1. Advantages of the Immersed Tube Tunnel across the İzmir Bay

The advantages of the immersed tube tunnel across the İzmir Bay are;

1. Contribution to the environment and the economy
2. Regional contribution

1.1.1. Contribution to the Environment and Economy:

Presently, the transportation needs between the two coasts of the İzmir Bay are provided by ferries and land transport. Since the ferry service is limited in capacity, people prefer highway transportation. The total distance traveled along the north and south coasts of İzmir Bay is almost 40 km and travel time is 60 min., as a rough estimate. However, if immersed tube tunnel is constructed across the İzmir Bay, this distance will be reduced to 7580 m, and the maximum travel time will be 10 min. Due to this considerable difference, the more savings in petrol usage will be realized and the less air will be polluted resulting from the exhaust gases. Thereby, the air quality of İzmir will be improved. In addition, due to the saving in imported petrol, a positive contribution to economy will be provided. Furthermore, since travel time will be reduced, the life quality of the region people will be increased.

1.1.2. Regional Contribution

If immersed tube tunnel is constructed:

1. Both the ferry traffic and highway traffic will be less between the Üçkuyular and Çiğli Sides,
2. The distance between Çiğli and Adnan Menderes Airport will be decreased by 8 km.
3. The traffic density will be dramatically diminished at the city center.
4. Distance from Çeşme Motorway to İzmir-Çanakkale Road at the north side of the bay will be reduced by 40 km.

According to the Republic of Turkey General Directorate of Highways (KGM) Annual Average Daily Traffic Report in 2005 the maximum traffic density in İzmir-Çeşme Motorway is observed in between July and August and in these months,

approximately 40000 vehicles use this motorway daily. Similarly, the same report state that the max traffic density realizes in between July and August in İzmir-Aydın Motorway and the average number of vehicle per day using this motorway is 37000. On the other hand, the capacity of İzmir Orbital Road is 40000 vehicles. Based on the these investigations, it can be assumed that if immersed tube tunnel is constructed on between Üçkuyular and Çiğli side, most probably at least 30000 vehicle will use this tunnel per day.

To make a rough estimate about the cost of the immersed tube tunnel, it is compared with the Marmaray Project. The unit cost of the immersed tube tunnel part of the Marmaray Project is about 100 million USD per km. Since the total length of the immersed tube tunnel recommended for the İzmir Bay is 7.6 km and its width about 1.33 times larger than the Marmaray, the approximate cost might be about $((39.8/15.3) \cdot 100 \cdot 7.6) = 2$ billion USD. However, if it is considered that the taken Marmaray unit cost price of 100M USD/km doesn't cover the below explained cost items of the IBITT tunnel, following costs can be added as an extra to the IBITT tunnel cost:

1. Add cost of 7 M m³ of soft material dredging is estimated as Lump Sum: 0.2B USD

2. Add cost of filling fine gravel to the sides of the tunnel, with a 1.5B m³ volume is estimated: 0.1B USD

3. Add cost of forming the first protective layer of the tunnel (40mx1mx7600m=0.3M.m³ of sand-cement mixture) underwater: 0.05B. USD

4. Add cost of forming the second protective layer of the tunnel (40mx1mx7600m=0.3M.m³ of armor rock) underwater: 0.05B USD

5. Add cost of expropriation of land as ROW (L=1km long and w=0.25 km wide on both sides, with a total area=0.5km²): 0.01B. USD

6. Add cost of two ventilation buildings on either side or three ventilation shafts in the sea ($h_{\text{sea}}=175$ m.): 0.19B USD

7. Add cost of ground improvement (compaction grouting) up to 30 m depth below seabed (w:50mxh:30mxL:7600m=11.4 M m³): 0.4B USD

If IBITT is not lowered by 10m from the existing seabed level (See Chapter 7), the total cost is estimated as 3 billion USD. However, if it is lowered by 10 m from the existing seabed level; this cost is increased to 3.3 billion USD.

The broad feasibility of the IBITT:

The total length of the tunnel: 7.58 km

The distance between Çiğli and İnciraltı by using surrounding highway: 50 km

The oil saving due to this difference:

$$(50.00 - 7.58) \cdot (30000) \cdot (6 \text{ lt}/100 \text{ km}) \cdot (2.5 \text{ USD}) \cdot (365) = 69.7 \text{ M USD} \quad (1.1)$$

The gain from the toll rate:

$$(30000 \text{ vehicle}) \cdot (5 \text{ USD}/\text{vehicle}) \cdot (365 \text{ day}) = 55 \text{ M USD} \quad (1.2)$$

Annual total benefits:

$$(69.7 + 55) = 124.7 \text{ M USD}/\text{year} \quad (1.3)$$

If 4.7 M USD /year (% 3.33) of the early capital gains is assumed as the early maintenance cost of the tunnel, then the yearly capital gains become 120 M USD/year.

Thus, after construction the tunnel finances itself in the next:

$$\frac{3 \text{ B USD}}{120 \text{ M USD}/\text{year}} = 25 \text{ years} \quad \text{or} \quad \frac{3.3 \text{ B USD}}{120 \text{ M USD}/\text{year}} = 27.5 \text{ years} \quad (1.4)$$

Since the project pays itself back in roughly 25/27.5 years, it becomes attractive (feasible) for Built-Operate-Transfer (BOT) type financing and 30 year BOT period is quite reasonable.

It should be noted in here that since there was not enough data to make a detailed cost analysis the cost estimation presented here is based on the Marmaray Project. However, both the soil properties of the İzmir Bay and the structural properties of the recommended tunnel are considerably different from the Marmaray Project. Hence, a better cost estimation of the immersed tube tunnel can be provided after the full feasibility report, which should include a detailed site investigation along the tunnel route.

1.3. Scope of This Study

This study consists of five main parts:

1. Introduction
2. Properties of the proposed İzmir Bay Immersed Tube Tunnel
3. Current seabed properties
4. Static analysis for the preliminary design
5. Seismic analysis of the immersed tube tunnel
6. Ground improvement along the tunnel alignment
7. Conclusion

In the first part, immersed tube tunnels and their applicability to various types of soils is described. Then, considering the soil type existing at the İzmir Bay, the applicability of the immersed tube tunnel at that location was investigated using the soil data obtained from the DLH.

In the second part, the possible route and geometric/technical properties of the tunnel was determined.

In the third part, the ultimate and allowable bearing capacity of the soil was calculated. Then, it was investigated that whether the current seabed soil has liquefaction potential or not.

In the fourth part, in order to evaluate the displacement and stresses occurring during and after construction, the static analysis was made by using Calculix finite element program.

In the fifth part, the seismic requirement for the tunnel was investigated by an equivalent static analysis method that is based on a seismic design procedure adopted in Taiwan High Speed Railway Project, whereby the analyses were performed by using the SAP 200 structural program.

In the sixth part, the aim of the ground improvement was explained and the most appropriate improvement type for İzmir Bay is determined. Then, all analyses were made again according to new situation of the seabed soil.

In the seventh part, which is the conclusion of the study, the obtained results of the study have been summarized and some suggestions were made about the İzmir Bay.

1.4. Possible Crossing Alternatives

There are two alternatives to cross the İzmir Bay: by means of a bridge or a tunnel. Nevertheless, the feasibility either depends on many factors such as water depth, distance, depth to rock below seabed, and subsoil profile of the seabed. Therefore, before determining the crossing type, the feasibility of various bridges and underwater tunnel types should be examined.

1.4.1. Bridges

Bridges are water-crossing structures used by people. It is built over rivers, lakes, ravines, canyons, railroads, and highways. There are seven main types of bridges: Beam bridges, cantilever bridges, truss bridges, arch bridges, cable bridges, suspension bridges, floating bridges.

A beam or "girder" bridge is the most common bridge type used in highway construction. It is simplest kind of all bridge designs. It is usually recommended for crossing short distances (less than 80 m.)

A cantilever bridge, which is a complex version of the beam-truss type bridges, is constructed by using cantilevers. Generally, it is made up with three spans and is supported only at one end. Because of the fact that it carries heavy vertical loads, the soil where the cantilever bridge foundation is placed should have high bearing capacity. Moreover, the cantilever bridge is suitable if the distance between the two coasts is less than 1000 m.

An arch bridge is the oldest type of bridge construction and it is the most durable type of bridges. It is constructed from stone, cast iron, steel, and reinforced concrete. Firstly, the total load of the structure is transferred to the abutment shaped arches and then to the soil. Because of their heavy weight, the soil under an arch bridge should be stiff. Beside an arch bridge should be considered only for short spans.

A truss bridge is one of the oldest types of modern bridges. Despite its lightweight, it can carry heavy loads. Furthermore, it has a simple design and it is economical to build due to efficient use of steel material. Nevertheless, this bridge type is considered only for crossing up to 1000 m distances.

A suspension bridge is a type of bridge, which consists of two main cables supporting the weight of the bridge and transfer the total load to anchorages and two towers. It is recommended for large distances more than 1000 m. Due to the relatively low deck stiffness, it is difficult to carry heavy live loads such as traffic loads. Thus, it is not recommended for weak foundation soil such as loose silt and sand (Murowchick 2008).

A cable-stayed bridge is a variation of the suspension bridge and is designed for intermediate lengths between 1000 m. and 2000 m. However, its principle and construction method is quite different from a suspension bridge. For instance, the cable-stayed bridges have tall towers like suspension bridges, but the roadway is attached to the towers by a series of diagonal cables. Such bridges are much lighter and stiffer compared to suspension bridges. This leads to a less deformation of the deck under the live loads. In addition, they are economic and construction time is shorter than the suspension bridges because cable stayed bridges do not need anchorages (Huang, et al. 2005).

A floating bridges is connected on top of pontoons that float on water. Due to the advantage of natural buoyancy of water, the total load anchored to the soil can be reduced. Therefore, it is more practical solution than other bridges types when the waterbed is extremely soft. However, floating bridges is appropriate for large water depths (30 m-60 m) (Watanabe and Utsunomiya 2003).

1.4.2. Underwater Tunnels:

Underwater tunnels are preferred when the soil profile of the waterbed or the weather condition is not proper for a bridge to be constructed above water. There are three alternative underwater tunnel types for crossing the water: Bored tunnels, floating tube tunnels, immersed tube tunnels.

Bored tunnel shall be constructed when the ground or waterbed is appropriate for excavating and preferred for deep tunnels. There are two alternative methods to build a bored tunnel: Drilling-blasting method or by using a tunnel-boring machine. Although a TBM machine with a circular cross-section excavates the soil without disturbing it and produces a smooth tunnel wall, bored tunnel is only suitable for self-retaining soils (TCRP Report/NCHRP Report 2006).

A **submerged floating tunnel** also known as an archimed bridge is a very new concept in the world. Only, Norwegian and Chinese have submerged floating tunnel projects in the design phase. Unlike the traditional underwater tunnels, submerged floating tunnel (SFT) is not buried to the seabed; it is suspended above the water floor and anchored to the ground with pontoons. It requires less substructure and excavation compared to the other two alternatives. Nonetheless, SFT is only appropriate for fjords, deep seas, and deep lakes (Hakkaart, et al.1993).

An immersed tube tunnel is made up of many prefabricated tubes constructed on land, which are then floated and moved to its dredged location by romorks in the sea. The tubes are lowered and connected with each other underwater. Then, the water is pumped out and the segments are covered with the backfill materials. It is preferred if the water depth is not larger than 60 m. and the waterbed is suitable for dredging, such as soft sandy, silty or alluvial soils(Baltzer and Hehengeber 2003).

1.5. Soil Profile of the İzmir Bay Bottom

İzmir Bay seabed consists of mixture of very loose silt, sand and alluvial materials, which are either non-cohesive or have very low cohesion values. Moreover, the rock layer depth is found approximately at 50 m below the sea level in the Üçkuyular side and 250 m-280 m below the sea level in the Çiğli side. Therefore, its ultimate bearing capacity is very low. Moreover, since the water depth of the İzmir Bay is less than 25 m, this is an advantage for an immersed tube tunnel to be built. Considering these properties, it has been decided that the immersed tube tunnel type of construction is the most suitable one for crossing the İzmir Bay.

1.6. Application History of the Immersed Tube Tunnel

The important immersed tube tunnels were listed below (Grantz, et al. 1993):

The immersed tube tunnel was heard firstly in the world in 1910 with the construction of the Detroit River Tunnel between USA and Canada. This immersed tube tunnel has been constructed 24 m below the water level and consists of eleven pieces of tubes. Each tube length is 80 m, height is 9.4 m, and width is 17 m, yielding to a total length of 800 m.

On the other hand, the first immersed tube tunnel in Europe is the Mass Transit Tunnel in Netherland constructed in 1941. The total length of this highway tunnel is 584 m. The tunnel consists of nine concrete box tubes, which are 61.35 long, 8.39 m in height and have a width of 24.77 m.

In 1958, prestressed concrete boxes were used for the first time in the construction of an immersed tube tunnel in Cuba. The total length of the tunnel is 520 m. The lengths of the tubes varies between 90 m and 107.5 m, the width is 21.85, and the height is 7.10 m. This highway tunnel was built 23 m under the sea level.

The Dees Tunnel in Canada was the first project considering the earthquake loads and was constructed 22 m below the sea level, with a total length of 629 m. It includes concrete tubes, with lengths of 104.9 m, height of 7.16 m and width of 23.80 m.

The Scheldt E3 (JFK) Tunnel, built in 1969 in Belgium, has the biggest tubes, which had ever been constructed in the world among all of the immersed tube tunnels. The width of the prestressed concrete boxes was 47.85 m, height was 10.1 m, while the length varies between 99 m and 115 m and the weight of each tube was nearly 47000 tons.

The Bay Area Rapid Transit (BART) Tunnel is the longest existing immersed tube tunnel in the world. The tunnel is in use in San Francisco California and constructed in 1970. The total tunnel length is 5825 m. and it has been operating as a railway. The tunnel consists of 58 tubes and each has a length of 110 m, a height of 6.5 m and width of 14.6 m. At a maximum depth of 41 m below the sea level, the Bay Area Rapid Transit Tunnel is one of the deepest vehicular tubes in service today.

The Oresund Tunnel constructed between Denmark and Sweden is the world's largest immersed tunnel in terms of volume. The total length of immersed tube tunnel section is 3510 m and the widht of the tubes are 40 m.

The first example of the immersed tube tunnels constructed in Turkey is the Marmaray Project that is being built on the İstanbul Bosphorus Waterway. It will be the deepest immersed tube tunnel in the world when the construction is completed (Marmaray 2007).

There were 108 immersed tube tunnels in the world until 1997. 48 of them in Europe, 27 of them in North America, 20 of them in Japan, 9 of them in South Asia(except Japan) and 4 of them in other countries (Marmaray 2007).

CHAPTER 2

PROPERTIES OF THE PROPOSED İZMİR BAY IMMERSED TUBE TUNNEL

2.1. Possible Route of the Immersed Tube Tunnel

The determination of a possible route of the tunnel and the access roads, through residential and undeveloped areas was examined by using Google Earth. (Google Earth 2008). A visual examination of the area leads to a decision of the İnciraltı-Çiğli tunnel route (See Figure 2.1). This selection is made based on two reasons. First, the İnciraltı and Çiğli sides are unpopulated and owned by the government. Second, the two sides allow the tunnel to be built on a straight route. This is essential to limit earthquake damage and water leakage risks. Furthermore, the Greater Municipality of the İzmir City (IZBB) and State Railways, Ports, Airports Authority (DLH) were consulted about whether there are any drawbacks with regard to the route of the tunnel. Consequently, after their approval, the current alignment between İnciraltı and Çiğli sides has been assigned as the route of the İzmir Bay Immersed Tube Tunnel. The possible route of the tunnel and corresponding water depths on this alignment were illustrated in Figures 2.1, and 2.2, respectively.

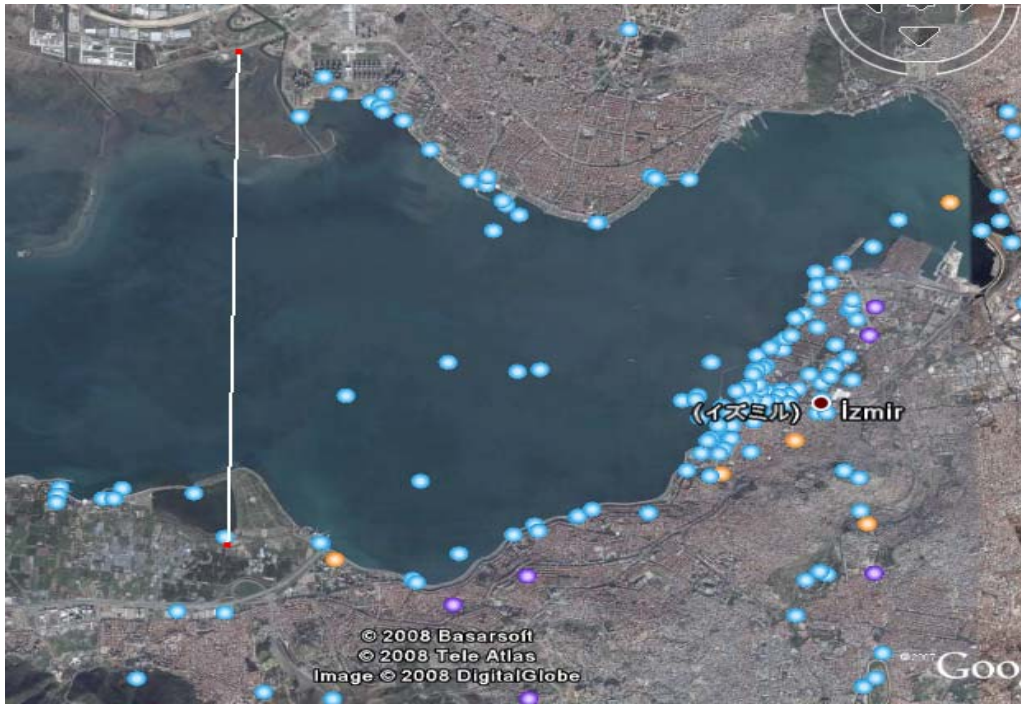


Figure 2.1. The possible route of tunnel
(Source: Google Earth 2008)

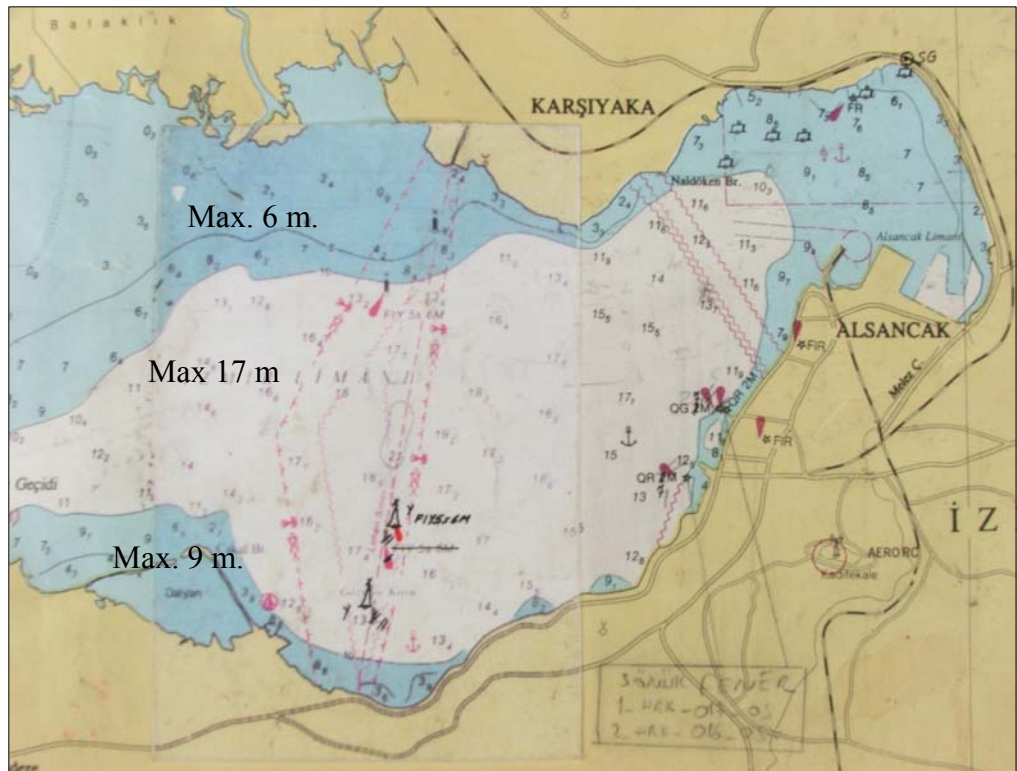


Figure 2.2. The water depths on the possible route of tunnel

2.2. Geometric Properties of the Tube

The İzmir Bay Immersed Tube Tunnel (IBITT) is composed of two land tunnel parts on each shore and an immersed-tube tunnel part at the center. The total length is 7580m, including an immersed tunnel section of 5560m in the middle. The tunnel has about 76 tunnel units. Each unit includes a two lane railway in the middle (width=10.6m) and three lane highways (width=13m) one on each side. The shape of each tunnel element has 39.8 m width, 10m height and the length varies 100m~120m, and its weight is approximately 38195t. The technical properties and typical cross section of the immersed tube tunnel unit were illustrated in Figure 2.3 and 2.4, respectively.

From the İnciraltı shore to the Çiğli shore, the tunnel starts with a 2.5% declination (station: km 0+000 m) for 1120 m. This is station: km 1+120 m, at which the inclination becomes zero for 2240 m (station: km 3+360 m). Afterwards, the road climbs with a 1% slope towards the Çiğli exit (station: km 7+580m). The deepest point of the top of the tunnel is 18.5 m. below the sea level and this depth is constant between station: km 1+120 m and station: km 3+660m. The longitudinal section of the immersed tube tunnel was illustrated in Figure 2.5

It should be noted in here that during the full feasibility report, detailed site investigation should be done. This study should include studies like bathymetric (seawater depth) and seismic fault line studies, current seawater quality of the dredged sediment disposal areas, shipping lane surveys etc. A contractor or its appointed subcontractor with a sub consultant can do these surveys, but overall independent consultant authorized by the client (DLH) should check all studies, reports, recommendations, and the works during the construction stage. It is emphasized that the current max. seawater depth record 18.5 m is not sufficient for any big cargo/contianier ship or for very large crude oil carrier if the existing İzmir Port does not move to out of the bay and will continue to be used in the future. In this case, there is a need of min 25 m seawater depth at the ship lane passage, indicating that IBITT should be further lowered by 10 m, making the max seawater depth equal to 28.5 m.

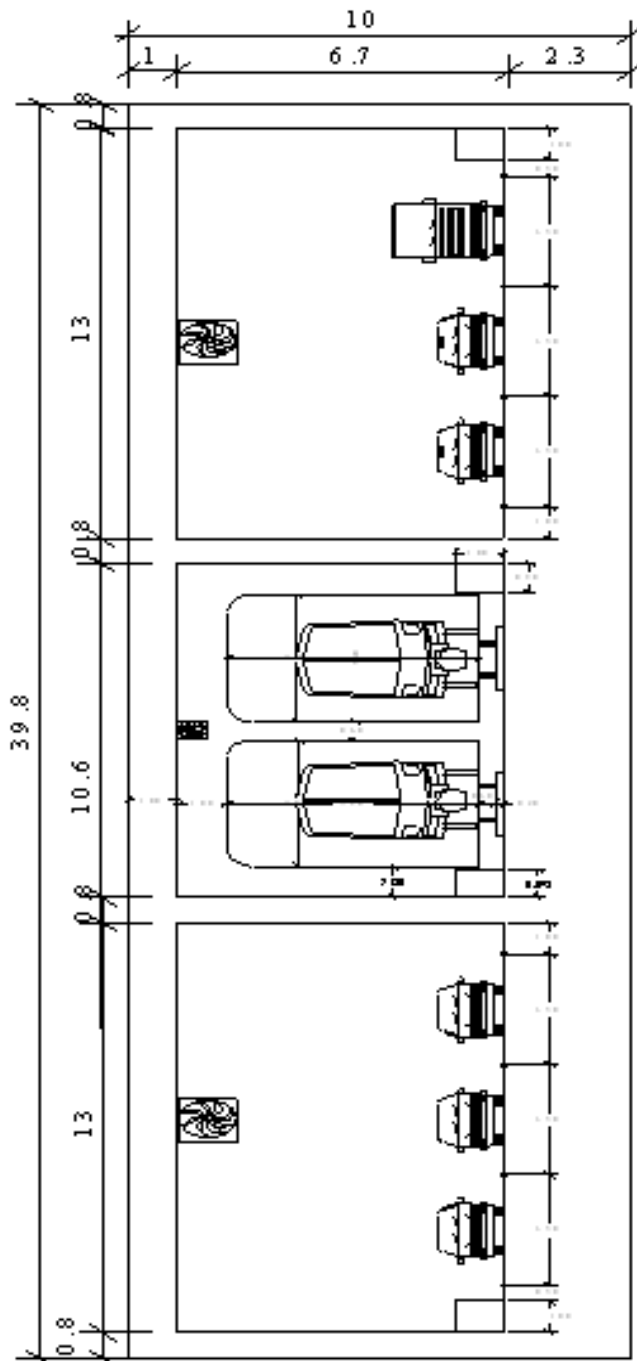


Figure 2.3. The technical properties of the IBITT

CROSS-SECTION A-A

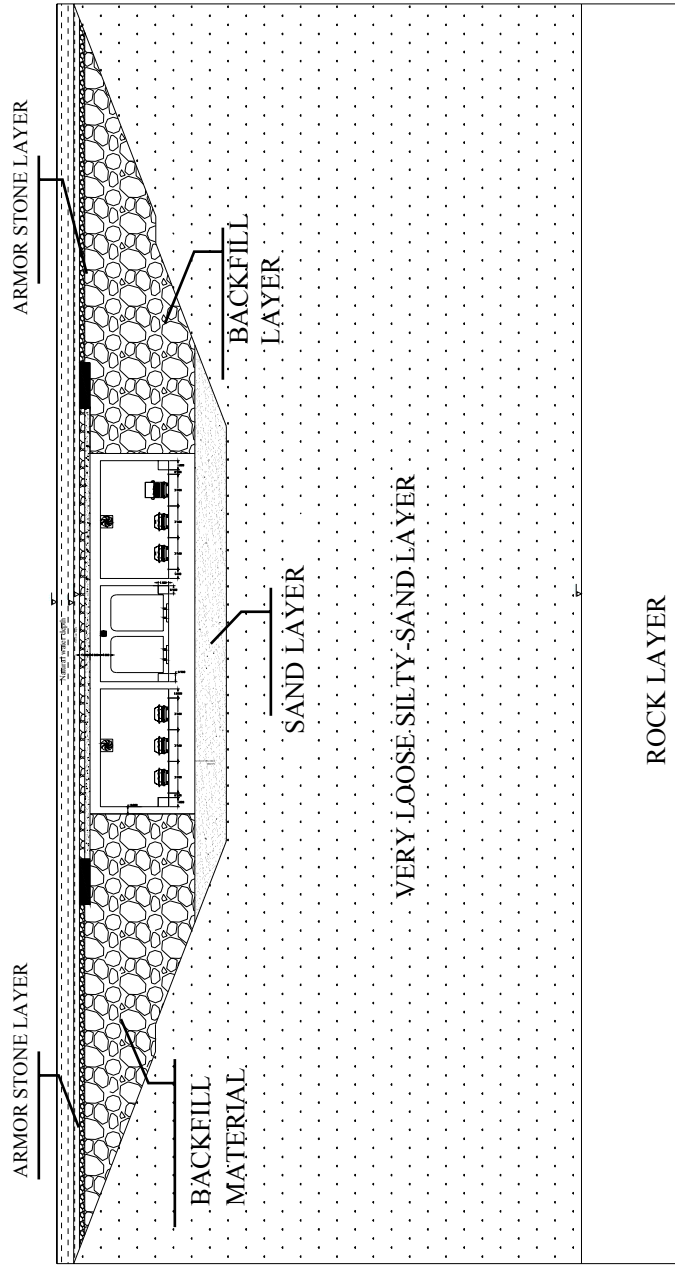


Figure 2.4. The cross-section section of the IBITT

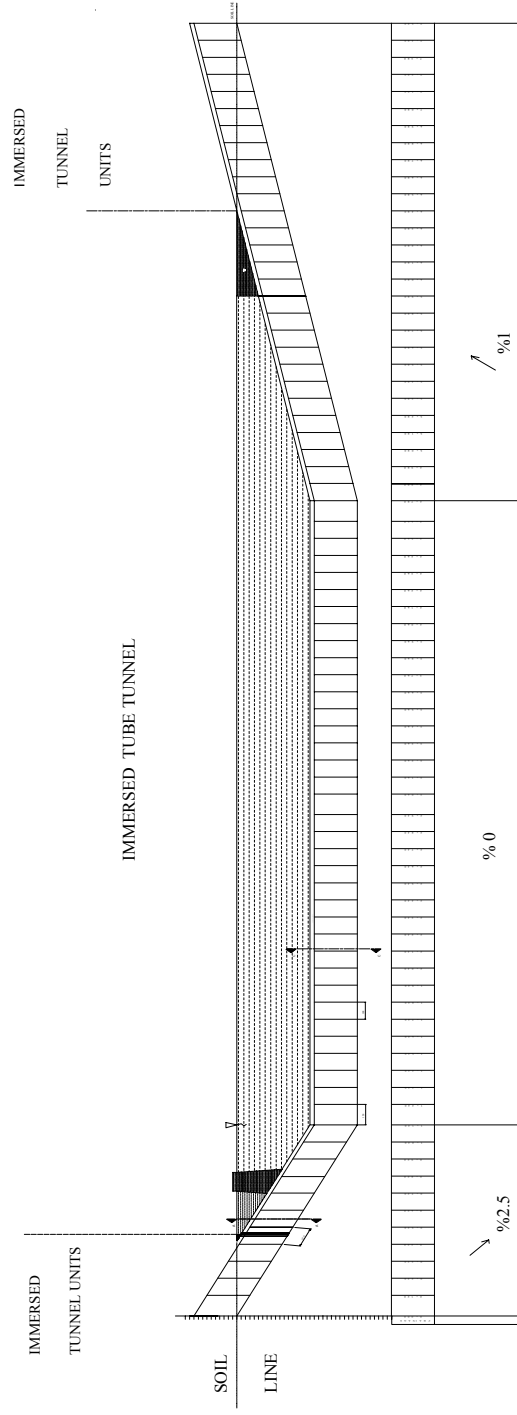


Figure 2.5. The longitudinal section of the IBTT

CHAPTER 3

CURRENT SEABED-SOIL PROPERTIES

3.1. Allowable Bearing Capacity

Using soil-boring data from the existing 3 boreholes nearest to the tunnel alignment, it was seen that the subsoil is mostly non-cohesive very loose to loose silty-sand or sandy-silt, with depths to bedrock varying between about 50 m on the Ückuyular side and about 280 m on the Çigli side. However, these preliminary site results should be confirmed by additional site investigations along the route, during the feasibility study or the preliminary design stages. Now, before describing bearing capacity values, firstly some definitions should be given;

- Bearing capacity is the capacity of soil to withstand the pressure from any engineered structure placed upon it, without producing any shear failure and large settlement.
- The ultimate bearing capacity (q_u) is the maximum pressure value that can be applied to the soil without causing shear failure.
- The allowable bearing capacity (q_a) is the maximum permissible pressure that can be applied to the soil so that shear failure does not occur and the maximum tolerable settlement is not exceeded.

The allowable bearing capacity of a soil can be calculated in terms of two different criteria:

a) The allowable bearing pressure based on ultimate capacity: This method is based on the relationship between the shear strength and allowable bearing capacity of the soil. According to this criterion, the allowable bearing capacity of the soil is equal to the ultimate bearing capacity of soil divided by a factor of safety.

b) The allowable bearing pressure based on tolerable settlement: In this method, it is assumed that the allowable bearing capacity of soil is equal to the maximum pressure without leading to intolerable settlement. (less than 2.5 cm)

It is recommended that, the allowable bearing capacity of soil should be calculated according to two different methods, respectively. In order to stay on the safe side, the smaller one should be used.

a. The allowable bearing pressure based on ultimate capacity: According to TENG (1962), the ultimate bearing capacity divided by a selected factor of safety, gives the allowable bearing capacity.” *A factor of safety of 3 is used under normal loading conditions and a factor of safety of 2 under combined maximum load*” (TENG 1962).

For long footings:

$$q_{ult} = 3 \cdot N^2 \cdot B \cdot R'_w + 5 \cdot (100 + N^2) \cdot D \cdot R_w \quad (psf) \quad (3.1)$$

$$q_{ult} = 0.048 \cdot N^2 \cdot B \cdot R'_w + 0.08 \cdot (100 + N^2) \cdot D \cdot R_w \quad (t / m^2) \quad (3.2)$$

$$q_a = \frac{q_{ult}}{FS} \quad (3.3)$$

where N is the standard penetration resistance, (number of blows per foot), B is the width of footing in meters unit, D is the depth of footing measured from ground surface to bottom of footing in meters, and R_w and R'_w are the correction factors for position of water level that can be obtained from Fig 3.1, and FS is the factor of safety.

b. The allowable bearing pressure based on tolerable settlement: Allowable bearing capacity for maximum settlement of 2.5 cm is given by TENG (1962) as;

$$q_a = 720 \cdot (N_{cor} - 3) \cdot \left(\frac{B+1}{2B} \right)^2 \cdot R_w \quad (psf) \quad (3.3)$$

$$q_a = 3.5 \cdot (N_{cor} - 3) \cdot \left(\frac{B+0.3048}{2B} \right)^2 \cdot R_w \quad (t / m^2) \quad (3.4)$$

where N_{cor} is the corrected SPT_N value,

$$N_{cor} = N \cdot \left(\frac{35}{p + 7} \right) \quad (3.4.a)$$

where, N is the SPT value obtained from the field, p' is the effective overburden pressure in t/m^2 unit and can be calculated by the following formula.

$$p' = \gamma' \cdot h \quad (3.4.b)$$

where, h is the half of the height between the sea level and the rock layer in meter, and γ' is the effective density of the soil in t/m^3 and it can be calculated from the following formula,

$$\gamma' = \gamma_{sat} - \gamma_w \quad (3.4.c)$$

where, γ_{sat} is the density of the saturated soil and γ_w is the density of the sea water.

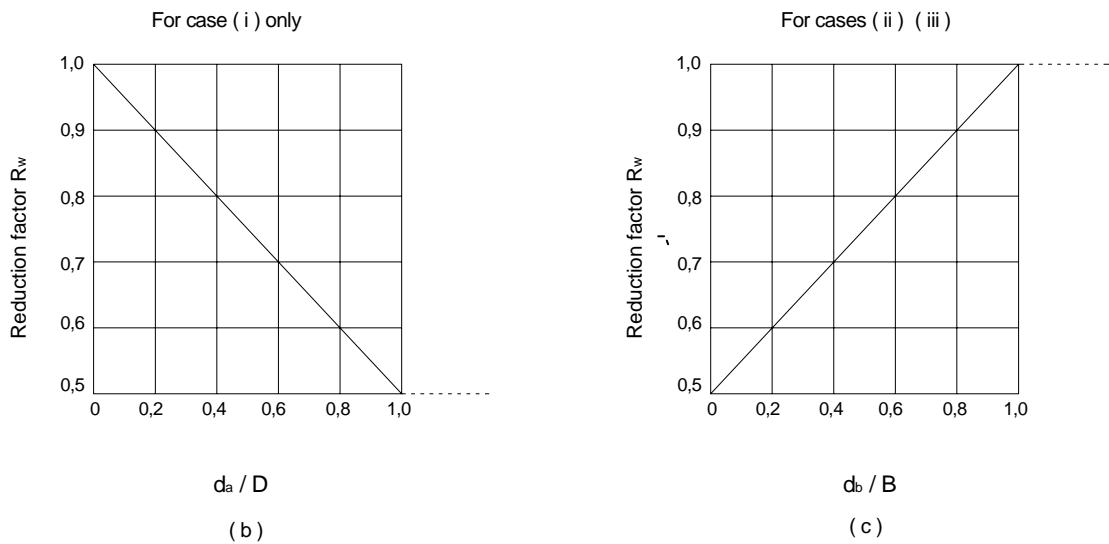
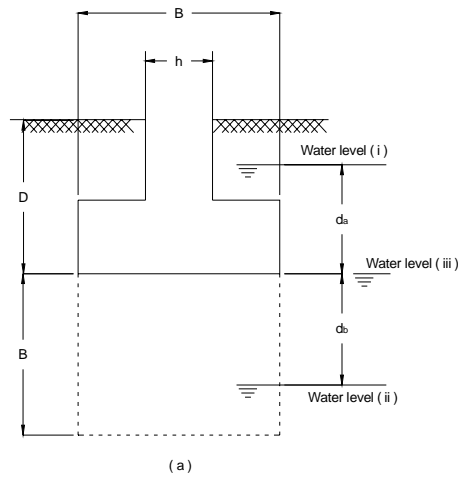


Figure 3.1. Correction factor for position of water level: (a) depth of water level with respect to dimension of footing; (b) water level above base of footing (c): water level below base of footing . (Source: Teng 1962)

3.1.1. SPT Results of the İzmir Bay

SPT-N value: A standard sampler is driven 450 mm into the ground at the bottom of drilled borehole by a drop hammer with a weight of 63.5 kg falling through a height of 76 cm. The number of blows is recorded at each 150 mm increments. The SPT-N is the number of blows required to achieve penetration from 15-45cm (Sivrikaya and Toğrol 2003).

For this study, there was no opportunity to make standard penetration tests (SPT) along the tunnel route. Therefore, test results that were obtained in the past is investigated by. Among these, data nearest to the tunnel route were used and the SPT results are presented in Table 3.1. These values are used to calculate the allowable bearing capacity of the seabed soil of the proposed IBITT across the İzmir Bay can be calculated. The borehole locations of the SPT are shown in Figure 3.2.

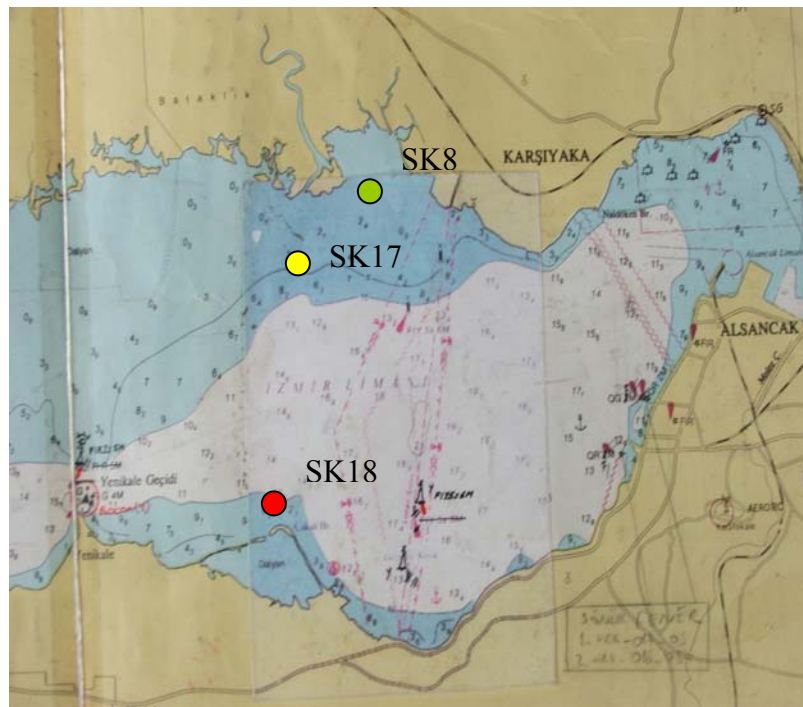


Figure 3.2. The locations of the 3 existing SPT boreholes nearest the IBITT route

Table 3.1 The SPT results obtained from DLH İzmir
(Source: DLH 1985)

Borehole Location : SK-18				
Depth(m)	Sample Number	The Number of Blow		
		0-15	15-30	30-45
4.10	SPT-1	1	1	1
5.50	SPT-2	10	12	15
7.10	SPT-3	15	17	17
8.60	SPT-4	12	17	19
10.10	SPT-5	15	15	17
11.60	SPT-6	15	16	16
13.10	SPT-7	23	11	12
14.60	SPT-8	18	17	17
16.10	SPT-9	15	15	18
17.60	SPT-10	15	15	18
Borehole Location : SK-8				
Depth(m)	The Number of sample	The Number of Blow		
		0-15	15-30	30-45
3.00	SPT-1	1	1	1
4.50	SPT-2	1	1	2
6.00	SPT-3	2	2	2
7.50	SPT-4	2	2	3
9.00	SPT-5	2	3	4
10.50	SPT-6	2	2	3
12.00	SPT-7	3	3	4
Borehole Location : SK-17				
Depth(m)	The Number of sample	The Number of Blow		
		0-15	15-30	30-45
9.85	SPT-1	-	-	-
11.35	SPT-2	-	-	-
12.85	SPT-3	1	1	1
14,35	SPT-4	1	1	1
15.85	SPT-5	1	1	1
15.85	SPT-6	1	1	1

i) At the borehole location SK-18, the penetration values are:

$$\text{SPT-1 (at 4.10 m.)} \quad N = N(15 - 30) + N(30 - 45) = 1 + 1 = 2$$

$$\text{SPT-2 (at 5.50 m.)} \quad N = N(15 - 30) + N(30 - 45) = 12 + 15 = 27$$

$$\text{SPT-3 (at 7.10 m.)} \quad N = N(15 - 30) + N(30 - 45) = 17 + 17 = 34$$

$$\text{SPT-4 (at 8.60 m.)} \quad N = N(15 - 30) + N(30 - 45) = 17 + 19 = 36$$

$$\text{SPT-5 (at 10.10 m.)} \quad N = N(15 - 30) + N(30 - 45) = 15 + 17 = 32$$

SPT-6 (at 11.60 m.)	$N = N(15 - 30) + N(30 - 45) = 16 + 16 = 32$
SPT-7 (at 13.10 m.)	$N = N(15 - 30) + N(30 - 45) = 11 + 11 = 22$
SPT-8 (at 14.60 m.)	$N = N(15 - 30) + N(30 - 45) = 17 + 17 = 34$
SPT-9 (at 14.60 m.)	$N = N(15 - 30) + N(30 - 45) = 15 + 18 = 33$
SPT-10 (at 17.60 m.)	$N = N(15 - 30) + N(30 - 45) = 15 + 18 = 33$

ii) At the borehole location SK-8, the penetration values are:

SPT-1 (at 3.00 m.)	$N = N(15 - 30) + N(30 - 45) = 1 + 1 = 2$
SPT-2 (at 4.50 m.)	$N = N(15 - 30) + N(30 - 45) = 1 + 2 = 3$
SPT-3 (at 6.00 m.)	$N = N(15 - 30) + N(30 - 45) = 2 + 2 = 4$
SPT-4 (at 7.50 m.)	$N = N(15 - 30) + N(30 - 45) = 2 + 3 = 5$
SPT-5 (at 9.00 m.)	$N = N(15 - 30) + N(30 - 45) = 3 + 4 = 7$
SPT-6 (at 10.50 m.)	$N = N(15 - 30) + N(30 - 45) = 2 + 3 = 5$
SPT-7 (at 12.00 m.)	$N = N(15 - 30) + N(30 - 45) = 3 + 4 = 7$

iii) At the borehole location SK-17, the penetration values are:

SPT-1 (at 9.85 m.)	$N = N(15 - 30) + N(30 - 45) = 0 + 0 = 0$
SPT-2 (at 11.35 m.)	$N = N(15 - 30) + N(30 - 45) = 0 + 0 = 0$
SPT-3 (at 12.85 m.)	$N = N(15 - 30) + N(30 - 45) = 1 + 1 = 2$
SPT-4 (at 14.35 m.)	$N = N(15 - 30) + N(30 - 45) = 1 + 1 = 2$
SPT-5 (at 15.85 m.)	$N = N(15 - 30) + N(30 - 45) = 1 + 1 = 2$
SPT-6 (at 17.85 m.)	$N = N(15 - 30) + N(30 - 45) = 1 + 1 = 2$

Based upon the three testing stations (SK18, SK8, SK17), average values of the N values can be taken so that,

- i) SPT_N=29 for areas that are close to the İnciraltı side,
- ii) SPT_N=4 for areas that are close to the Çiğli side
- iii) SPT_N=2 for the middle of the IBITT route.

3.1.2. Allowable Bearing Capacity of the Seabed Soil of the İzmir Bay

The allowable bearing capacity will be calculated for SPT_N= 4 only. The other locations are compared according to this result.

a.) First method: The allowable bearing Pressure based on ultimate capacity

The ultimate bearing capacity based on shear failure of the soil is calculated by Eq 3.2:

$$q_{ult} = 0.048 \cdot N^2 \cdot B \cdot R'_w + 0.08 \cdot (100 + N^2) \cdot D \cdot R_w \quad (t/m^2)$$

$$B = 39.8 \text{ m} \quad D = 285 \text{ m}$$

$$da/D = 1 \quad R_w = 0.5 \quad R'_w = 0 \quad \text{from Figure (3.1)}$$

$$q_{ult} = 0.048 \cdot 4^2 \cdot 39.8 \cdot 0 + 0.08 \cdot (100 + 4^2) \cdot 28.5 \cdot 0.5 \quad (t/m^2)$$

$$q_{ult} = 132 \text{ t/m}^2$$

The allowable bearing capacity of the soil is calculated by Eq 3.2:

$$q_a = \frac{q_{ult}}{FS}$$

where FS is taken as 3. (Bowles 1988)

$$q_a = \frac{132}{3} = 44 \text{ t/m}^2$$

b) Second Method: The allowable bearing capacity based on 2.5 cm tolerable settlement

First, p' is calculated by Eq 3.4.b:

$$p' = \gamma' \cdot h$$

$$\gamma' = 1.800 - 1.027 = 0.773 \text{ t/m}^3$$

Assuming the rock layer is present at a depth of 150 m below the sea level, h is calculated as follows.

$$h = \frac{150}{2} = 75 \text{ m}$$

$$p' = 0.773 \cdot 75 = 58 \text{ t/m}^2$$

If the overburden pressure exceeds 28.12 t/m² (40 psi), it takes the value of 28.12 t/m² (40 psi) (Teng 1962). Thus; p' is taken as 28.12 t/m² (40 psi)

Second, corrected SPT_ N value (N_{cor}) is found by Eq 3.4.a:

$$N_{cor} = N \cdot \left(\frac{50}{p+10} \right) = 4 \cdot \left(\frac{50}{40+10} \right)$$

$$N_{cor} = 4$$

Last, the allowable bearing capacity of the soil is calculated by Eq 3.4:

$$q_a = 3.5 \cdot (N_{cor} - 3) \cdot \left(\frac{B + 0.3048}{2B} \right)^2 \cdot R_w \quad (\text{t/m}^2)$$

$$B = 39.8 \text{ m} \quad R_w = 0.5$$

$$q_a = 3.5 \cdot (4 - 3) \cdot \left(\frac{39.8 + 0.3048}{2 \cdot 39.8} \right)^2 \cdot 0.5$$

$$q_a = 0.44 \text{ t/m}^2$$

A comparison of the above based on two different approaches shows that the second approach yields a smaller value. This means that the soil fails because of

intolerable settlement, before it fails due to shear failure. Thus, the result found from the second approach is used as the allowable bearing capacity of the soil.

The allowable bearing capacity of soil is very small, and it seems clear that it is smaller than the net total pressure applied at foundation level, hence ground improvement is definitely recommended

The SPT-N value is assumed as 2 in the Çiğli coastal area side. Therefore, in this side, the allowable bearing capacity of the soil is less than 0.44 t/m^2 . It can be said that if the SPT-N is less than 3 the soil does not have enough capacity to carry the net foundation pressure applied on the seabed soil. Based on the existing SPT-N value results, it can be concluded that the allowable bearing capacity of the Çiğli seabed soil is less than the net pressure applied to it. Thus ground improvement is needed. In the İnciraltı side the SPT-N value was assumed as to be 29, Hence, the soil has enough bearing capacity to carry the pressure transferred to it. However, since the soil consists of sand and gravel in this part, it is recommended to compact the soil by making grouting up to at least 30 m (0.75B) depth below the seabed. There are no SPT results for the middle alignment of the tunnel (based on the DLH study); and therefore the allowable bearing capacity of the soil could not be calculated

3.2. Liquefaction Potential of the Seabed Soil

If loose saturated and unconsolidated granular soil is subjected to cyclic loading such as earthquake loading, its pore pressure will increase. As a result of this, the soil particles lose its effective stress and the medium acts as a liquid. (Das 1983). This behavior is called liquefaction and generally occurs in loose to moderately compacted granular soils (such as silty sands or sands and gravels) under water, with poor drainage conditions. Figure 3.3 explains the liquefaction process of the soil.

To decide whether the soil has been under the liquefaction risk or not, there are several methods, such as laboratory investigations and observations on the field. Based on the existing test results, the liquefaction risk of the İzmir Bay's seabed is examined by using two different analyses:

1. Liquefaction analysis by using depth and SPT data relationship
2. Liquefaction analysis by using the simplified procedure

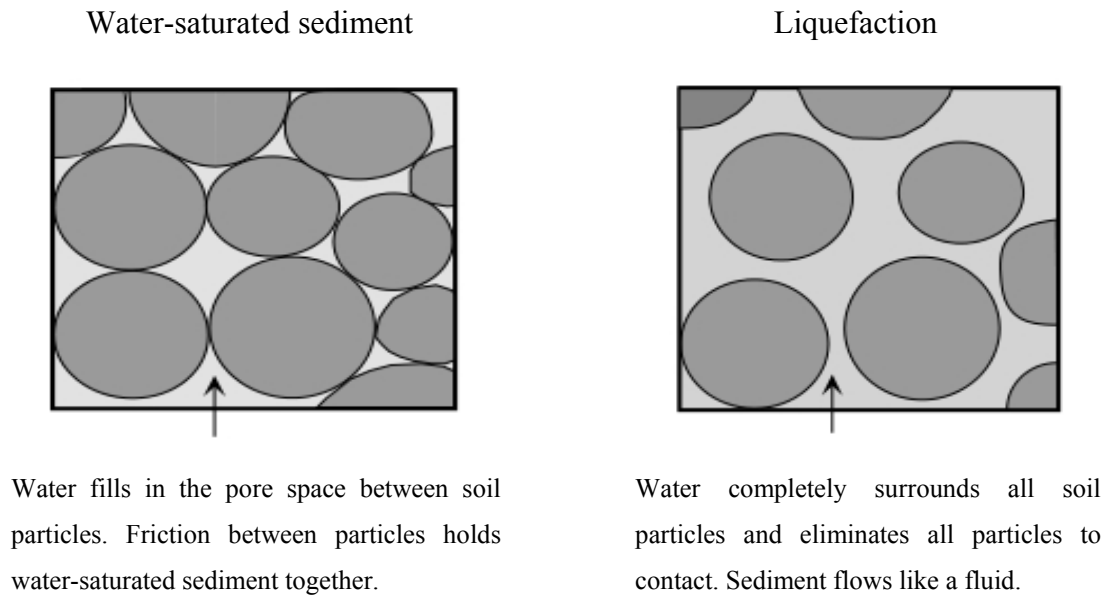


Figure 3.3. Liquefaction process of the soil
(Source: Tulane University 2004)

3.2.1. Liquefaction Analysis by using Depth and SPT Data Relationship

In this method, the liquefaction potential of the soil is examined by using a relationship between the SPT-N values and their corresponding depth (Tezcan and Özdemir 2004). For instance, by using three SPT data, which were provided from three different locations (nearest to the route) of the İzmir Bay, the liquefaction risk of the tunnel soil can be revealed by means of the graph in Figure 3.4. SK18 is the name of the borehole location near the İnciraltı side, SK17 is the name of the borehole location between the İnciraltı side and the Çiğli side, and SK8 is the name of the borehole location near the Çiğli side. The locations of the boreholes are shown in Figure 3.2.

Two curves plotted in Figure 3.4 show the degree of liquefaction potential of the soil. The processed data from Table 3.1 is inserted into this graph, revealing the degree of liquefaction risk of the soil. It can be seen that the Çiğli side is under high risk and the İnciraltı side is under low risk. According to this depth and SPT data relationship, ground improvement appears to be necessary

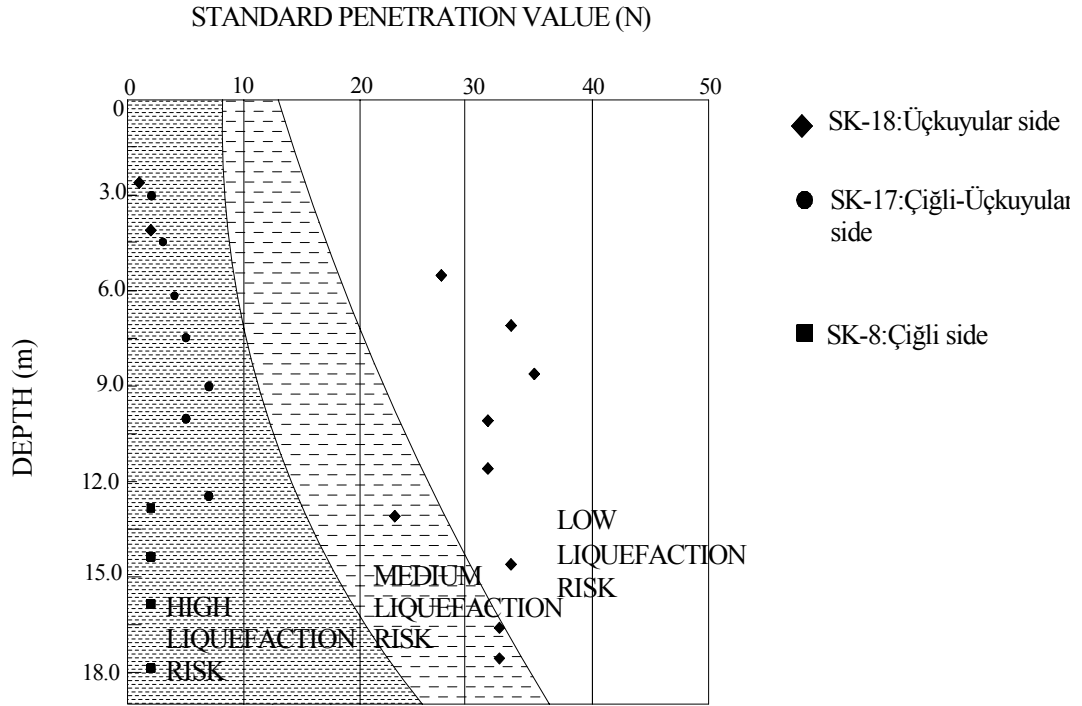


Figure 3.4. Relationship between the possibility of liquefaction and N values
(Source: Tezcan and Özdemir 2004)

3.2.2. Liquefaction Analysis by using Simplified Procedure

The simplified procedure is originally developed by Seed and Idriss in 1971 following the disastrous earthquake in Alaska, USA and in Nigata, Japan in 1964. This procedure is based on the relationship between the cyclic resistance ratio (CRR) and cyclic stress ratio (CSR). Dividing the CRR to CSR, the factor of safety FS is found. At locations, where FS is less than unity, liquefaction is expected to occur (Tezcan and Özdemir 2004).

The factor of safety, FS , expressed as the capacity over demand is:

$$FS = \frac{Capacity}{Demand} = \frac{CRR}{CSR} \quad (3.5)$$

FS should be bigger than 1 to avoid liquefaction risk.

3.2.2.1. Earthquake Induced Shear Stress Ratio (CSR)

A transient earthquake motion is converted to an equivalent series of uniform cycles of shear stress. The number of equivalent cycles, a function of the duration of motion is correlated with the magnitude of the earthquake (Lee and Seed, 1967). The actual time history of shear stress at any point in a soil deposit during an earthquake will have an irregular form. Therefore, the average equivalent stress, $r_b=65\%$ of the maximum shear stress, is used for $M_w=7.5$ earthquake magnitude expected in İzmir Bay. To calculate the cyclic stress ratio (CSR) the following formula is developed in the field, due to earthquake shaking (Tezcan and Özdemir 2004).

$$CSR = \frac{\tau_{av}}{\sigma'_{vo}} = r_b \cdot \frac{a_{max}}{g} \cdot \frac{\sigma_{vo}}{\sigma'_{vo}} \cdot r_d \quad (3.6)$$

$$\tau_{av} = r_b \cdot \left(\frac{a_{max}}{g} \right) \cdot \sigma_{vo} \cdot r_d \quad (3.7)$$

where, τ_{av} : the average horizontal shear stress developed on the soil element,

σ'_{vo} : effective overburden pressure,

σ_{vo} : total vertical overburden pressure,

a_{max} : peak ground acceleration

g : acceleration of gravity

r_d : depth reduction coefficient (see Sec. 3.2.2.2.)

r_b : coefficient for effective average level of acceleration,

$$r_b = 0.1 \cdot (M_w - 1) \quad (3.8.a)$$

$$r_b = 0.65 \text{ for } M_w = 7.5 \quad (3.8.b)$$

3.2.2.2. Depth Reduction Factor

The depth reduction factor, r_d , is introduced to take into account the fact that the amplitudes of horizontal accelerations decrease, as the depth below the ground surface increases (Similar to the acceleration response values in high-rise buildings). Seed and Idris (1971) recommended using the following r_d values, which account for the flexibility of the soil profile, in regard to routine practice and non-critical projects (Tezcan and Özdemir 2004).

$$r_d = 1 - 0.00765 \cdot z \quad \text{for } z \leq 9.15 \quad (3.9.a)$$

$$r_d = 1.174 - 0.0267 \cdot z \quad \text{for } 9.15 \leq z \leq 23 \quad (3.9.b)$$

$$r_d = 0.744 - 0.0082 \cdot z \quad \text{for } 23 \leq z \leq 30 \quad (3.9.c)$$

$$r_d = 0.50 \quad \text{for } z \geq 30 \quad (3.9.d)$$

where z is the depth to the midpoint of the layer below the seabed surface in m.

3.2.2.3. Cyclic Resistance Ratio (CRR)

To determine the capacity of seabed soil to resist liquefaction, cyclic resistance ratio-CRR is determined by use of field correlations from insitu tests or laboratory tests on representative samples of the soil deposits. The three most routinely used methods to evaluate the liquefaction resistance, CRR, are:

- i: The standard penetration test (SPT),
- ii: The cone penetration test (CPT),
- iii: The seismic shear wave velocity (V_s) test (Tezcan and Özdemir 2004).

For this work, the CRR value is calculated by using the SPT results.

Corrected factors for SPT Values are;

$$(N_1)_{60} = C_N \cdot C_E \cdot C_B \cdot C_R \cdot C_S \cdot N_m \quad (3.10)$$

where,

$(N_1)_{60}$: Corrected SPT number

C_N : Overburden correction factor

C_E : Correction factor for the SPT hammer energy ratio

C_B : Correction factor for the borehole diameter

C_R : Correction factor for the rod length

C_S : Correction factor for the sampling method

N_m : Insitu measured Standard Penetration resistance value

The correction factors C_N, C_E, C_B, C_R, C_S are summarized in Table 3.2.

After calculating the corrected SPT number, the CRR can be found by using charts developed by different researches.

Curves by Seed et al. (1983): *Practical charts are proposed by Seed et. al. (1983) regarding evaluation of the liquefaction potential for different magnitude earthquakes, by representing the behavior of sands with $D_{50} > 0.25$ mm, under level ground conditions, and penetration resistance, N_1 , as shown in Figure 3.5 (Tezcan and Özdemir 2004).*

Table 3.2. The correction factor values for corrected SPT values

(Source: Tezcan and Özdemir 2004)

Symbol	Correction factor value															
C_N (overburden pressure correction factor) σ'_{vo} is in kg/cm ²	$C_N = \frac{1}{\sqrt{\sigma'_{vo}}}$ (Liao and Whitman, 1986)															
	$C_N = 0.77 \cdot \log\left(\frac{20}{\sigma'_{vo}}\right)$ (Peek ,et al. 1974)															
	$C_N = 1 - 1.25 \cdot \log \sigma'_{vo}$ (Tokimatsu and Yoshimi, 1983)															
	$C_N = \frac{1.7}{0.7 + \sigma'_{vo}}$ (Seed and Idriss, 1983)															
C_E (Energy ratio correction factor)	$C_E = \frac{\text{Efficiencyratio}}{0.60}$ <p>where efficiency ratio(ER) is the for percentage of the theoretical SPT impact hammer energy actualay transmitted to hammer</p> <table border="1"> <thead> <tr> <th><u>Equipment</u></th> <th><u>ER</u></th> <th><u>C_E</u></th> </tr> </thead> <tbody> <tr> <td>Donnut hammer⁽¹⁾</td> <td>0.30 to 0.60</td> <td>0.5 to 1.0</td> </tr> <tr> <td>Donnut hammer⁽²⁾</td> <td>0.70 to 0.85</td> <td>1.2 to 1.4</td> </tr> <tr> <td>Safety hammer</td> <td>0.40 to 0.75</td> <td>0.7 to 1.2</td> </tr> <tr> <td>Automatic-trip Donut hammer</td> <td>0.50 to 0.80</td> <td>0.8 to 1.3</td> </tr> </tbody> </table>	<u>Equipment</u>	<u>ER</u>	<u>C_E</u>	Donnut hammer ⁽¹⁾	0.30 to 0.60	0.5 to 1.0	Donnut hammer ⁽²⁾	0.70 to 0.85	1.2 to 1.4	Safety hammer	0.40 to 0.75	0.7 to 1.2	Automatic-trip Donut hammer	0.50 to 0.80	0.8 to 1.3
<u>Equipment</u>	<u>ER</u>	<u>C_E</u>														
Donnut hammer ⁽¹⁾	0.30 to 0.60	0.5 to 1.0														
Donnut hammer ⁽²⁾	0.70 to 0.85	1.2 to 1.4														
Safety hammer	0.40 to 0.75	0.7 to 1.2														
Automatic-trip Donut hammer	0.50 to 0.80	0.8 to 1.3														
C_B (Borehole diam. correction factor)	<table> <tbody> <tr> <td>D=65~115 mm</td> <td>$C_B=1.0$</td> </tr> <tr> <td>D=150 mm</td> <td>$C_B=1.05$</td> </tr> <tr> <td>D=200 mm</td> <td>$C_B= 1.15$</td> </tr> </tbody> </table>	D=65~115 mm	$C_B=1.0$	D=150 mm	$C_B=1.05$	D=200 mm	$C_B= 1.15$									
D=65~115 mm	$C_B=1.0$															
D=150 mm	$C_B=1.05$															
D=200 mm	$C_B= 1.15$															
C_R (Rod lenght correction factor)	<table> <tbody> <tr> <td>L<3 m</td> <td>$C_R=0.75$</td> </tr> <tr> <td>3<L≤4</td> <td>$C_R=0.80$</td> </tr> <tr> <td>4<L≤6</td> <td>$C_R=0.85$</td> </tr> <tr> <td>6<L≤10</td> <td>$C_R=0.95$</td> </tr> <tr> <td>10<L≤30</td> <td>$C_R=1.00$</td> </tr> </tbody> </table>	L<3 m	$C_R=0.75$	3<L≤4	$C_R=0.80$	4<L≤6	$C_R=0.85$	6<L≤10	$C_R=0.95$	10<L≤30	$C_R=1.00$					
L<3 m	$C_R=0.75$															
3<L≤4	$C_R=0.80$															
4<L≤6	$C_R=0.85$															
6<L≤10	$C_R=0.95$															
10<L≤30	$C_R=1.00$															
C_S (Sampling method correction factor)	<table> <tbody> <tr> <td>Standard sampler</td> <td>$C_S=1.00$</td> </tr> <tr> <td>Sampler without lines</td> <td>$C_S=1.10$ Loose soils</td> </tr> <tr> <td></td> <td>$C_S=1.30$ Dense soils</td> </tr> </tbody> </table>	Standard sampler	$C_S=1.00$	Sampler without lines	$C_S=1.10$ Loose soils		$C_S=1.30$ Dense soils									
Standard sampler	$C_S=1.00$															
Sampler without lines	$C_S=1.10$ Loose soils															
	$C_S=1.30$ Dense soils															

The application of the simplified procedure for this study based on the İzmir Bay's soil properties is described below;

i) The cyclic stress ratio (CSR) is:

The total stress under 2.5B depth of the tunnel base:

$$\sigma_{vo} = (h_1 \times \gamma_{water}) + (h_2 \times \gamma_{armor-stone}) + (h_3 \times \gamma_{sand-concrete}) + \left(\frac{V_{tube} \cdot \gamma_{concrete}}{A_{tubebase}} \right) + (h_5 \times \gamma_{soil}) \quad (3.11)$$

$$\sigma_{vo} = (17.5 \times 1.027) + (0.5 \times 2.6) + (0.5 \times 2.1) + \left(\frac{15278 \cdot 2.5}{39.8 \cdot 100} \right) + (100 \times 1.60)$$

$$\sigma_{vo} = 189.92 t / m^2 = 19 kg / cm^2$$

The effective stress under 2.5B depth of the tunnel base,

$$\sigma'_{vo} = \sigma_{vo} - ((17.5 + 1 + 10 + 100) \times 1.027) = 57.95 t / m^2 = 5.8 kg / cm^2 \quad (3.12)$$

The depth reduction factor:

$$z = h_1 + h_2 + h_3 + h_4 + h_5 = 17.5 + 0.5 + 0.5 + 10 + 100 = 128.5$$

$$z \geq 30 m \quad rd = 0.50 \quad (\text{from Eq 3.9.d})$$

The cyclic stress ratio is calculated by Eq 3.6. as below;

$$CSR = \frac{\tau_{av}}{\sigma'_{vo}} = r_b \cdot \frac{a_{max}}{g} \cdot \frac{\sigma_{vo}}{\sigma'_{vo}} \cdot r_d$$

$$a_{max} = 0.34 g \quad (\text{from Table 3.3.})$$

$$r_b = 0.65 \quad (\text{from Eq 3.8.b})$$

$$CSR = 0.65 \cdot \left(\frac{0.34 \cdot g}{g} \right) \cdot \left(\frac{189.92}{57.95} \right) \cdot 0.50$$

$$CSR = 0.362$$

Table 3.3 Ground Acceleration Coefficients and Peak Ground Acceleration
(Source: Taiwan High speed Rail Project Contract C240 2003)

Level of Earthquake	Ground Acceleration Coefficient (Z_t)	Peak Ground Acceleration (a_{max}) m/s ²
Type I (severe)	0.34	3.34
Type II (moderate)	0.11	1.11

ii) The cyclic resistance ratio (CRR) is:

Firstly, the correction factors are obtained from Table 3.2.

The overburden correction factor C_N is:

To calculate the overburden pressure correction factor value the formula developed by Liao and Whitman was used. Thus,

$$C_N = \frac{1}{\sqrt{\sigma'_{vo}}} = \frac{1}{\sqrt{5.8}} = 0.415 \quad (3.11)$$

The energy ratio correction factor C_E is:

$$C_E = \frac{\text{Efficiency Ratio}}{0.60} \quad (3.12)$$

Assume that the donut hammer was used for the SPT and ER=0.60.

$$\text{for } ER = 0.60 \rightarrow C_E = 1.0 \quad (3.13)$$

The borehole diameter correction factor C_B is:

Note that, N is too small when an oversize borehole is drilled (Bowles 1988).

Hence,

$$C_B = 1.15 \quad (3.14)$$

The rod length correction factor C_R is:

Note that, N is too high for $L > 10$ m (Bowles 1988). Thus,

$$C_R = 1.00 \quad (3.15)$$

For loose soils sampling method correction factor C_s is:

$$C_s = 1.10 \quad (3.16)$$

Assumption: At 17.5 m. depth (the part, where the inclination of the tunnel is zero), the N value was taken as 4 (as an average value), based on the other SPT results due the fact that there was no SPT results for this part of the tunnel.

Finally, the corrected SPT_N value $(N_1)_{60}$ is found from Eq 3.10:

$$(N_1)_{60} = C_N \cdot C_E \cdot C_B \cdot C_R \cdot C_s \cdot N_m$$

$$(N_1)_{60} = 0.415 \cdot 1.0 \cdot 1.15 \cdot 1.0 \cdot 1.10 \cdot 4$$

$$(N_1)_{60} = 2.1$$

From Figure 3.5. the CRR value is,

$$\text{for } (N_1)_{60} = 2.1 \text{ and } M_w = 7.5 \rightarrow CRR = 0.02$$

At last, factor of safety can be calculated from Eq 3.5 as below;

$$CSR = 0.362$$

$$CRR = 0.02 \dots$$

$$FS = \frac{CRR}{CSR} = \frac{0.02}{0.362} = 0.06$$

$$FS = 0.06 < 1.25$$

Thus, the soil has high liquefaction potential.

Three SPT testing borehole results along the IBITT route are evaluated for this study. They are used to calculate the allowable bearing pressure and give an idea about the site's liquefaction potential. However, there are a number of drawbacks in using these data. First, the numbers of boreholes are not enough. Second, the boreholes do not reach to the depth of the IBITT, which is designed to be at a depth of 28.5 meters.

The calculated allowable bearing capacities may not be reliable. These capacities are based on equations that are developed for line footings. In the current study, on the other hand, the magnitude of the tunnel width is 10-30 times larger than a regular footing. As is the case with the allowable bearing capacity analysis, the stress ratio and penetration resistance analysis, also suggests that the site of interest has high liquefaction potential. Based on the results of the two methods, ground improvement appears to be necessary along the IBITT route.

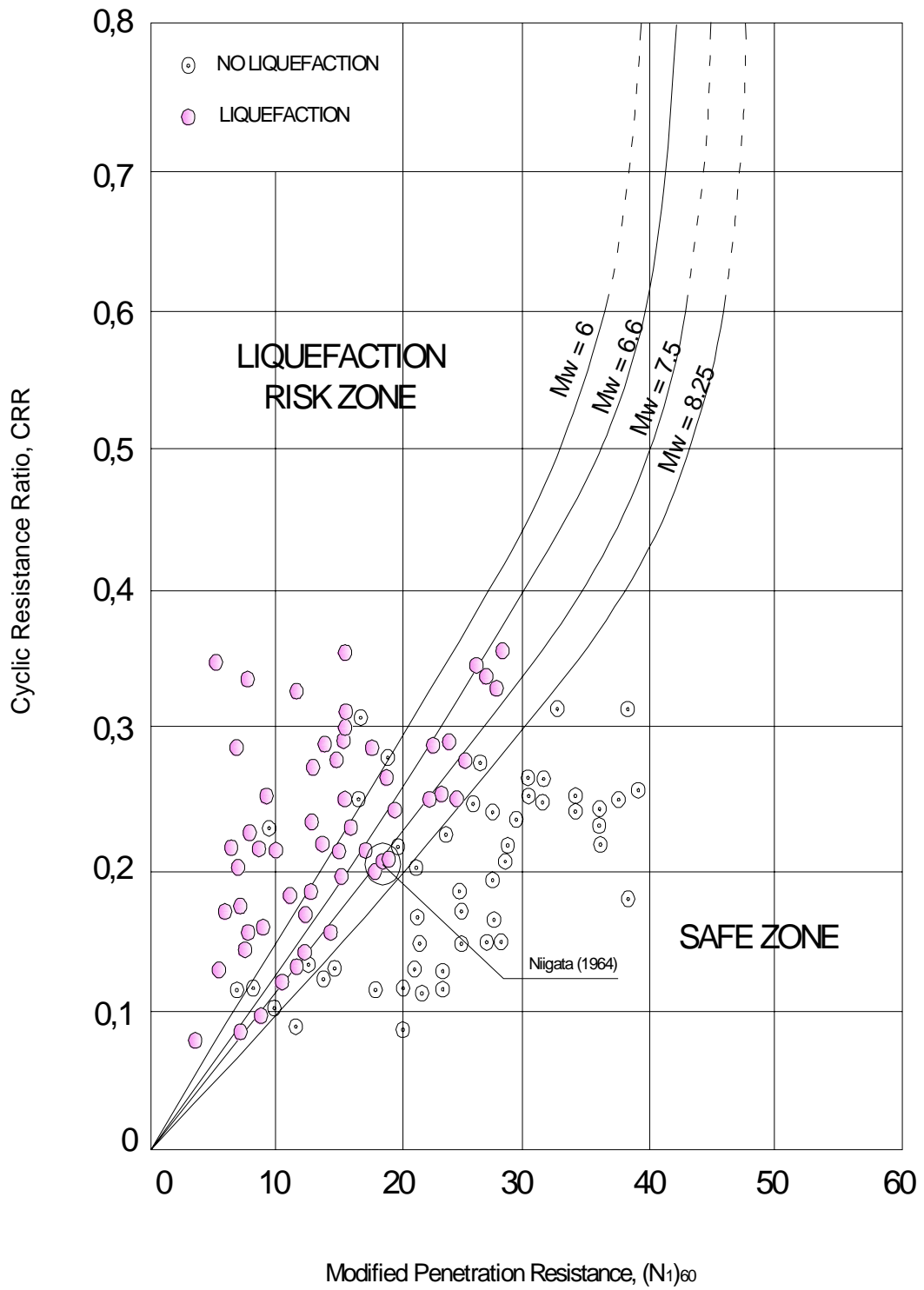


Figure 3.5. Stress ratio and penetration resistance
(Source Tezcan and Özdemir 2004)

CHAPTER 4

STATIC ANALYSIS FOR PRELIMINARY DESIGN

The aim of the static analysis was to calculate the displacements of the seabed subsoil (beneath the immersed tube tunnel) under static loads and investigate whether they are acceptable or not. The first part of this chapter consists of the calculation of the modulus of subgrade reaction. This modulus is used to calculate the equivalent soil stiffness property. Two methods are available to calculate this modulus of subgrade reaction. One that is based on the $\sigma-\varepsilon$ relation, and another that depends on the allowable bearing capacity of the soil. Once the soil stiffness property is at hand, the soil settlement is calculated with a worst case loading. For the static analysis, a finite element program called Calculix was chosen and two analyses were carried out for two cases:

1. The static analysis to find the displacements occurring in the subsoil as soon as the tube is immersed onto the seabed.
2. The static analysis to find the displacements during operation of the tunnel:

4.1. Estimation of the Modulus of Subgrade Reaction

The modulus of subgrade reaction k_s is a relationship between the applied soil pressure and deflection experienced by the structure that is widely used in soil-structure interaction problems. In a mechanical sense, k_s could be based on plate-load test data, which is given as follows (Bowles 1988).

$$k_s = \frac{q}{\delta} \quad (4.1)$$

where q is the soil pressure and, δ is the deflection of the soil. Here, the value of q is calculated by dividing the applied force by the plate δ must be measured.

However, it is difficult to make plate-load tests at foundation level, except for very small plate. Therefore, k_s should be calculated by using other relationships, containing

either the stress-strain modulus, E_s , or allowable soil pressure, q_a , as described below. After a brief explanation of the two methods, their application to the IBITT problem follows.

4.1.1. Finding the Modulus of Subgrade Reaction from Stress

Strain modulus, E_s (First method)

This approximation shows existence of a direct relationship between k_s and E_s as explained below (Bowles 1988):

$$k_s = \frac{\Delta q}{\Delta H} = \frac{1}{B \cdot E'_s \cdot I_s \cdot I_f} \quad (4.2)$$

where Δq is the stress increase in stratum from footing or pile load, ΔH is the settlement of foundation, E'_s is the corrected modulus of elasticity and can be calculated as below:

$$E'_s = \frac{(1 - \mu^2)}{E_s} \quad (4.3)$$

E_s is the modulus of elasticity of soil in ksf unit, μ is poisson ratio of soil, B is the width of the structure base in ft unit, I_f is factor based on the D/B ratio found by Figure 4.1, and I_s is the settlement influence factor based on H/B and L/B

$$I_s = I_1 + \frac{1 - 2\mu}{1 - \mu} \cdot I_2 \quad (4.4)$$

I_1, I_2 : Influence factors which depend on L'/B' , thickness of the stratum H, Poisson's ratio μ and the embedment depth D . They are found from Table 4.1.

$L' = L/2$ for center; $L' = L$ for corner

$B' = B/2$ for center; $B' = B$ for corner

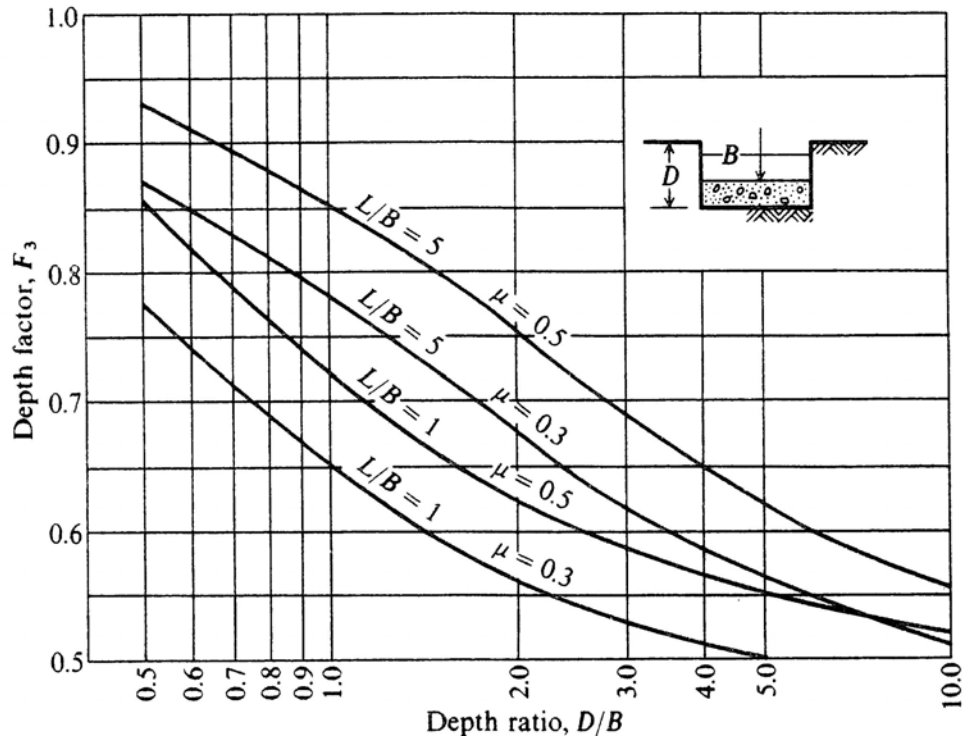


Figure 4.1. Influence factor I_f for a footing at a depth D .

(Source: Bowles 1988)

4.1.2. Finding the Modulus of Subgrade Reaction from Allowable Soil Pressure, q_a (Second method)

In this approximation, the k_s value is calculated with respect to the allowable soil bearing capacity. It is noted that the computed allowable soil pressures and bending moments (in case of eccentric loads) are not very sensitive to what value is used for k_s . This is because the structural member stiffness is usually 10 or more times greater than the soil stiffness, (Bowles 1988). Therefore, the following equation is proposed to approximate k_s .

$$k_s = 40 \cdot (FS) \cdot q_u = 40 \cdot q_a \text{ (kN / m}^3\text{)} \quad (4.5)$$

where q_a is the allowable bearing pressure in kPa units and FS is the factor of safety.

Table 4.1. Values of I_1 and I_2 to compute the Steinbrenner influence factor

(Source: Bowles 1988)

H/B'	L/B = 1, 0	1,1	1,2	1,3	1,4	1,5	1,6	1,7	1,8	1,9	2,0
0,2	0,009	0,008	0,008	0,008	0,008	0,008	0,007	0,007	0,007	0,007	0,007
	0,041	0,042	0,042	0,042	0,042	0,042	0,043	0,043	0,043	0,043	0,043
0,4	0,033	0,032	0,031	0,030	0,029	0,028	0,028	0,027	0,027	0,027	0,027
	0,066	0,068	0,069	0,070	0,070	0,071	0,071	0,072	0,072	0,073	0,073
0,6	0,066	0,064	0,063	0,061	0,060	0,059	0,058	0,057	0,056	0,056	0,055
	0,079	0,081	0,083	0,085	0,087	0,088	0,089	0,090	0,091	0,091	0,092
0,8	0,104	0,102	0,100	0,098	0,096	0,095	0,093	0,092	0,091	0,090	0,089
	0,083	0,087	0,090	0,093	0,095	0,097	0,098	0,100	0,101	0,102	0,103
1,0	0,142	0,140	0,138	0,136	0,134	0,132	0,130	0,129	0,127	0,126	0,125
	0,083	0,088	0,091	0,095	0,098	0,100	0,102	0,104	0,106	0,108	0,109
1,5	0,224	0,224	0,224	0,223	0,222	0,220	0,219	0,217	0,216	0,214	0,213
	0,075	0,080	0,084	0,089	0,093	0,096	0,099	0,102	0,105	0,108	0,110
2,0	0,285	0,288	0,290	0,292	0,292	0,292	0,292	0,292	0,291	0,290	0,289
	0,064	0,069	0,074	0,078	0,083	0,086	0,090	0,094	0,097	0,100	0,102
3,0	0,363	0,372	0,379	0,384	0,389	0,393	0,396	0,398	0,400	0,401	0,402
	0,048	0,052	0,056	0,060	0,064	0,068	0,071	0,075	0,078	0,081	0,084
4,0	0,408	0,421	0,431	0,440	0,448	0,455	0,460	0,465	0,469	0,473	0,476
	0,037	0,041	0,044	0,048	0,051	0,054	0,057	0,060	0,063	0,065	0,069
5,0	0,437	0,452	0,465	0,477	0,487	0,496	0,503	0,510	0,516	0,522	0,526
	0,031	0,034	0,036	0,039	0,042	0,045	0,048	0,050	0,053	0,055	0,058
6,0	0,457	0,474	0,489	0,502	0,514	0,524	0,534	0,542	0,550	0,557	0,563
	0,026	0,028	0,031	0,033	0,036	0,038	0,040	0,043	0,045	0,047	0,050
7,0	0,471	0,490	0,506	0,520	0,533	0,545	0,556	0,566	0,575	0,583	0,590
	0,022	0,024	0,027	0,029	0,031	0,033	0,035	0,037	0,039	0,041	0,043
8,0	0,482	0,502	0,519	0,534	0,549	0,561	0,573	0,584	0,594	0,602	0,611
	0,020	0,022	0,023	0,025	0,027	0,029	0,031	0,033	0,035	0,036	0,038
9,0	0,491	0,511	0,529	0,545	0,560	0,574	0,587	0,598	0,609	0,618	0,627
	0,017	0,019	0,021	0,023	0,024	0,026	0,028	0,029	0,031	0,033	0,034
10,0	0,498	0,519	0,537	0,554	0,570	0,584	0,597	0,610	0,621	0,631	0,641
	0,016	0,017	0,019	0,020	0,022	0,023	0,025	0,027	0,028	0,030	0,031
20,0	0,529	0,553	0,575	0,595	0,614	0,631	0,647	0,662	0,677	0,690	0,702
	0,008	0,009	0,010	0,010	0,011	0,012	0,013	0,013	0,014	0,015	0,016
500,0	0,560	0,587	0,612	0,635	0,656	0,677	0,696	0,714	0,731	0,748	0,763
	0,000	0,000	0,000	0,000	0,000	0,000	0,001	0,001	0,001	0,001	0,001

H/B'	L/B = 2,5	4,0	5,0	6,0	7,0	8,0	9,0	10,0	25,0	50,0	100,0
0,2	$I_1 = 0,007$	0,006	0,006	0,006	0,006	0,006	0,006	0,006	0,006	0,006	0,006
	$I_2 = 0,043$	0,044	0,044	0,044	0,044	0,044	0,044	0,044	0,044	0,044	0,044
0,4	0,026	0,024	0,024	0,024	0,024	0,024	0,024	0,024	0,024	0,024	0,024
	0,074	0,075	0,075	0,075	0,076	0,076	0,076	0,076	0,076	0,076	0,076
0,6	0,053	0,051	0,050	0,050	0,050	0,049	0,049	0,049	0,049	0,049	0,049
	0,094	0,097	0,097	0,098	0,098	0,098	0,098	0,098	0,098	0,098	0,098
0,8	0,086	0,082	0,081	0,080	0,080	0,080	0,079	0,079	0,079	0,079	0,079
	0,107	0,111	0,112	0,113	0,113	0,113	0,113	0,114	0,114	0,114	0,114
1,0	0,121	0,115	0,113	0,112	0,112	0,112	0,111	0,111	0,110	0,110	0,110
	0,114	0,120	0,122	0,123	0,123	0,124	0,124	0,124	0,125	0,125	0,125
1,5	0,207	0,197	0,194	0,192	0,191	0,190	0,190	0,169	0,188	0,188	0,188
	0,118	0,130	0,134	0,136	0,137	0,138	0,138	0,139	0,140	0,140	0,140
2,0	0,284	0,271	0,267	0,264	0,262	0,261	0,260	0,259	0,257	0,256	0,256
	0,114	0,131	0,136	0,139	0,141	0,143	0,144	0,145	0,147	0,147	0,148
3,0	0,402	0,392	0,386	0,382	0,378	0,376	0,374	0,373	0,368	0,367	0,367
	0,097	0,122	0,131	0,137	0,141	0,144	0,145	0,147	0,152	0,153	0,154
4,0	0,484	0,464	0,479	0,474	0,470	0,466	0,464	0,462	0,453	0,451	0,451
	0,082	0,110	0,121	0,129	0,135	0,139	0,142	0,145	0,154	0,155	0,156
5,0	0,543	0,554	0,552	0,548	0,543	0,540	0,536	0,534	0,522	0,519	0,519
	0,070	0,098	0,111	0,120	0,128	0,133	0,137	0,140	0,154	0,156	0,157
6,0	0,585	0,609	0,610	0,608	0,604	0,601	0,598	0,595	0,579	0,576	0,575
	0,060	0,087	0,101	0,111	0,120	0,126	0,131	0,135	0,153	0,157	0,157
7,0	0,618	0,653	0,658	0,658	0,656	0,653	0,650	0,647	0,628	0,624	0,623
	0,053	0,078	0,092	0,103	0,112	0,119	0,125	0,129	0,152	0,157	0,158
8,0	0,643	0,688	0,697	0,700	0,700	0,698	0,695	0,692	0,672	0,666	0,665
	0,047	0,071	0,084	0,095	0,104	0,112	0,118	0,124	0,151	0,156	0,158
9,0	0,663	0,716	0,730	0,736	0,737	0,736	0,735	0,732	0,710	0,704	0,702
	0,042	0,064	0,077	0,088	0,097	0,105	0,112	0,118	0,149	0,156	0,158
10,0	0,679	0,740	0,758	0,766	0,770	0,770	0,770	0,768	0,745	0,738	0,735
	0,038	0,059	0,071	0,082	0,091	0,099	0,106	0,112	0,147	0,156	0,158
20,0	0,756	0,856	0,896	0,925	0,945	0,959	0,969	0,977	0,982	0,965	0,957
	0,020	0,031	0,039	0,046	0,053	0,059	0,065	0,071	0,124	0,148	0,156
500,0	0,832	0,977	1,046	1,102	1,150	1,191	1,227	1,259	1,532	1,721	1,879
	0,001	0,001	0,002	0,002	0,002	0,003	0,003	0,003	0,008	0,016	0,031

4.1.3. Application of the First and Second Methods in this Study

In this study, k_s was calculated by two different approaches, and to stay on the safe side the smaller one was taken as the k_s design value.

1. Estimation of k_s by using the first (E_s) method:

The modulus of elasticity for silty-sand soils changes between 5 and 20 MPa. In this study, as the immersed tube is designed with respect to worst conditions, E_s was taken as 5 MPa. In addition, Poisson's ratio for this type was assumed as 0.35 (Bowles 1988).

The design parameters;

$$B = 39.8\text{ m} \quad L = 100\text{ m} \quad D = 10\text{ m}$$

$$E_s = 5\text{ MPa} \quad \mu = 0.35$$

Corrected E'_s value is calculated by Eq 4.3:

$$E'_s = \frac{(1 - \mu^2)}{E_s} = \frac{(1 - 0.35^2)}{5 \cdot 10^6} = 1.755 \cdot 10^{-7} \frac{\text{m}^2}{\text{N}}$$

For the center, H was taken as 1.25B. Because the depth of stress influence (stress bulb) due to added net foundation pressure, for very large structures is reduced from 2.5B to 0.75B (Egeli, et al. 1983).

$$H = 1.25 \cdot B = 49.75\text{ m} \quad B' = \frac{B}{2} = 19.9\text{ m}$$

$$\frac{H}{B'} = \frac{1.25B}{0.5B} = 2.5 \rightarrow I_1 = 0.343 \text{ from Table 4.1}$$

$$\frac{L}{B} = \frac{100}{39.8} = 2.5 \rightarrow I_2 = 0.113 \text{ from Table 4.1.}$$

The settlement influence factor calculated by using Eq 4.4:

$$I_s = 0.343 + \frac{1 - 2 \cdot 0.35}{1 - 0.35} \cdot 0.113$$

$$\frac{D}{B} = \frac{10}{39.8} = 0.25 \rightarrow I_f = 0.85 \text{ from Figure 4.1}$$

Then the modulus of subgrade reaction was founded by using Eq 4.2:

$$k_s = \frac{1}{B' \cdot E'_s \cdot I_s \cdot I_f}$$

$$k_s = \frac{1}{(19.9) \cdot (1.755 \cdot 10^{-7}) \cdot (0.395 \cdot 4) \cdot (0.85)} = 213203 \text{ N/m}^3$$

For corner,

$$\frac{H}{B'} = \frac{1.25B}{B} = 1.25 \rightarrow I_1 = 0.382$$

$$\frac{L}{B} = \frac{100}{39.8} = 2.5 \rightarrow I_1 = 0.067$$

$$I_f = 0.85$$

$$I_s = 0.382 + \frac{1 - 2 \cdot 0.35}{1 - 0.35} \cdot 0.067 = 0.418$$

$$k_s = \frac{1}{(39.8) \cdot (1.755 \cdot 10^{-7}) \cdot (0.418) \cdot (0.85)} = 402944 \text{ N/m}^3$$

For the average value of k_s , four center contributions and one corner contribution is used. In other words, the values must be weighted (Bowles 1988).

$$k_{s(av)} = \frac{4 \cdot 213203 + 402944}{5} = 251151 \text{ N/m}^3$$

2. Estimation of k_s by using the second (q_a) method:

The allowable bearing capacity of the soil was calculated in Section 3.1 and had been found as 0.446 t/m^2 (4.374 kN/m^2). The modulus of subgrade reaction value is calculated by Eq 4.5:

$$k_s = 40 \cdot q_a \quad \text{kN/m}^3$$

$$k_s = 40 \cdot 4.374 = 174.96 \text{ kN/m}^3 = 174960 \text{ N/m}^3$$

In order to stay on the safe side, the smaller value of the two approaches is used as the modulus of subgrade reaction of the supporting soil. The results are shown in Table 4.2.

Table 4.2. The modulus of subgrade reaction (k_s) values obtained from 2 different approaches

The modulus of subgrade reaction (k_s) (N/m^3)	First Method	Second Method	Used Value
	251151.43	174500	174500

4.1.4. Calculation of the Spring Constants

A single tube of 100 m in length is divided into five pieces of 20 m, each. These pieces are modeled by a mesh of 18 m hexahedral (20 noded) elements. The bottom face of such a meshed segment that rests on soil is shown in Figure 4.4. The soil is modeled as linear spring elements, which are connected to the nodes indicated in Figure 4.4. An

isoperimetric view of the meshed tube segment, together with the spring element is shown in Figure 4.2. The spring constants at each node are obtained by the multiplication of the modulus of subgrade reaction with the area of the face of the corresponding element and are weighted by a factor, as is shown in Figure 4.3. Thus,

$$K_i^j = A_j \cdot k_s \cdot \alpha_i \quad (4.6)$$

where; K_i^j is the spring constant connected to the i^{th} node of the element j , A_j is the face area(that is in contact with soil) of the j^{th} element, and α_i is the weighting factor of the i^{th} node. (See Figure 4.3)

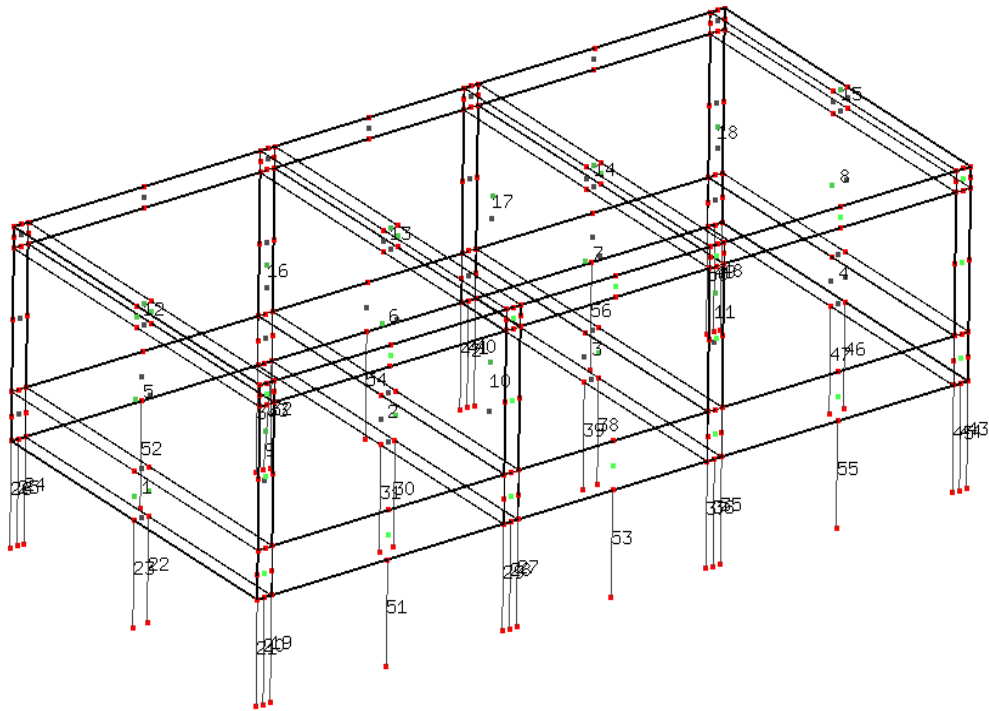


Figure 4.2. The modeling of the tube unit and the elastic foundation in Calculix

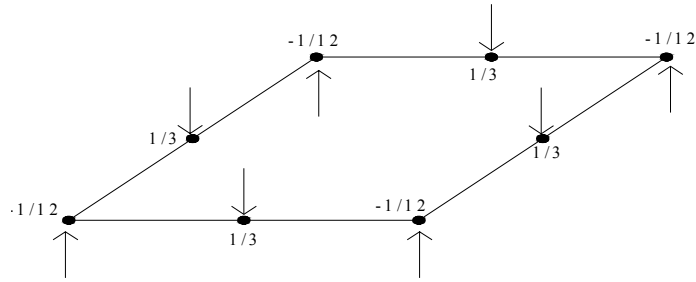


Figure 4.3. The weights for vertical spring constants corresponding to each node of a hexahedral element face (Source: Calculix 1.7 2007)

The above figure illustrates the distribution of the K_i value over the element surface (tunnel unit's soil base). If an edge or a corner node is shared by more than one element, the spring stiffness of that node is simply superimposed.

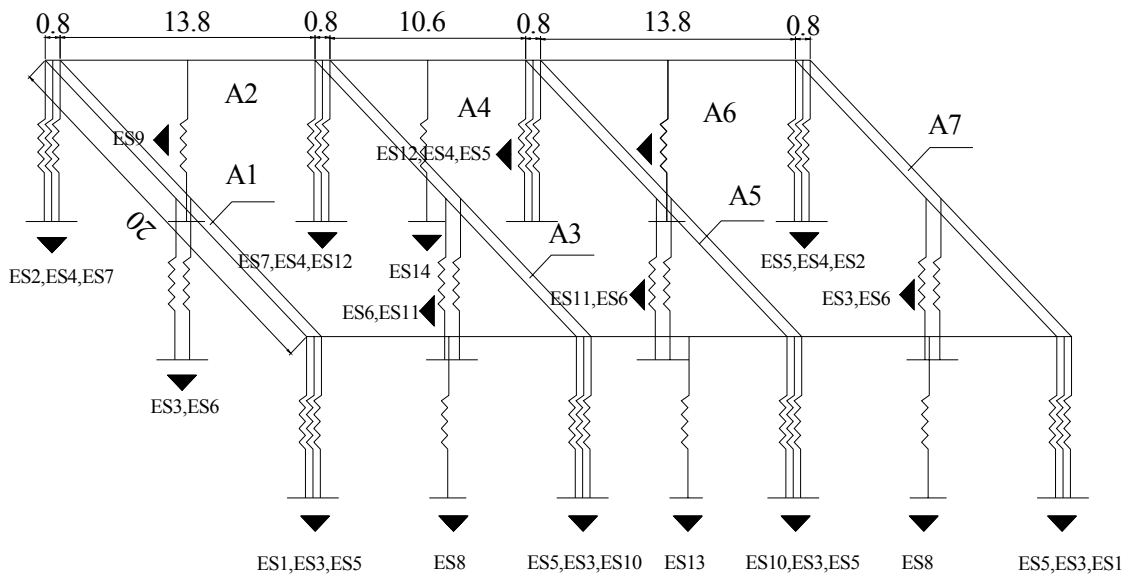


Figure 4.4. The modeling of the elastic foundation of the tube unit.

The areas of the base surface of the tube from Figure 4.3.

$$A1 = A3 = A5 = A7 = 0.8 \times 20 = 16m^2 \quad (4.7)$$

$$A2 = A6 = 13 \times 20 = 260m^2 \quad (4.8)$$

$$A4 = 10.6 \times 20 = 212m^2 \quad (4.9)$$

Considering the meshing model, 13 different vertical spring constants were calculated by using Eq 4.6.

$$ES1 = (-1/12) \cdot (175000) \cdot (16) = -233333 \text{ N/m} \quad (4.6.a)$$

$$ES2 = (-1/12) \cdot (175000) \cdot (16) = -233333 \text{ N/m} \quad (4.6.b)$$

$$ES3 = (1/3) \cdot (175000) \cdot (16) = 933333 \text{ N/m} \quad (4.6.c)$$

$$ES4 = (1/3) \cdot (175000) \cdot (16) = 933333 \text{ N/m} \quad (4.6.d)$$

$$ES5 = (-1/12) \cdot (175000) \cdot (260) + ES1 = -4025000 \text{ N/m} \quad (4.6.e)$$

$$ES6 = (1/3) \cdot (175000) \cdot (260) + ES3 = 16100000 \text{ N/m} \quad (4.6.f)$$

$$ES7 = (-1/12) \cdot (175000) \cdot (260) + ES1 = -4025000 \text{ N/m} \quad (4.6.g)$$

$$ES8 = (1/3) \cdot (175000) \cdot (260) = 15166667 \text{ N/m} \quad (4.6.h)$$

$$ES9 = (1/3) \cdot (175000) \cdot (260) = 15166667 \text{ N/m} \quad (4.6.i)$$

$$ES10 = (-1/12) \cdot (175000) \cdot (212) + ES1 = -3325000 \text{ N/m} \quad (4.6.j)$$

$$ES11 = (1/3) \cdot (175000) \cdot (212) + ES3 = 13300000 \text{ N/m} \quad (4.6.k)$$

$$ES12 = (-1/12) \cdot (175000) \cdot (212) + ES1 = -3325000 \text{ N/m} \quad (4.6.l)$$

$$ES13 = (1/3) \cdot (175000) \cdot (212) = 12366667 \text{ N/m} \quad (4.6.m)$$

$$ES13 = (1/3) \cdot (175000) \cdot (212) = 12366667 \text{ N/m} \quad (4.6.n)$$

4.2. Static Analysis of the Tunnel for Worst Case Scenario

Tunnel units are built at the shore and below the sea level. The construction procedure of each tube unit undergoes four basic steps:

- i) Construction at land,
- ii) Coverage of its open ends, so that it floats on water, and can be pulled to its position
- iii) It is slowly lowered down to the seabed by allowing water to drain into the tube. Positioning is accomplished by using steel cables, GPS and divers.
- iv) Finally, the sides are filled with sand and gravel in a slurry form with the help of pumps.

The aim here is to investigate the amount of subsoil settlement when the water-filled tube with water is placed upon it. If the settlement value of the subsoil is bigger than the tolerable settlement value (2.5 cm), the subsoil needs to be improved.

The static analysis was made only for the tube placed to the dredged trench location with the greatest depth of seawater (17.5 m). Hence, there was no need for another analysis, because it was assumed that the elastic properties of the tunnel seabed soil are the same along the tunnel route; since a limited borehole data was available (the worst borehole data in Çiğli side was used in the analysis). Moreover, the effective pressure on the subsoil is the same during immersion of each tube unit. Therefore, there was no need to make displacement (i.e. settlement) analysis for each tube unit. The Calculix model of the tube that was illustrated in Figure 4.2 consists of a mesh with twenty noded brick elements (C3D20) (see Figure 4.5) and the elastic foundation was assembled with two noded linear spring elements. Each tube unit model consists of 90 C3D20 elements and 130-spring elements. Boundary conditions were applied such that only vertical motion was allowed. Only the base of the springs was fixed in all directions. In addition, it was assumed that the side fills had no effect on the vertical motion of the tube under its gravity loads. Pressures acting on to the subsoil (as soon as the water-filled tube with water is placed upon it) are illustrated in Figure 4.6 and

calculated as below. The displacement analysis should be carried out for the worst case (maximum loading on the soil). Two scenarios can be considered: One during the placement of the tube, another during service failure.

1. If no problem occurs during immersion process of the tubes, there will be no excessive loads acting onto the seabed. However, in the design phase, a worst-case scenario must be considered. Water leakage, and hence a tunnel unit that is completely filled with water is an undesirable, but possible stage during construction. Therefore, this analysis case consists of a tunnel unit being placed onto its seabed, its top covered with an extra protective material layer, and the inside of the tunnel being filled with water.

2. When the tunnel is in service, the additional loads come from the sidewalks and the traffic, only. Here, the worst-case scenario is the tube filled with cars, trucks, trains, and water due to a water leakage in the joints.

The failure scenario described in item number two will result in larger pressure acting on the subsoil. Therefore, only one analysis will suffice to find the maximum displacement.

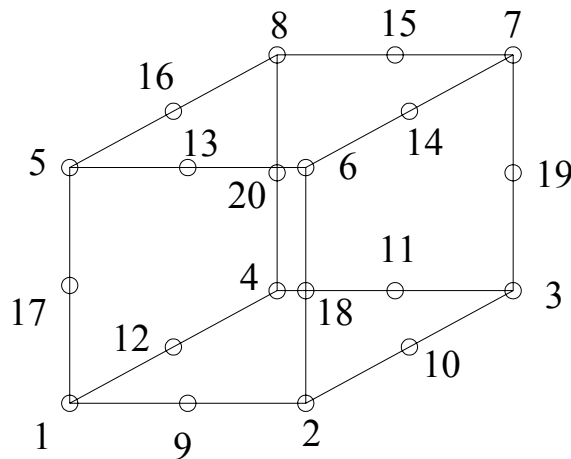
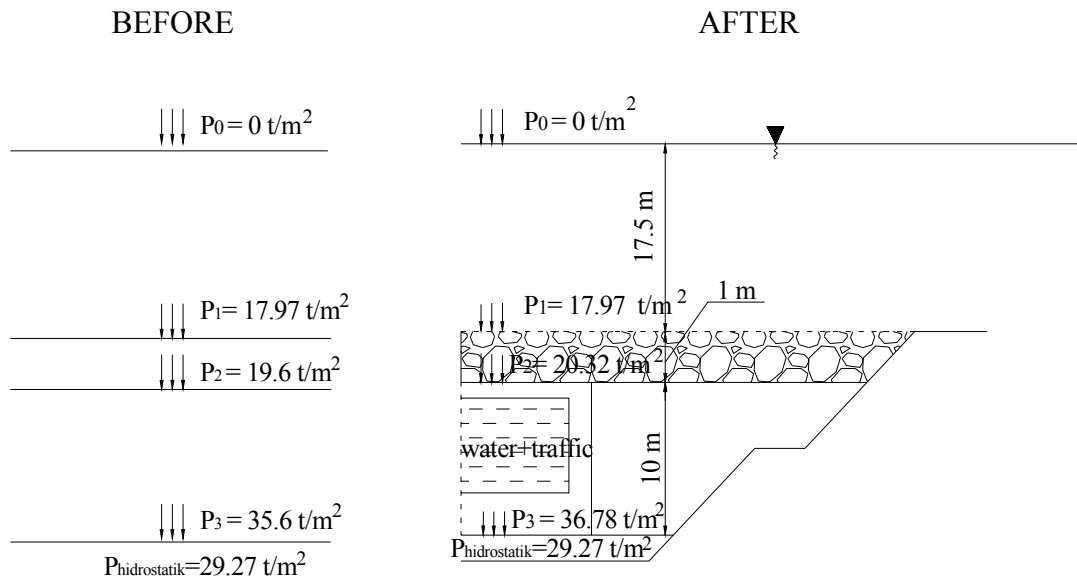


Figure 4.5. Twenty-noded brick element (C3D20) in Calculix

(Source: Calculix 1.7 2007)



a) Pressure transferring on the seabed soil before dredging

b) Pressure transferring on the seabed soil after dredging

Figure 4.6. The foundation pressure on the seabed soil before and after construction of the IBITT

4.2.1 Total Pressure Transferred to the Seabed Soil

a) Checking the floatability during transportation of the empty tunnel unit to its dredged location:

The total width of the tunnel is 39.8 m, and height is 10 m. The widths of the highways are 13 m and height is 6.7 m, and the width of the railway is 10.6 m, and the height is 6.7 m. The length of the tube is 100 m. The density of reinforced concrete is 2.5 t/m^3 and seawater is 1.027 t/m^3 .

Subtracting the volumes of each hole from the total volume of the tube, the concrete volume of the tube could be calculated.

$$V_{net} = (39.8 \times 100 \times 10) - (13 \times 6.7 \times 100) - (10.6 \times 6.7 \times 100) - (13 \times 6.7 \times 100) = 15278 \text{ m}^3 \quad (2.1)$$

If the density of concrete is multiplied by the concrete volume of the tube, the total weight of the tube will be found:

$$W_{tube} = (15278 \times 2.5) = 38195 \text{ t} \quad (2.2)$$

The natural buoyancy of water applied from foundation level to sea level:

$$F_{buoyancy} = (39.8 \times 10 \times 100) \times 1.027 = 40874 \text{ t} \quad (2.3)$$

$$F_{buoyancy} > W_{tube} \rightarrow \text{The tube floats, which is O.K.}$$

b) Checking the sinkability of the tunnel unit during lowering to its dredged location:

The unit weight of the armor stone per square m.:

$$P_{armorstone} = 0.5 \times 2.6 = 1.30 \text{ t} / \text{m}^2 \quad (2.4)$$

The unit weight of the sand-concrete per square m.:

$$P_{sand - concrete} = 0.5 \times 2.1 = 1.05 \text{ t} / \text{m}^2 \quad (2.5)$$

The pressure on the seabed soil due to the water layer on the tube:

$$P_{water-positive} = 17.5 \times 1.027 = 17.97 \text{ t} / \text{m}^2 \quad (2.6)$$

To sink the tunnel element, there is no need to completely fill it with water. A water depth of 1 m inside the tube is sufficient.

$$W_{water_intube} = (2 \times (13 \times 1.0 \times 100) + (10.6 \times 1 \times 100)) \times 1.027 = 3759 \text{ t} \quad (2.7)$$

Thus, the weight of the 1m water filled tunnel unit is:

$$W_{semifilled_tube} = W_{tube} + W_{water} = 38195 + 3759 = 41954 \text{ t} \quad (2.8)$$

$W_{semifilled_tube} > F_{buoyancy} \rightarrow$ The tunnel element sinks to its dredged location.

However, as it is mentioned in Section 4.2. to be prepared for the worst case conditions, the maximum settlement calculation should be made considering the tunnel is in service and due to a water leakage it is full filled with water. (Scenario 2, see page 49).

The weight of the fully filled tube is calculated as below:

$$W_{waterfilled_tube} = 39800 + ((2 \times 13 \times 6.7 \times 100) + (10.6 \times 6.7 \times 100)) \times 1.027 = 63379 \text{ t} \quad (2.9)$$

The unit weight of the full-filled tube is calculated as below:

$$P_{waterfilledtube} = \frac{63379}{39.8 \times 100} = 15.92 \text{ t / m}^2 \quad (2.10)$$

The weight of the traffic loads is calculated as below. The train load is calculated according to S (1950) Freight Train from “Alman Federal Demiryolları-Çelik Demiryol Köprüleri için Hesap Esasları (BE)” technical code. The Figure... shows the distribution of the loads in S (1950) Freight Train.

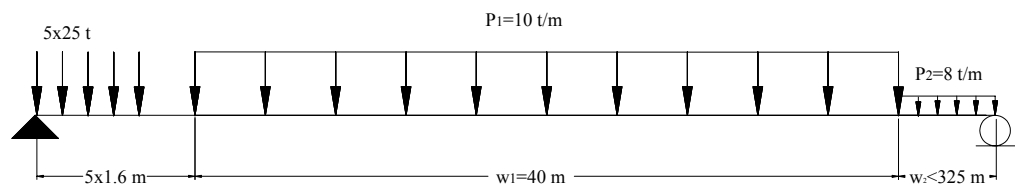


Figure 4.7. S (1950) load train

(Source: Alman Federal Demiryolları-Çelik Demiryol Köprüleri için Hesap Esasları (BE))

$$W_{loading\ train} = 2 \times (5 \times 25 + 40 \times 10.4 + 52 \times 8) = 1882\ t \quad (2.11)$$

There are 3 line in highway and it is assumed that max. 25 cars can be placed in a line and the weight of the car with people is 1.9 tons can be assumed.

$$W_{car} = 2 \times (25 \times 3 \times 1.9) = 285\ t \quad (2.12)$$

The pressure occurring due to the traffic effect can be calculated as below:

$$P_{traffic} = \frac{(1882 + 285)}{(39.8 \times 100)} = 0.54\ t / m^2 \quad (2.13)$$

The total pressure transferred to the soil is calculated:

$$P_{total} = P_{filledtube} + P_{water-positive} + P_{protectivelayer} + P_{traffic} - P_{water-negative} \quad (2.14)$$

$$P_{total} = 15.92 + 17.97 + (1.05 + 1.30) + 0.54 - (28.5 \times 1.027) = 7.51\ t / m^2$$

The net effective soil stress at the dredged foundation level of the tunnel, which is 11 m below of the seabed soil:

$$P_{soil} = 11 \times (1.6 - 1.027) = 6.30\ t / m^2 \quad (2.15)$$

Subtracting the permanent total pressure transferred to the soil from the net effective soil stress at the dredged foundation level, the net effective stress increase can be calculated as below:

$$P'_{neteffective} = 7.51 - 6.30 = 1.21\ t / m^2 \quad (2.16)$$

Due to the increase of the net effective pressure on the seabed soil, the vertical displacement of the tunnel was calculated as 6.59 cm but this value is above the permissible settlement value of 2.5 cm for each immersed tube unit. The permissible

settlement value is a serviceability requirement for tunnels and immersed tube tunnels containing railroads and highways, designed and constructed in the Far East (Egeli 1996). At first glance, it might appear reasonable to decrease the tunnel dimensions, in order to decrease the stress on the subsoil. Nevertheless, no matter what dimensions are used, settlement value is likely to be exceeded.

Also, remember that the mass is necessary to overcome the buoyancy (lift) forces of the water. Thus, dimensions cannot be decreased. To overcome this drawback, compaction grouting type ground improvement is suggested for the seabed soil. Moreover, this is a good precaution against the seismic forces risk and overcoming its induced further settlement. (See Chapter 5). The static analysis result in Calculix is shown in Figure 4.8.

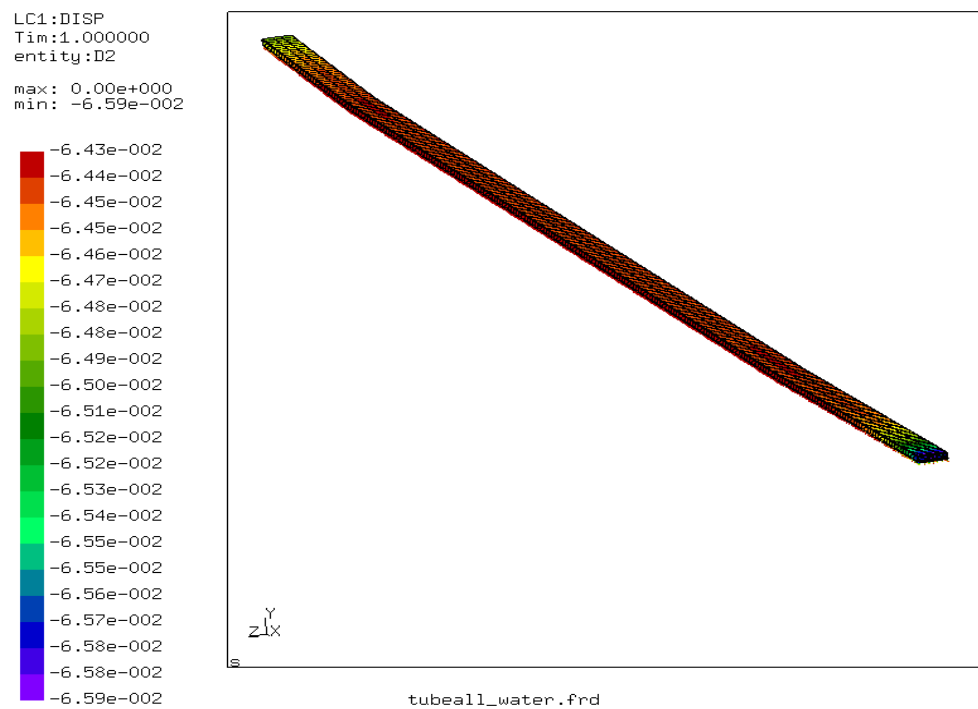


Figure 4.8. Maximum vertical displacement of the tunnel

CHAPTER 5

SEISMIC ANALYSIS OF THE IMMERSED TUBE TUNNEL

It is principally recognized that underground structures is affected less from earthquakes than buildings on the ground surface (Kouretzis, et al. 2006). Therefore, in the past, most tunnel structures were designed and built without regard to seismic effects (Taylor, et al. 2005). A seismic design procedure was applied to a tunnel project for the first time in the 1960s by civil engineers for immersed tube tunnel; The Deas Tunnel is the first project that is designed taking the earthquake effects into consideration (Wang 1993, Grantz, et al.1993). For instance, the Bay Area Rapid Transit (BART) tunnel in San Francisco, California and Osaka South Port (OSP) immersed tube tunnel in Japan have been subjected to strong seismic shaking. Nevertheless, since these tunnels had been designed considering the seismic effects, both tunnels behaved exceptionally well, by sustaining no measurable damage (Anastasopoulos, et al. 2007). On the other hand, the Alameda Tubes in the San Francisco Bay Area, which were some of the earliest immersed tube tunnels built in 1927 and 1963, were designed without any seismic design considerations. Therefore, during the Loma Prietta Earthquake (1989), some cracking was experienced in the ventilation buildings and limited water leakage into the tunnels was observed. (Hashash, et al. 2001).

The purpose of this chapter was to develop a pre-seismic design of the immersed tube tunnel in order to give the structure the capacity to withstand the loads or deformations/displacements applied to it during an earthquake. A seismic design should cover all components of the tunnel including, portal buildings, ventilation buildings, approach structures etc. However, in this study only the immersed tube units, the joints of the tube units and the elastic foundation underneath were considered.

5.1. Types of Deformations

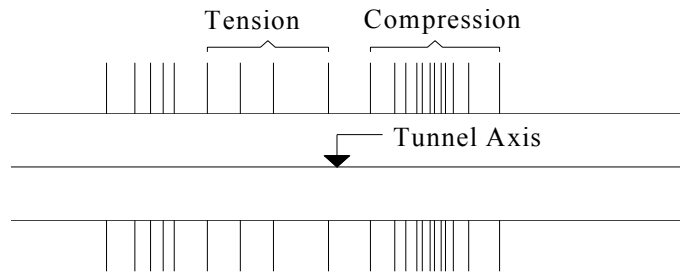
The response of tunnels to seismic shaking motions was explained below (Wang 1993):

1. Axial and Lateral Deformations: Axial and lateral deformations develop in a linear tunnel, when seismic waves propagate either parallel or oblique to the tunnel. The tunnel lining considerations for these types of deformations are in the tunnel longitudinal direction along the tunnel axis. The idealized representations of axial and lateral deformations are illustrated in Figure 5.1. Vertical deformations are also present during an earthquake. These are less detrimental, because the vertical stiffness of the tube only one tenth of its lateral stiffness. Therefore, vertical deformations are not considered in the analysis.

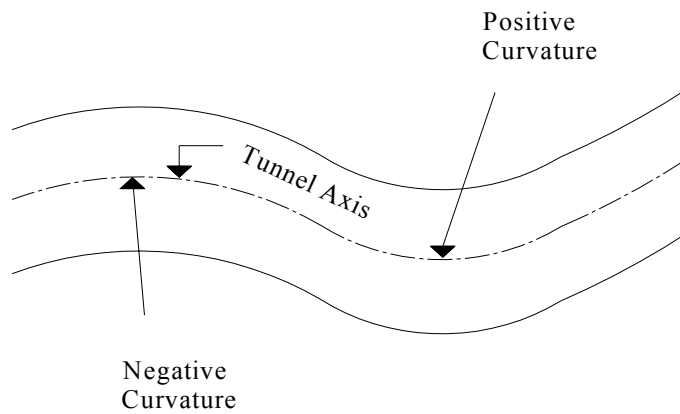
2. Ovaling (for circular tunnels) or racking (for rectangular tunnels): Since the dimensions of a typical lining cross-section of the tunnel are small compared with the earthquake wavelengths, the ground motions produce racking effect (Penzien 2000). Ovaling or racking deformations may develop in tunnel structures, when waves propagate in a direction perpendicular or nearly perpendicular to the tunnel axis, resulting in a distortion of the cross-sectional shape of the tunnel lining (Wang 1993). The racking deformation of the rectangular tunnel section is shown in Figure 5.2.

5.2. Seismic Analysis Procedures

The seismic design of underground structures differs from the design of surface structures. Surface structures are not only directly subjected to the excitations of the ground. They experience amplification of the shaking motions depending on their own vibratory characteristics. Underground structures, on the other hand, are constrained by the surrounding medium. Hence, they can not progress to a considerable amount of deformation, independently from the medium nor can they be subjected to a vibration amplification (Wang 1993).



A. Axial deformation along the tunnel (top view of the tunnel)



B. Curvature deformation along the tunnel (top view of the tunnel)

Figure 5.1. Axial and lateral deformations along a tunnel
(Source: Wang 1993)

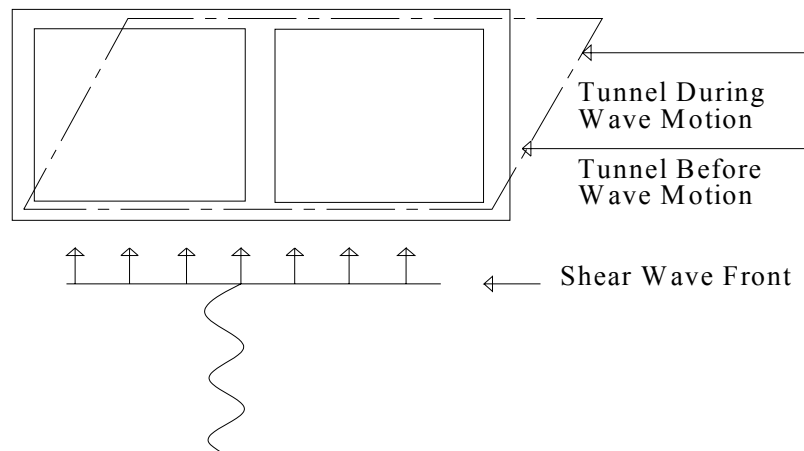


Figure 5.2. Racking deformation of a rectangular tunnel
(Source: Wang 1993)

5.2.1. Free-Field Deformation Approaches

The term ‘free-field deformation’ describes ground strains caused by seismic waves in the absence of structures or excavation. In this approach, the interaction between the underground structure and the surrounding ground is ignored.

The free-field deformation method provides a simple and effective design, if the ground is very stiff and has low shaking intensity or the structure is more flexible than the surrounding medium. For soft soils (the structure is stiffer than the medium), this approach provides a first-order estimate of the anticipated structural deformation (Hashash, et al. 2001). The axial and lateral deformation of the tunnel lining by using a free field deformation approach can be estimated by using a structural analysis program or by a hand calculation. The strains of the tunnel due to the seismic wave propagation according to the simplified procedure are explained below.

5.2.1.1. Closed Form Solution Method (Simplified Procedure)

For practical purposes, Newmark developed a simplified approach in 1968. This method is one of the free-field deformation approaches. According to this method, the structure and the ground in the free field experience the same strains (Wang 1993). Figure 5.3 shows free-field ground deformation along a tunnel axis due to a sinusoidal shear wave with a wavelength, L , a displacement amplitude, D , and an angle of incidence, a . The axial and lateral deformations of the ground and the shear (racking) deformation of the tunnel, due to the shear wave is calculated by using Eq 5.1 and 5.3, respectively.

The axial (longitudinal) strain;

$$\varepsilon = \frac{V_s}{C_s} \cdot \sin a \cdot \cos a \quad (5.1)$$

The lateral;

$$\left(\frac{1}{r}\right) = \frac{A_s}{C_s^2} \cdot \cos^3 a \quad (5.2)$$

The shear (racking) deformation;

$$\gamma = \frac{V_s}{C_s} \cdot \cos^2 a \quad (5.3)$$

where a is the angle of incidence with respect to the tunnel axis, r is the radius of lateral, V_s is the peak particle velocity for shear wave, C_s is the effective propagation velocity of the shear wave, and A_s is peak particle acceleration of the shear wave.

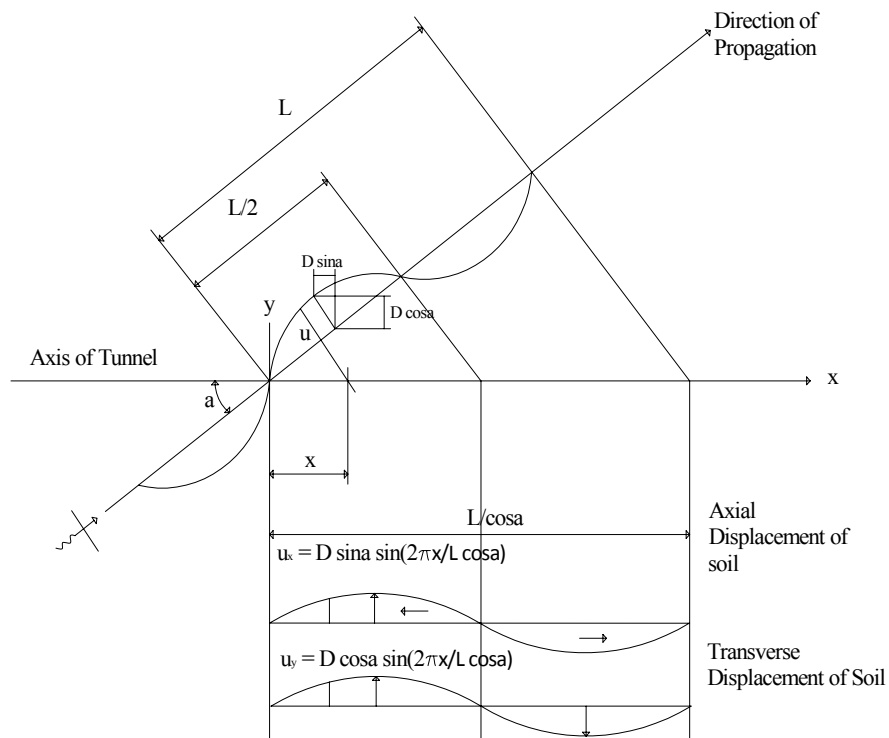


Figure 5.3. The propagation of the S wave along the tunnel axis
(Source: Wang 1993)

This method has also been used successfully for seismic design of long, linear tunnel structures in several major transportation projects including the San Francisco BART stations and tunnels as well as those for the Los Angeles Metro (Wang 1993). Nevertheless, for rectangular box structures in soft soils, this method gives very conservative designs since free-field ground distortions in soft soils are generally large

and also underground structures are typically designed with stiff configurations to resist static loads (Hashash, et al. 2001).

As a conclusion, a free-field deformation approach is not recommended for rectangular structures in soft soil. For this type of structures, however, a soil-structure interaction approach is suggested.

5.2.2. Soil-Structure Interaction Approach

A tunnel-ground interaction analysis that considers both the tunnel stiffness and the ground stiffness is necessary, in order to find the true tunnel response. The tunnel-ground interaction system is simulated as a beam on an elastic foundation, with the theory of wave propagating in an infinite, homogeneous, isotropic medium (Hashash, et al. 1998). The calculation procedures are explained below:

5.2.2.1. Dynamic Earth Pressure

This method typically assumes earthquake loads to be caused by the inertial force of the surrounding soil. Among the dynamic earth pressure methods, most widely used one is the Monobe-Okabe method. However, for rectangular cross sections, under plain strain conditions, this method leads to unrealistic results and is not suggested to be used for typical tunnel cross sections (Hashash, et al. 2000).

5.2.2.2. Closed Form Solution Method to Calculate Axial and Bending Stresses

This method is based on the beam-on-elastic foundation approach and it ignores dynamic (inertial) interaction effects (Shamsabadi 2001). When the tunnel is subjected to the axial and lateral deformations due to the traveling seismic waves in the ground, the tunnel is experienced to have the sectional forces below:

- Axial forces, acting on the cross section because of the axial deformation
- Bending moments, M , and shear forces, V , acting on the cross section due to the lateral deformation. (Wang 1993)

Simplified Interaction Equations:

The axial forces caused by a shear wave with 45 degree angle of incidence can be obtained from:

$$Q_{\max} = \frac{\frac{K_a L}{2\pi}}{1 + 2\left(\frac{K_a}{E_c A_c}\right)\left(\frac{L}{2\pi}\right)^2} D_a \quad (5.4)$$

where, L is the wavelength of an ideal sinusoidal shear wave, K_a is the longitudinal spring coefficient of medium in force per unit deformation per unit length of tunnel, D_a is the free-field displacement response amplitude of an ideal sinusoidal shear wave, E_c is the modulus of elasticity of tunnel lining, and A_c is the cross-section area of tunnel lining.

The maximum axial strain can be obtained from the equation below:

$$\varepsilon_{axial} = \frac{Q_{\max}}{E_c \cdot A_c} \quad (5.5)$$

$$M_{\max} = \frac{K_t \left(\frac{L}{2\pi}\right)^2}{1 + \left(\frac{K_t}{E_c I_c}\right)\left(\frac{L}{2\pi}\right)^4} D_b \quad (5.6)$$

where, I_c is the moment of inertia of the tunnel section, K_t is the transverse spring coefficient of medium in force per unit deformation per unit length of tunnel, D_b is the free-field displacement response amplitude of an ideal sinusoidal shear wave.

Once the maximum bending moment is found by Eq 5.6, the corresponding stress at the tunnel sides are evaluated as follows:

$$\sigma_{\max} = \frac{M_{\max} \cdot (B/2)}{I_c} \quad (5.7)$$

The maximum bending strain is calculated from the equation below:

$$\varepsilon_{bending} = \frac{M_{\max} \cdot (B/2)}{E_c \cdot I_c} \quad (5.8)$$

The maximum shear force corresponding to the maximum bending moment is derived as:

$$V_{\max} = M_{\max} \cdot \frac{2\pi}{L} \quad (5.9)$$

Once the design parameters are found, they should be checked against the allowable values. For concrete, the allowable shear strength is calculated by the formula given below:

$$V_c = 0.22 \cdot f_{cd} \cdot A_{shear} \quad (5.10)$$

The maximum strain should be less than the allowable strain:

$$\varepsilon_{\max} = \varepsilon_{axial} + \varepsilon_{bending} \leq \varepsilon_{allowable} \quad (5.11)$$

where $\varepsilon_{allowable}$ is the allowable tensile strain of the concrete. In the equations above, K_a and K_t are different from the conventional beam on elastic foundation problems, since the spring coefficients should be representative of the dynamic modulus of the ground under seismic loads. In addition, the derivations should consider the fact that loading felt by the surrounding soil (medium) is alternately positive and negative due to an assumed sinusoidal seismic wave. For a preliminary design, the expression suggested by St. John and Zahrah (1987) should serve the purpose:

$$K_t = K_a = \frac{16\pi \cdot G_s (1 - \nu_s)}{(3 - \nu_s)} \cdot \frac{H}{L} \quad (5.12)$$

where, G_s is the shear modulus of the medium, ν_s is the poisson's ratio of the medium, H is the height of a rectangular structure (or diameter of a circular tunnel), and L is the wavelength.

The wavelength is not known, but it can be estimated by using the shear wave velocity.

$$L = T \cdot C_s \quad (5.13)$$

where, the predominant natural period, T , can be estimated from the soil deposit at a tunnel site (Wang 1993):

$$T = \frac{4H_s}{C_s} \quad (5.14)$$

where, H_s is the soil deposit thickness over rigid bedrock and C_s is the shear wave velocity of the medium.

5.2.2.3. Numerical Analysis Method to Calculate Axial and Bending Stresses

Another method to determine the displacements and stresses developing in the tunnel's longitudinal direction during a seismic activity is by using numerical methods. The numerical analysis of underground structures can be made by using either lumped mass/stiffness methods or by finite element/difference methods (Hashash, et al. 2001).

5.2.2.4. Closed Form Solution Method to Calculate Racking Deformations

Rectangular tunnels are usually built in shallow soils and design of such tunnels requires careful consideration of soil structure interaction analysis for two reasons:

1. There is a larger deformation during an earthquake in shallow soils than in deeper soils, because of the decreased stiffness of the surrounding soils, due to a lower overburden pressure. Thus, the site amplification effect is high.

2. Rectangular tunnel linings are usually built stiffer than circular tunnel linings in their transverse direction and hence, they are less tolerant to deformations (Husam, et al. 2005).

Then, the racking deformation of a tunnel was calculated by using two different approaches:

1. Simple Frame Analysis Model: In this approach, only the tube unit is modeled without the surrounding soil under simple boundary conditions, as shown in Figure 5.6. This approach should be used for a first-order estimate, although conservative results can be obtained. The simplicity of the modeling makes the analysis worthwhile and gives a relationship between the shear deformation flexibilities of the tunnel and the soil.

The procedure to calculate the racking deformation in rectangular tunnels is defined below (Wang 1993):

Firstly, the earthquake design parameters should be determined, including at least the magnitude of the earthquake, peak ground accelerations, $a_{\max}(Z_t)$, and C_s , according to level earthquake parameters, which are Type I (severe) earthquake and Type II (moderate) earthquake. Then, based on the soil properties and the design earthquake parameters, the free-field shear strains/deformations of the ground are determined.

$$\gamma_s = \frac{V_s}{C_s} \quad (5.15)$$

$$V_s = R_v \cdot a_s \quad (5.16)$$

where, R_v is the ratio of peak ground velocity to peak ground acceleration and determined from Table 5.2., a_s is the peak particle acceleration associated with S waves and found from the formula below:

$$a_s = R_a \cdot a_{\max} \quad (5.17)$$

in here, R_d is the ratio of the ground motion at the tunnel base depth to the motion at the ground surface and is determined from Table 5.1, and $a_{\max}(Zt)$ is the peak ground acceleration, determined from Table 3.3.

Then, the free-field deformation is calculated by Eq 5.18:

$$\Delta_{free-field} = \gamma_s \cdot H \quad (5.18)$$

where, H is the height of the structure

Table 5.1. Ratios of ground motion at the tunnel foundation (base) level to the motion at the ground surface (Source: Power, et al. 1996).

Tunnel depth (m)	Ratio of the ground motion at tunnel foundation level to motion at the ground surface
≤ 6	1.0
6-15	0.9
15-30	0.8

Table 5.2. Ratios of peak ground velocity to peak ground acceleration at the surface in rock and soil (Source: Power, et al. 1996).

Moment Magnitude(M_w)	Ratio of peak ground velocity (cm/s) to peak ground acceleration (g)		
	Source-to-site distance (km)		
	0-20	20-50	50-100
Rock ^a			
6.5	66	76	86
7.5	96	97	109
8.5	127	140	152
Stiff Soil ^a			
6.5	94	102	109
7.5	140	127	155
8.5	180	188	193
Soft Soil			
6.5	140	132	142
7.5	208	165	201
8.5	269	244	251

Note: ^a in this table, the sediment types represent the following shear wave velocity ranges: rock ≥ 750 m/s; stiff soil 200-750 m/s; and soft soil < 200 m/s. The relationship between peak ground velocity and peak ground acceleration is less certain in soft soils.

The relative stiffness (flexibility ratio) is derived from the expressions below:

The angular distortion of a soil when subjected to shear strain is calculated by Eq 5.19:

$$\gamma_s = \frac{\tau}{G_s} = \frac{\Delta_{free-field}}{H} \quad (5.19)$$

After rearranging this equation, the shear or flexural stiffness of the tunnel element can be written as the ratio of the shear stress to a corresponding angular distortion:

$$\frac{\tau}{\gamma_s} = \frac{\tau}{(\Delta/H)} = G_s \quad (5.20)$$

A distributed force, P , is applied along the tube length to the top of the structure, acting in the transverse direction (Figure 5.4). The resulting lateral displacement, Δ , is calculated by a structural analysis program. Once the displacement, Δ , corresponding to the applied force, P , is obtained, a linear relationship between the two can be written as follows:

$$P = S_1 \cdot \Delta \quad (5.21)$$

where, S_1 is the force per length that is required to cause a unit racking deflection of the structure.

The applied shear stress can also be converted into a concentrated force, P , by multiplying it by the width of the structure (B) and its unit length, resulting in the following expression for angular distortion:

$$\gamma_s = \frac{\Delta}{H} = \frac{P}{H \cdot S_1} = \frac{\tau \cdot B \cdot 1}{H \cdot S_1} \quad (5.22)$$

Combining Eq 5.19 and Eq 5.22, the flexibility ratio of the structure can be calculated as follows:

$$\gamma_{s \text{ structure}} = \gamma_{s \text{ soil}}$$

$$\frac{\tau_{str} \cdot B \cdot 1}{H \cdot S_1} = \frac{\tau_{soil}}{G_s}$$

$$F = \frac{\tau_{soil}}{\tau_{structure}} = \frac{G_s \cdot B \cdot 1}{H \cdot S_1}$$

$$F = \frac{G_s \cdot B}{S_1 \cdot H} \quad (5.23)$$

where G_s is the shear modulus of soil, H is the height of the structure, and B is the width of the structure.

The shear modulus can be calculated as follows:

$$G_s = \rho \cdot C_s^2 \quad (5.24)$$

where ρ is the density of the saturated soil

In this expression, the unit racking stiffness is the reciprocal of the lateral racking deflection, $S_1 = 1/\Delta_1$ caused by a unit concentrated force. It can be obtained from simple static analysis of the box structure, without including the surrounding soil but under simple boundary condition, as shown in Figure 5.4 (Ostadan and Penzien 2001).

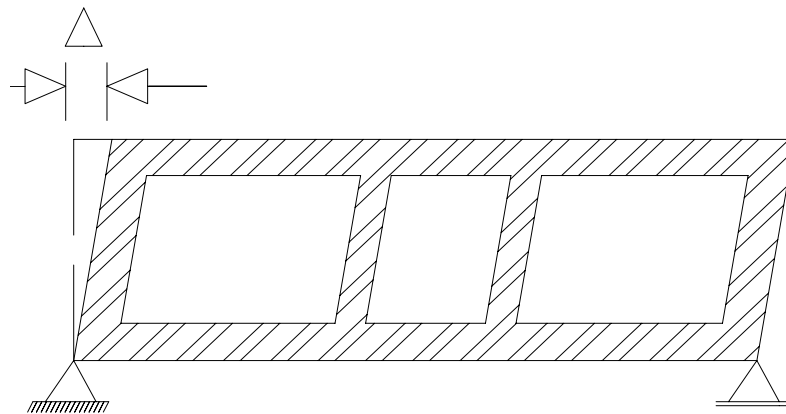


Figure 5.4. The racking deflection of the tunnel when applying unit displacement sideway (Source: Wang 1993)

The flexibility ratio gives an idea about the response of the structure and the surrounding medium (Wang 1993):

$F \rightarrow 0.0$: The structure is rigid, so it will not rack regardless of the distortion of the ground (i.e. the structure must take the entire load)

$F < 1.0$: The structure is considered stiff relative to the medium and will therefore deform less

$F = 1.0$: The structure and medium have equal stiffness, so the structure will undergo approximately free-field distortions.

$F > 1.0$: The racking distortion of the structure is amplified relative to the free field, though not because of dynamic amplification. Instead, the distortion is amplified because the medium now has a cavity, providing lower shear stiffness than non-perforated ground in the free field.

$F \rightarrow \infty$: The structure has no stiffness; soil will undergo deformations identical to the perforated ground.

Based on the flexibility ratio, the racking coefficient R defined as the normalized structure racking distortion with respect to the free-field ground distortion can be estimated from Figure 5.5.

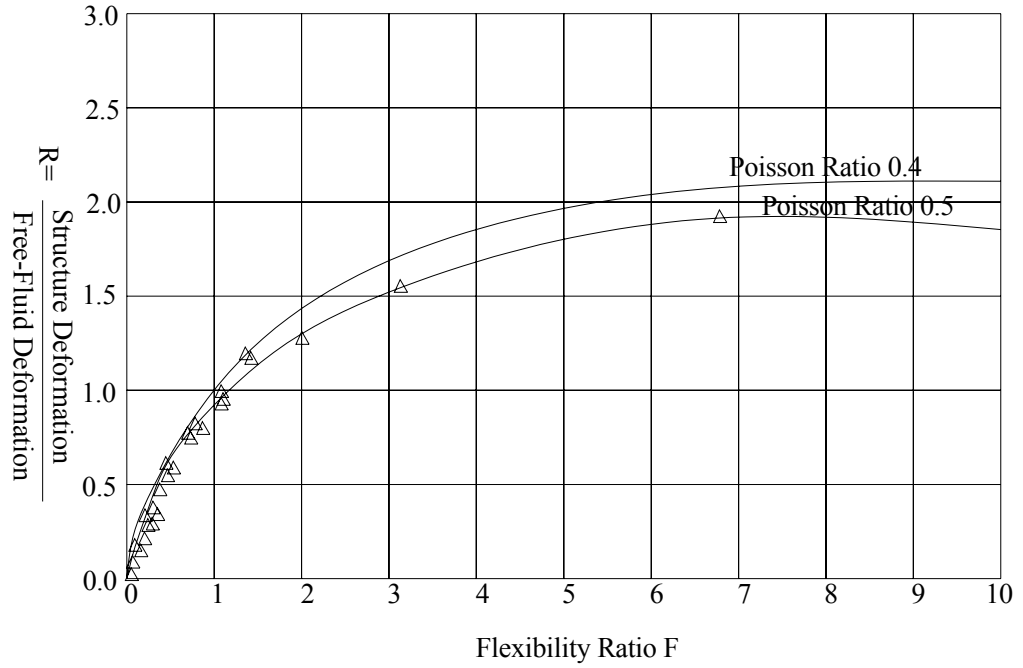
$$R = \frac{\gamma_s}{\gamma_{free-field}} = \frac{\left(\frac{\Delta_s}{H} \right)}{\left(\frac{\Delta_{free-field}}{H} \right)} = \frac{\Delta_s}{\Delta_{free-field}} \quad (5.25)$$

where, γ_s is the angular distortion of the structure, Δ_s is the lateral racking deformation of the structure, $\gamma_{free-field}$ is the shear distortion/strain of the free-field, and $\Delta_{free-field}$ is the lateral shear deformation of the free-field.

After determining the racking coefficient, the lateral racking deformation of the structure is calculated by multiplying it by the free-field deformation as below:

$$\Delta_s = R \cdot \Delta_{free-field} \quad (5.26)$$

Then, the stresses in the tunnel section are determined by performing a structural analysis with an applied racking deformation is shown in Figure 5.6.



Note: Triangular symbols: For rectangular tunnels
 Solid Lines: For circular tunnels

Figure 5.5. Normalized structure deflections, circular versus rectangular tunnels
 (Source: Wang 1993)

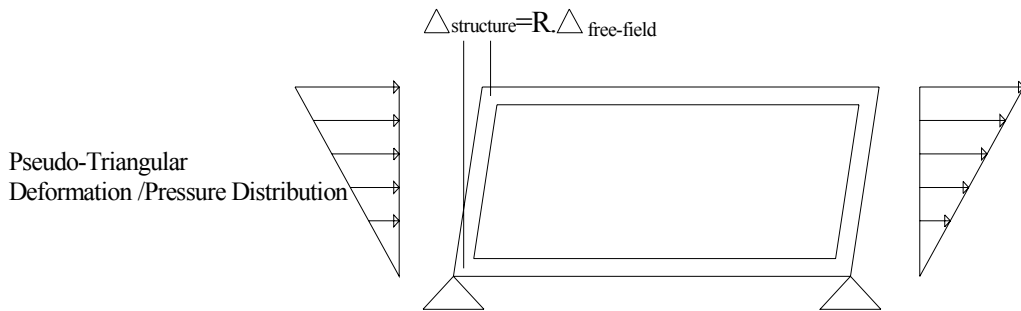


Figure 5.6. Simplified frame analysis model
 (Source: Wang 1993)

2. The Soil-Structure Interaction Approach: Both the subsoil and the surrounding medium are modeled together with the tunnel structure. The free field displacements are applied as boundary condition to the outer edges of the modeled soil

medium. The use of soil-structure interaction is highly recommended, because only a few assumptions are made in this method. Thus, a more reliable result can be expected.

5.3. Application of the Seismic Design Procedures in This Study

The axial and lateral deformations within the immersed tube tunnel, due to received seismic waves, were calculated by using the tunnel-ground interaction approach, since the seabed of the İzmir Bay is very soft. First, it was assumed that the earthquake wave is applied to the structure in longitudinal direction and the max stresses and deformations were found. These investigations were made by using both the closed form solution method (simple hand calculation) and by a numerical analysis (finite element) method. Assuming that the earthquake wave is applied to the tunnel in the horizontal direction, the max stress in the tunnel was found. This calculation was made by using both the simple frame analysis method and the soil-structure interaction approach. Then the results were compared and results that are more realistic were taken as the design values in the study.

5.3.1. Calculation of the Axial and Lateral Deformations of the Immersed Tube Tunnel due to an Expected Seismic Wave Action

In the study, it was assumed that a shear wave propagating at 45 degree (angle of incidence) to the tunnel axis would create the most critical axial strain within the tunnel structure. The effective shear wave velocity (C_s) of the ground was taken as 130 m/s. This value is based on the İzmir Metro-Stage 1 Halkapınar-Uçyol Underground Railway Project. In this design-construction project, it was considered that the shear wave velocity (C_s), of the İzmir soil changes from 130 m/s to 140 m/s (Tezcan 2007). Moreover, this (C_s) value can be calculated as follows:

$$C_s = 80.6 \cdot N^{0.331} \quad (5.27)$$

$$C_s = 80.6 \cdot 4^{0.331} = 127 \text{ m/s}$$

where, the N value was taken as 4 in Chapter 3.

Geotechnical Parameters

The effective unit mass of the submerged soil is calculated as follows:

$$\rho'_s = \rho_s - \rho_{water} = 1.600 - 1.027 = 0.573 \text{ t} / \text{m}^3 \quad (5.28)$$

where ρ_s is the density of the saturated soil and ρ_{water} is the density of sea-water.

The poison ratio of the loose silty-sand soil: $\nu_s = 0.35$

Soil deposit thickness over the rigid bedrock: $H_s = 150 \text{ m}$ (assumed as an average value between 50 m on İnciraltı side and 250 m on Çiğli side)

Earthquake Parameters for Type I (Severe) Earthquake Design

The magnitude of earthquake: $M_w = 7.5$, source to distance: 10 km

Peak ground acceleration in soil from Table 3.3: $A_s = 3.34 \text{ m} / \text{s}^2$

The peak ground particle acceleration of the soil from Table 3.3: $a_{\max} = 0.34g$

The peak particle acceleration, a_s , associated with S waves is calculated as follows:

$$a_s = 0.8 \cdot a_{\max} = 0.8 \cdot 0.34 = 0.272g \quad (5.29)$$

where the 0.8 multiplier of 0.8 is depicted from the Table 5.2.

The peak particle velocity, V_s , associated with S waves is calculated as follows:

$$V_s = \frac{208}{g} \cdot a_s = \frac{208}{g} \cdot 0.272g = 56.58 \text{ cm} / \text{s} = 0.57 \text{ m} / \text{s} \quad (5.30)$$

where the multiplier of $\frac{208}{g} \text{ cm} / \text{s}$ was depicted from the Table 5.1.

Structural Parameters

The ultimate strength of concrete C30: $f_{ck} = 30 \text{ MPa}$

Concrete Young's modulus for C30: $E_c = 32000 \text{ MPa}$

Tunnel cross section area: $A_c = 157 \text{ m}^2$

Moment of inertia: $I_c = 21761 \text{ m}^4$

Width of the tunnel: $B = 39.8 \text{ m}$

Height of the tunnel: $H = 10 \text{ m}$

5.3.1.1. Closed Form Solution Method

Using the tunnel-ground interaction procedure

1. The predominant natural period of the soil deposit, T , is estimated by Eq 5.14:

$$T = \frac{4H_s}{C_s} = \frac{4 \cdot 150}{127} = 4.72 \text{ s}$$

2. The idealized wavelength, L , is estimated by Eq 5.13:

$$L = T \cdot C_s = 4.72 \cdot 127 \cong 600 \text{ m}$$

3. The shear modulus of the soil, G_s , is calculated by Eq 5.24:

$$G_s = \rho_s \cdot C_s^2 = 0.773 \cdot 127^2 = 90632245 \text{ N/m}^2 = 91 \text{ MPa}$$

4. The equivalent spring coefficients, K_a and K_t , of the soil are calculated by Eq 5.12:

$$K_t = K_a = \frac{16\pi \cdot G_s (1 - \nu_s)}{(3 - 4\nu_s)} \cdot \frac{H}{L} = \frac{16\pi \cdot 9.1 \times 10^7 \cdot (1 - 0.35)}{(3 - 0.35)} \cdot \frac{10}{600}$$

$$K_a = K_t = 30830069 \text{ N/m}$$

5. The ground displacement amplitudes, D_a and D_b are derived from the equations below (Newmark 1968):

$$\text{For free field axial strain: } \frac{V_s}{2C_s} = \frac{2\pi D_a}{L} \quad (5.31)$$

$$\Rightarrow D_a = \frac{0.57 \cdot 600}{2 \cdot 127 \cdot 2 \cdot \pi}$$

$$D_a = 0.214 \text{ m}$$

$$\text{For free-field bending lateral: } \frac{A_s}{C_s^2} \cos^3 45^\circ = \frac{4\pi^2 D_b}{L^2} \quad (5.32)$$

$$\Rightarrow D_b = \frac{A_s \cdot L^2 \cdot \cos^3 45}{C_s^2 \cdot 4\pi^2}$$

$$D_b = 0.669 \text{ m}$$

6. Maximum axial force and the corresponding axial strain of the tunnel lining are calculated.

The maximum axial force, Q_{\max} is calculated by Eq 5.4:

$$Q_{\max} = \frac{\frac{K_a L}{2\pi}}{1 + 2 \left(\frac{K_a}{E_c A_c} \right) \left(\frac{L}{2\pi} \right)^2} D_a = \frac{\frac{30830069 \cdot 600}{2\pi}}{1 + 2 \cdot \left(\frac{30830069}{32000000000 \cdot 157.42} \right) \left(\frac{600}{2\pi} \right)^2} \cdot 0.209$$

$$Q_{\max} = 5.68 \times 10^8 \text{ N}$$

The maximum axial strain, ε_{axial} , is found from Eq 5.5:

$$\varepsilon_{axial} = \frac{Q_{\max}}{E_c \cdot A_c} = \frac{5.68 \times 10^8}{32000000000 \cdot 157.42}$$

$$\varepsilon_{axial} = 0.00011$$

7. The maximum bending moment and corresponding bending strain of the tunnel lining are calculated.

The maximum bending moment, M_{max} , by using Eq 5.6 is calculated as follows:

$$M_{max} = \frac{K_t \left(\frac{L}{2\pi} \right)^2}{1 + \left(\frac{K_t}{E_c I_c} \right) \left(\frac{L}{2\pi} \right)^4} D_b = \frac{30830069 \cdot \left(\frac{600}{2\pi} \right)^2}{1 + \left(\frac{30830069}{32000000000 \cdot 21761} \right) \left(\frac{600}{2\pi} \right)^4} 0.669$$

$$M_{max} = 4.016 \times 10^{10} \text{ Nm}$$

The maximum bending strain, $\varepsilon_{bending}$, is found from Eq 5.8:

$$\varepsilon_{bending} = \frac{M_{max}(B/2)}{E_c \cdot I_c} = \frac{5.072 \cdot 10^{10} \cdot 39.8 \cdot 0.5}{32000000000 \cdot 21761 \cdot 0.5}$$

$$\varepsilon_{bending} = 0.0011$$

8. The total strain that may develop during seismic activity is compared with the allowable strain. The max axial strain, ε_{max} , is found by Eq 5.11:

$$\varepsilon_{max} = \varepsilon_{axial} + \varepsilon_{bending} \leq \varepsilon_{allowable}$$

$$\varepsilon_{max} = 0.0013 \leq 0.002 \Rightarrow O.K.$$

9. The maximum shear force, V_d , due to the bending lateral is calculated by Eq 5.9:

$$V_d = M_{\max} \frac{2\pi}{L} = 4.016 \times 10^{10} \cdot \frac{2\pi}{600}$$

$$V_d = 4.203 \times 10^8 \text{ N}$$

10. The allowable shear force, V_{\max} , is found by Eq 5.10:

$$V_c = 0.22 \cdot f_{cd} \cdot (A_{shear}) = 0.22 \cdot 20 \cdot (157 - (0.8 \cdot 6.7 \cdot 4)) \cdot 10^6$$

$$V_c = 6.423 \times 10^8 \text{ N}$$

$V_d < V_c$, the shear force does not exceed the allowable shear resistance. Therefore, the tunnel has enough capacity to resist the shear forces.

11. The maximum bending stress, σ_{\max} , is calculated by using Eq 5.7 as follows:

$$\sigma_{\max} = \frac{M_{\max} \cdot (B/2)}{I_c} = \frac{5.072 \times 10^{10} \cdot 39.8 \cdot 0.5}{28310.1}$$

$$\sigma_{\max} = 36723562 \text{ N/m}^2 = 36.72 \text{ MPa}$$

$$\sigma_{\max} = 36.72 \text{ MPa} > f_{cd} = 20 \text{ MPa}$$

where, f_{cd} is the design compressive strength of C30 concrete.

12. The minimum bending stress, σ_{\min} , is calculated by using Eq 5.33 as follows:

$$\sigma_{\min} = \left| \frac{-M_{\min} \cdot (B/2)}{I_c} \right| \quad (5.33)$$

$$\sigma_{\min} = 36.72 \text{ MPa} \quad (\text{in tension})$$

Note that (-) sign denotes tensional stress in the tunnel concrete.

$$|\sigma_{\min}| \gg f_{ctd} = 1.27 \text{ MPa}$$

where f_{ctd} is the design tensile strength of C30 concrete.

The concrete has not enough capacity to resist the bending stress occurring during the seismic activity. Therefore, the internal forces must be relieved which can be accomplished by increasing the flexibility of the structure. Section 5.4 discusses the seismic analysis after rubber (or neoprene) joints are introduced in between two adjacent tube unit.

5.3.1.2. Numeric Analysis Method (Finite Element Method)

In this study, the preferred method is the finite element analysis procedure which is implemented by using SAP 2000, a structural analysis program.

The analysis of the tunnel was performed at a selected mid-route location for a part of 1800 m, of the tunnel which corresponds to three-wave length of the seismic motion of the soil. A tube unit in 100 m length is divided into 90-cube elements. The model contains 1926 solid elements and 3456 joints. Since the seabed soil is very loose, in order to represent the soil-structure interaction, the soil is modelled as well. The seabed soil is represented by a solid surface springs in SAP 2000. In order to represent flexibility of the system, elastomeric joints are introduced between two adjacent tube units. The modulus of elasticity of the elastomeric material used in the model is 3 MPa, its poisson ratio is 0.49, and the length of each elastomeric joint is 0.5 m.

The seismic design loads imposed on the tunnel is defined as displacements. In other words, the earthquake loads for underground structures are represented in terms of deformations and strains applied on such structure by the surrounding medium (Hashash, et al. 2001). Turkey, on the other hand, has no code/standards for design and construction of tunnels and for immersed tube tunnels in particular as of today. Thus, the analysis of the system was conducted as an equivalent static analysis and the design was made for loading condition used in the Far Eastern Projects and defined as below (Egeli 1996, and Taiwan High Speed Railway Project 2003):

$$1DL + 1LL + 1EU \quad (5.34)$$

where DL is the dead load coming from the self weight of the structure, including material layer and the weight of the water layer above the tube. LL is the live load coming from the traffic loads and EU is the earthquake displacements (amplitude of the wave) due to the shear wave. They can be calculated by the formula below:

$$y_i = D \cdot (\cos a) \cdot \sin\left(2\pi \cdot \frac{x_i}{(L/\cos a)}\right) \quad (5.35)$$

where D is the amplitude of the wave, a is the angle of the shear wave with respect to the tunnel longitudinal axis, L is the length of the shear wave and x is the distance. In this equation, it was assumed that the amplitude of the shear wave is 1 m because. It is well known that a maximum probable amplitude value of any shear wave is assumed as 1 unit. The amplitudes D_a and D_b of the shear wave of the İzmir Bay was calculated as 0.214m and 0.669 m. Since, the calculations are made considering worst case scenario, in this study the amplitude of the shear wave is taken as 1 m. and the angle of the incidence is 45 degrees. The shear wave is imposed on the structure as shown in Figure 5.3. Since underground structures are constrained by surrounding medium and they move together with the ground, the motion of the shear wave is the same with the tunnel motion during an earthquake. In order to define the motion of the tunnel during an earthquake, the calculated coordinates in Eq 5.35 are imposed on the each node of the model in SAP2000 in lateral direction.

First, the analysis was made for the present situation of the seabed soil of the İzmir Bay. The used modulus of subgrade reaction (k_s) value was taken as 174500 N/m³ (See Section 4.1.3). As a result of the analysis, the max compressive stress in longitudinal direction was found as 21x10⁶ N/m² (21 MPa). It develops on the outer walls and the top corners of the tunnel, while in lateral direction, the max compressive stress was found as 45.5 MPa and it develops on the inner walls of the tunnel. The deformation of the structure during an earthquake is shown in Figure 5.7. The analysis results are shown in Figures 5.8 and 5.9.

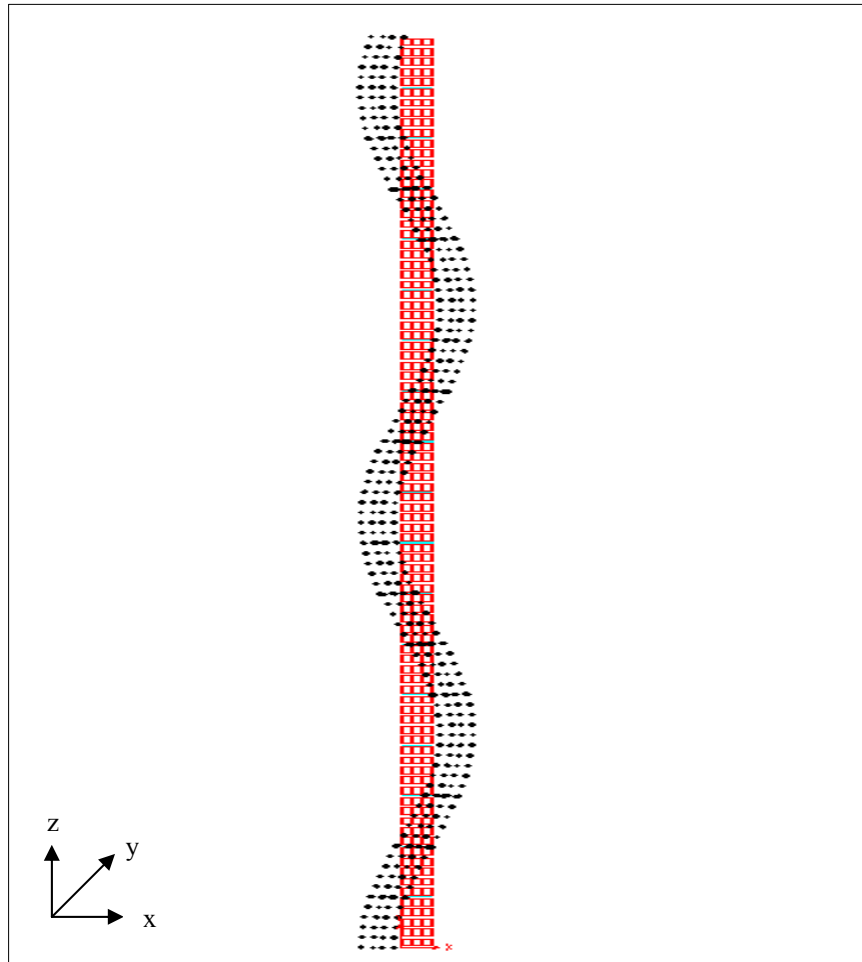


Figure 5.7. The deformation of the tube unit during an earthquake.

The analysis shows that the max stress is higher than the design compressive strength of the concrete (as the used concrete material is C30, $f_{cd}=20$ MPa). To eliminate this drawback, ground improvement should be applied to the seabed soil. Assuming that ground improvement was made and the min SPT_N value rises to 35 after the ground improvement, the new (k_s) of the soil is calculated as 5600144 N/m³. Then, a new analysis was made in SAP2000 by using the same model. As a result of this analysis, the max compressive stress on the tunnel in both longitudinal direction and lateral direction was decreased to 19.6×10^6 N/m² (19.6 MPa). It is less than the compressive strength of the C30 concrete. However, the opposite face of the tunnel is subjected to a tensile stress of the same magnitude (19.6 MPa). This value is considerably larger than the tensile strength of the concrete (for C30 $f_{ctd}=1.25$ MPa). In

order to strengthen the structure against tensile stresses, prestressed concrete can be used (Akan and Özen 2005). The analysis results obtained after ground improvement are shown in Figures 5.10 and 5.11.

The earthquake design of the tunnel was made by making quastatic analysis in SAP 2000. In order to apply the SAP2000 modeling procedures, 4 noded solid element was used and the soil fixed from x, y, and r_z (rotation in z dir) axis. Therefore, conservative stress values were found at the end of analysis. However, the tunnel is moved together with the surrounding soil during an earthquake, thus the stresses in lateral direction might be dramatically less than the finding. In addition, since the elastomer joints are were used, it is probable that less stresses develop on the tubes in both lateral and longitudinal direction during a seismic motion. Therefore, it is suggested that in design phase detailed earthquake analysis of the tunnel was made to obtain results that are more realistic.

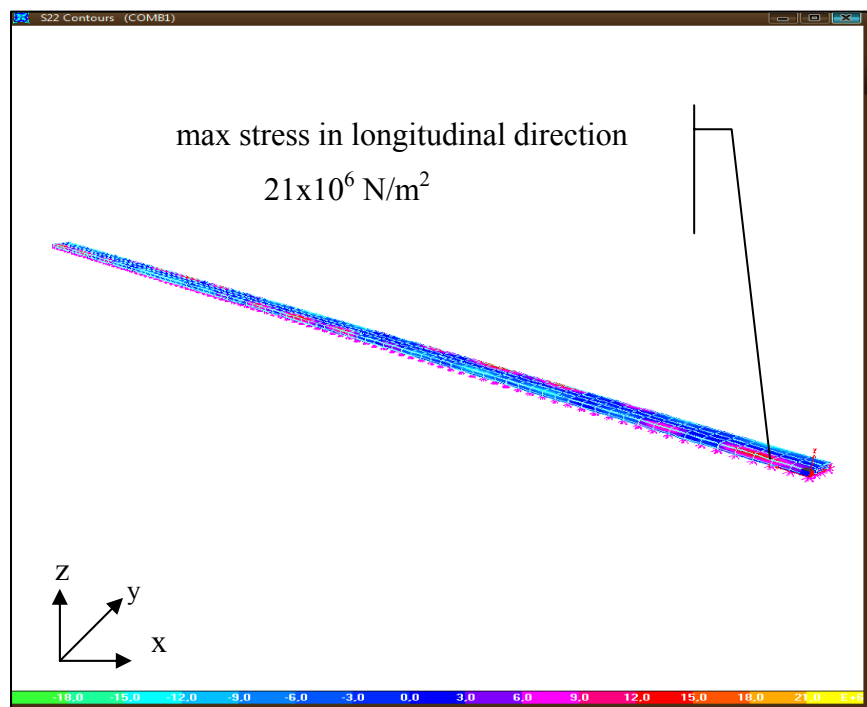


Figure 5.8. Max compressive stress on the tube in longitudinal direction (before ground improvement)

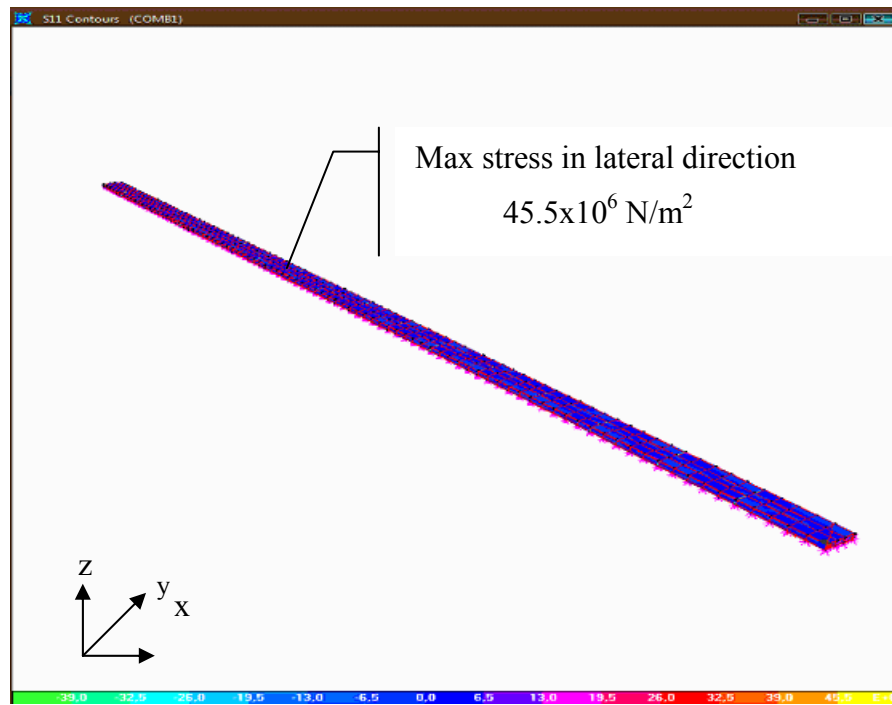


Figure 5.9. Max compressive stress on the tube in lateral direction (before ground improvement)

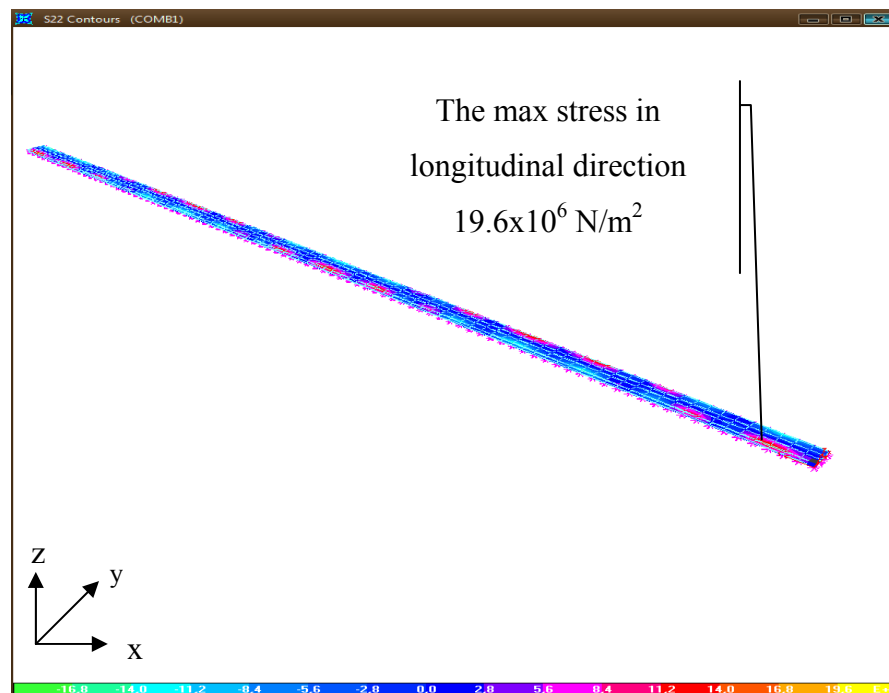


Figure 5.10. Max stress on the tube in longitudinal direction (after ground improvement)

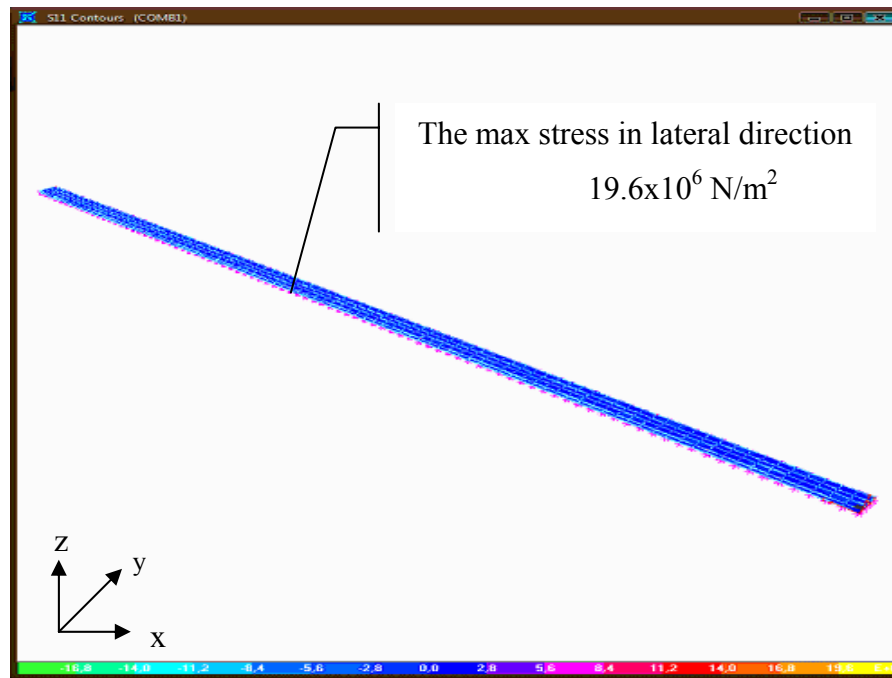


Figure 5.11. Max stress on the tube in lateral direction (after ground improvement)

It should be noted that to be economic, the min SPT_N value of the seabed soil should be increased to 35 from the base of the tunnel to a depth of $0.75 \times B$ ($0.75 \times 39.8 = 30\text{ m}$) depth. (Egeli, et al. 1983). As this is a large width structure where about 90% of the stress distribution within the seabed soil's occurs within this depth. After this point, SPT_N=15 is enough until $F.S. \times B$ ($1.25 \times 39.8 \cong 50\text{ m}$) depth. In this equation, $F.S$ denotes the safety factor, which is taken as 1.25 (Egeli 1996). Furthermore, it should be noted in here that, before placing the tube units to the seabed soil the SPT values should be verified by an independent and experienced ground improvement sub consultant authorized by the ultimate owner or the BOT operator of the structure.

5.3.2. Calculation of Racking Deformation and Stresses of the Immersed Tube Unit due to an Expected Seismic Wave Action

In this study, the racking deformation of the tube unit was calculated by using both a simple frame analysis model, and a soil-structure interaction approach. The results of the two different methods are tabulated for comparison.

5.3.2.1 Simple Frame Analysis Model:

First, the angular distortion of the soil is calculated by Eq 5.15:

$$\gamma_s = \frac{V_s}{C_s} = \frac{0.57}{127} = 0.0045$$

The free-field racking deformation is calculated by Eq 5.18

$$\Delta_{free-field} = \gamma_s \cdot H = 0.0045 \times 10 = 0.045 m$$

The shear modulus of soil is calculated by Eq 5.24

$$G_s = \rho_s \cdot C_s^2 = 0.573 \cdot 127^2 = 90632245 N / m^2 = 91 MPa$$

The following step is to calculate the force/length per unit displacement, which is a requirement that causes a unit racking displacement of 1 m. This is accomplished by modeling a 20 m segment of the tube. The reason why a length of 20 m was used here is that hour glassing occurred. There was no problem, however, in the results by using 20 noded brick elements over the full length of the model. At the end, the total model consisted of 18 elements (for the 20 m segment).

S_1 is calculated by Eq. 5.21:

$$S_1 = P / \Delta = (8.21 \times 10^9 / 20) / (1) = 4.11 \times 10^8 N / m^2$$

In the equation above, 20 is the length in meters of the length of the tube segment and 1 is the unit deformation in meters. The deflected shape of the tunnel is shown in Figure 5.12, and the force variable on the tube unit is illustrated in Figure 5.13.

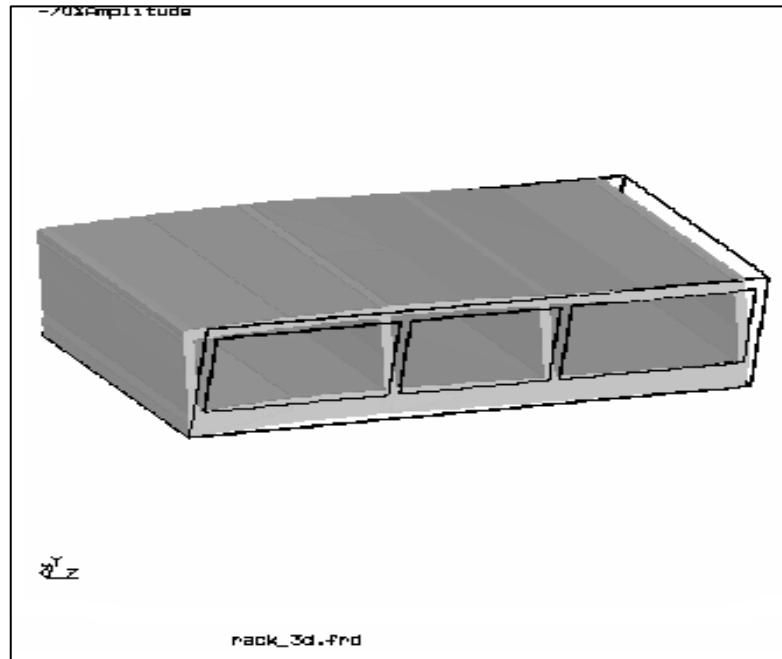


Figure 5.12. The deformation of the tube unit after applying unit-racking deflection.

The flexibility ratio is calculated by Eq 5.19:

$$F = \frac{G_s B}{S_1 H} = \frac{90632245 \times 39.8}{4.11 \cdot 10^8 \times 10} = 0.88$$

Since, the flexibility ratio is less than one; the structure is stiffer than the medium and it will not deform as much as the soil.

According to the flexibility ratio, the racking coefficient is determined from Figure 5.5.

For $F=0.88$, the racking coefficient is equal to 0.9

The racking deflection is determined by Eq 5.22:

$$\Delta_s = R \cdot \Delta_{free-field} = 0.9 \times 0.045 = 0.04 \text{ m}$$

This means that the racking deformation causes the top of the tube to deflect 0.04 m.

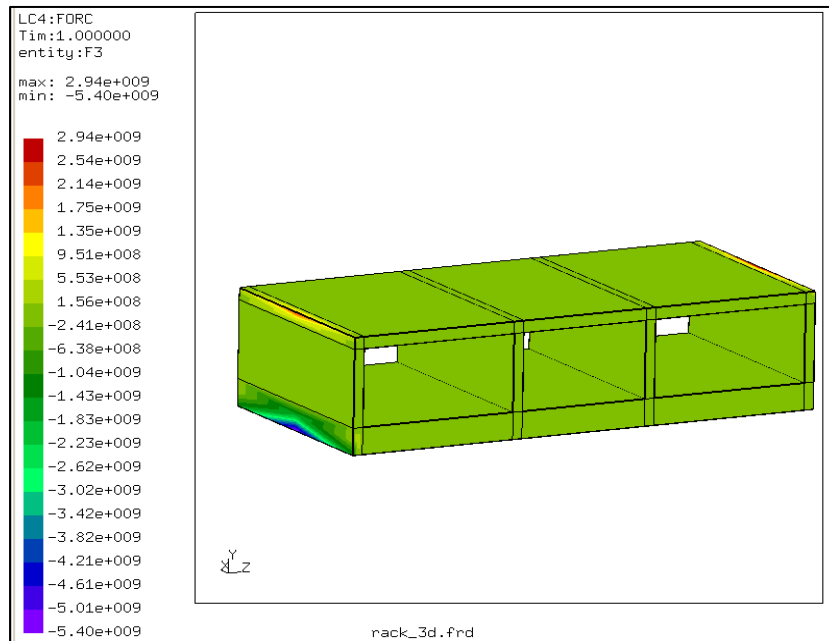


Figure 5.13. Force averaging on the tube unit after applying unit deflection in lateral direction

This deflection varies linearly over the height of the structure with no deformation at the base and the max occurs at the top. The resulting stress is found as $9.64 \times 10^6 \text{ N/m}^2$ and it develops upper right-hand corner of the tube. The analysis results are illustrated in Figures 5.14 and 5.15.

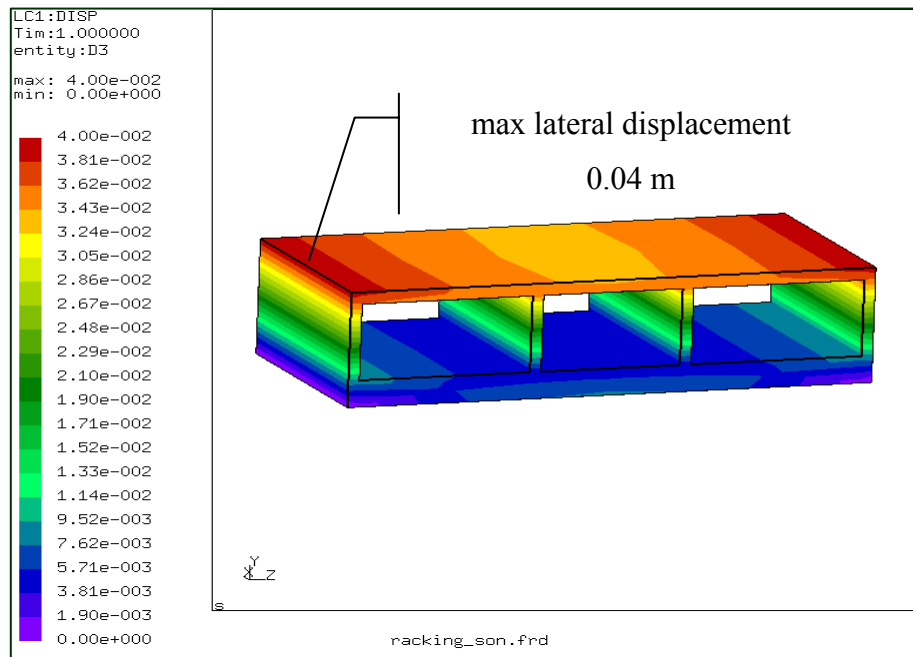


Figure 5.14. Maximum racking deflection of the tube unit according to the simple frame analysis model

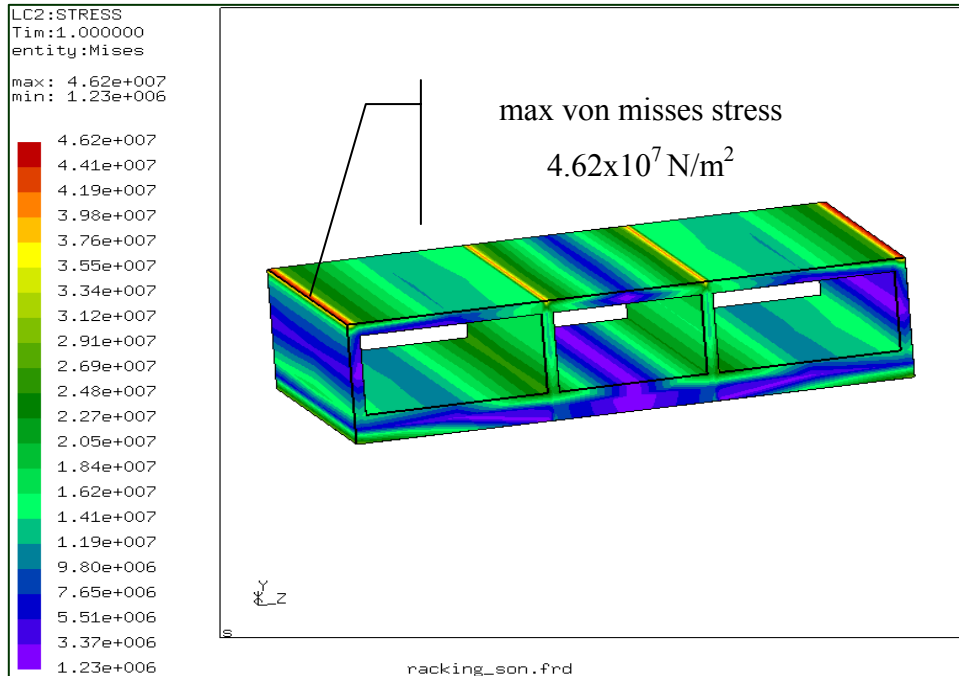


Figure 5.15. Maximum Von Misses stress of the tube unit according to simple frame analysis model

5.3.2.2. Soil-Structure Interaction Approach

In this approach, a finite element is constructed. The model consists of a 20 m segment in length of the tube tunnel together with the rock fill at the sides. Quadratic hexagonal and wedge elements are used to represent the tube and the rocks. The soil, on the other hand, is modeled by linear axial springs. The spring constants were calculated by multiplying the modulus of subgrade reaction, k_s , with the elements face area, and a model weighting factor (see Section 4.1.4 for the calculation of spring constants underneath a hexagonal element).

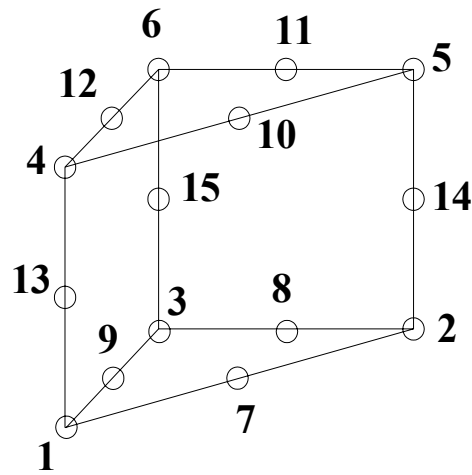


Figure 5.16. Fifteen noded wedge element in Calculix
(Source: Calculix 1.7 2007)

The racking analysis is performed by applying the free-field deformation to the outer spring ends. Zero displacement is applied to the depth of 10 m, and $\Delta_{free-field} = 0.045 m$ is applied at the top level of the tube. By using this soil-structure interaction approach, it was calculated that the tubes top surface is displaced by 0.0004 m which causes a Von Misses stress of only 3.37 MPa at the top of the tube. The analysis results are shown in Figures 5.17 and 5.18.

As it is seen, the results from the simple frame analysis model are much more conservative than the soil structure interaction approach. This is likely due to the fact that the simple frame analysis, as the name implies, is simpler and also it is based on a

number of assumptions (See Table 5.3 for the results). It is well known that whenever two or more elastic bodies interact with each other an analysis based on the finite element or finite difference method must be used. Since the tube structure, the side fill, and the soil are different elastic materials, it can be concluded that the soil-structure interaction result represents the real solution of the racking problem.

Table 5.3. Racking analysis results

Racking Analysis Results	Simplified Frame Analysis Model	Soil-Structure Interaction Approach
max lateral displacement (m)	0.04	0.0004
max von mises stress (N/m ²)	4.62x10 ⁷	3.37x10 ⁶

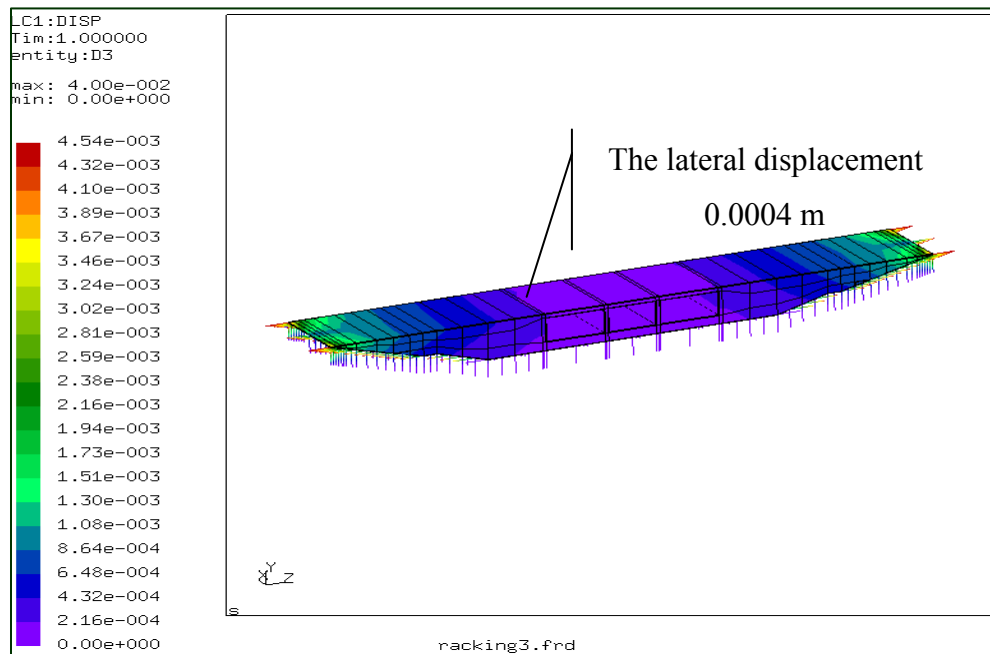


Figure 5.17. Racking deflection of the tube unit according to the soil-structure interaction approach

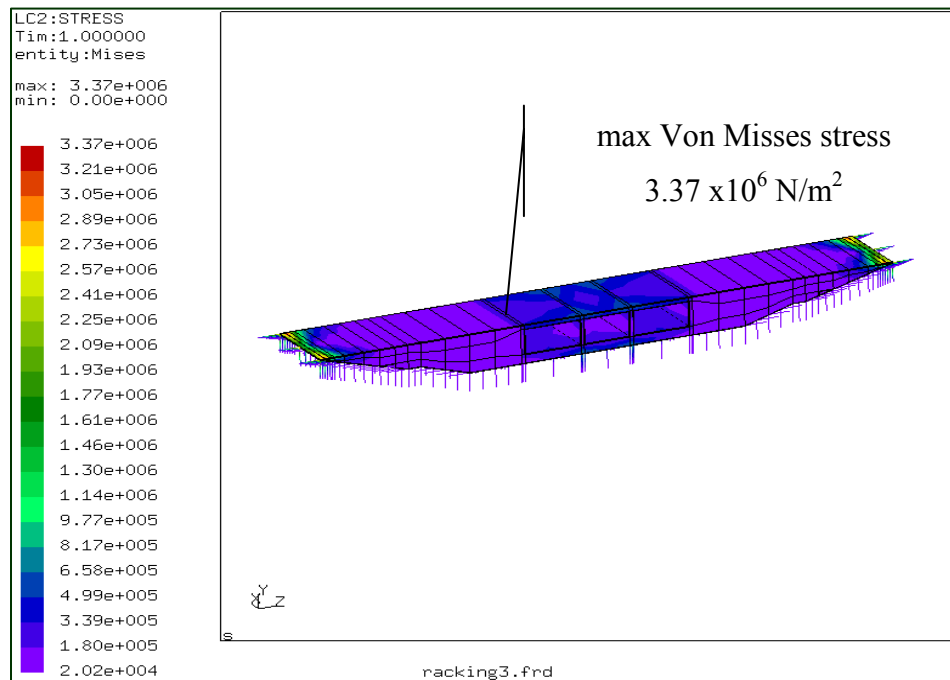


Figure 5.18. Von misses stress of the tube unit according to simple frame analysis model

5.4. Seismic Design Issues

The analysis in Section 5.3.1.1 concludes that high stresses develop in the tunnel, if all tube units are rigidly interconnected. These stresses can be relieved if elastomer joints are used in between two adjacent tube units. In addition, the tube tunnel should be made impermeable against water leakage. Hence, flexible joint is recommended for that reason too (Akimoto, et al. 2002).

Two different joint types are used to connect the adjacent tubes to each other:

a) Conventional Flexible Joint: This type of joint consists of rubber gasket and connection cables. The cables and gaskets carry tensile and compression forces respectively at joint parts. The cable-rubber gasket type flexible joint (conventional flexible joint) which has been especially used for immersed tube tunnels in Japan is shown in Figure 5.19. Due to possible lateral displacements of the tunnel, large openings can occur between two adjacent tube units. If large openings occur, they deteriorate the dewatering performance of the joints. Since, this type of joint cannot

provide the dewatering activity between the tunnel elements; a highly flexible joint is needed to absorb such large displacements (Kiyomiya, et al. 2004).

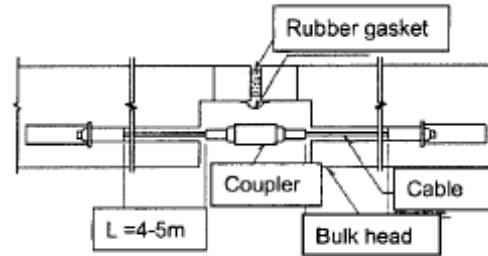


Figure 5.19. Conventional type flexible joint
(Source: Kiyomiya, et al. 2004)

b) Crown Seal Flexible Joint: This type of joint, which consists of a rubber block, installed at the outside of the bulkhead and flanges connected to the rubber block and fixed to an attachment plate, is a kind of pin structure. This type of joint shows excellent performance to absorb the possibly resulting large openings, displacements, and stresses induced by any seismic effect and by any differential settlement between the tunnel units. (Kiyomiya, et al. 2004)

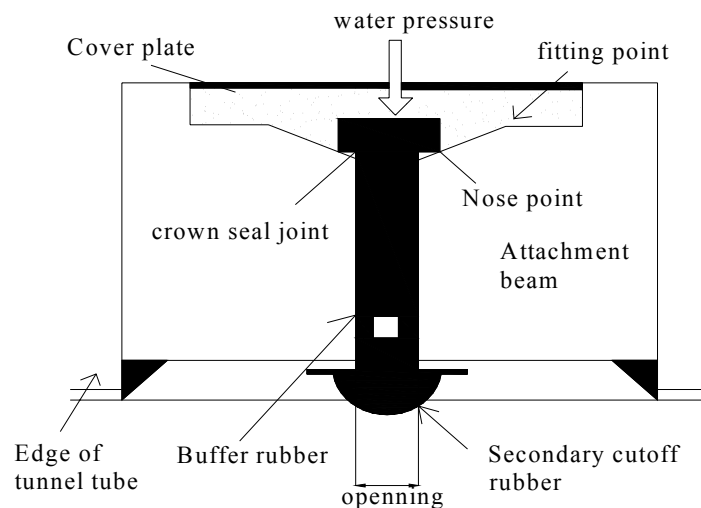


Figure 5.20. Crown seal flexible joint
(Source: Akimoto 2002)

5.5. Calculation of Longitudinal Movement between the Two Immersed Tube Units during an Earthquake

The tube tunnels cannot be rigidly interconnected, because the internal stresses may rise to such levels that cause structural failure during an earthquake. Therefore, it was suggested to use flexible joints, which introduce flexibility, and thus reducing the internal stresses.

The seismic shear waves cause the joints to be compressed in one side of the tube, and to be extended on the other side. This applies to the right-left, and the top-bottom sides of the tube interconnections, depending on the seismic wave's direction and properties. The top-bottom displacements are less important compared to the right-left ones, because the tube height is smaller than its width.

The amount of extension and compression for these joints are investigated in this section for a design specification. In this particular problem, the interconnection of the adjacent two units at the maximum lateral are considered (units 36 and 37). Figure 5.21 shows an exaggerated layout of these units.

The calculation can be made based on the geometry in Figure 5.21. The y_1 , y_2 , and y_3 values are the amplitudes of the earthquake wave at x_1 , x_2 , and x_3 distances and they are calculated by Eq 5.33. In addition, θ_1 , θ_3 are the angles between the units and the tube tunnel alignment, and θ_2 is the angle in between the two tube units.

The coordinates x_1 , x_2 , and x_3 in Figure 5.21 correspond to 3500th (i.e. station 3+500 km), 3600th, and 3700th meters of the immersed tube tunnel.

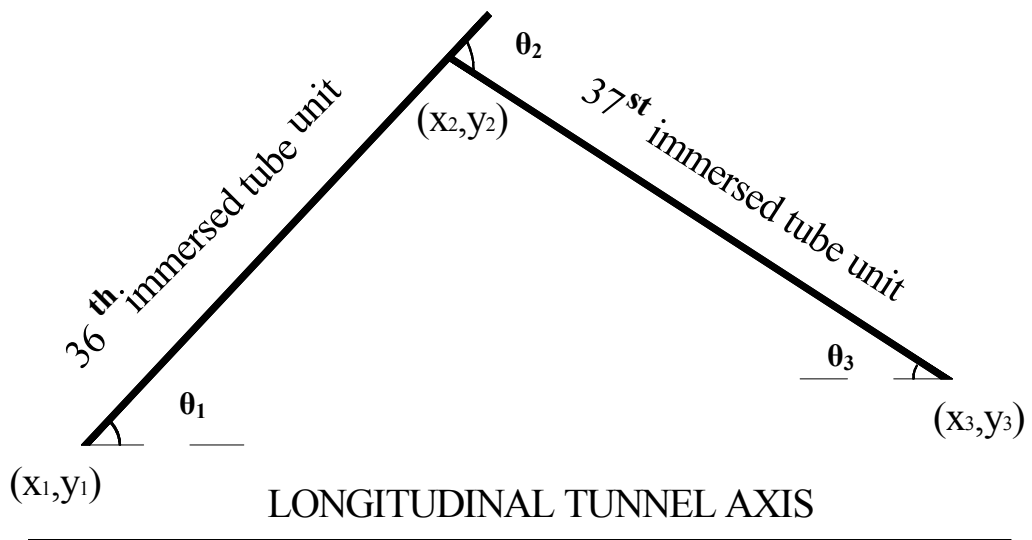
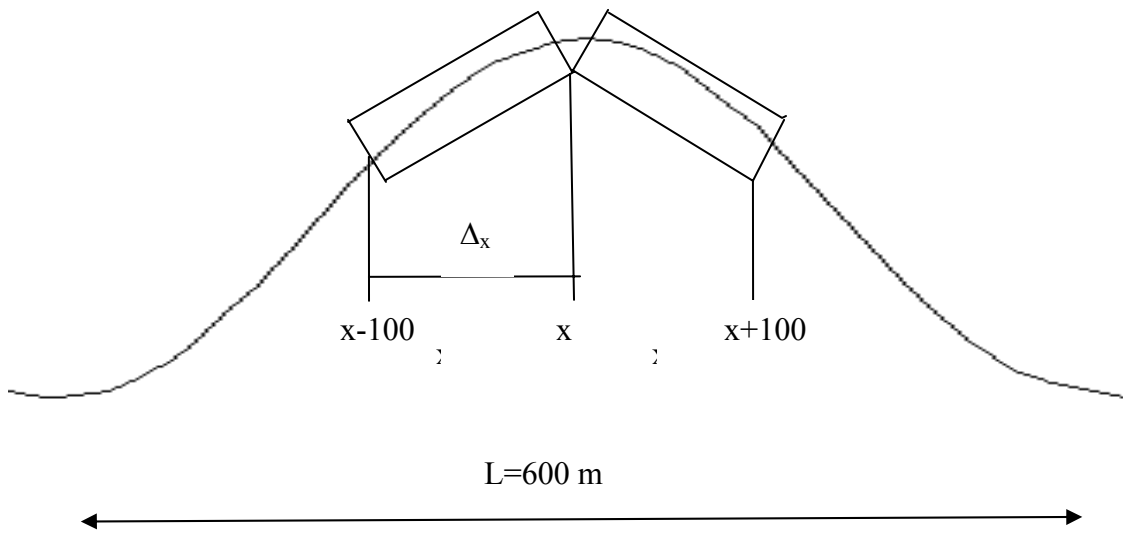


Figure 5.21. The shape of the immersed tube unit during an earthquake

This means that, the 3500th m. of the immersed tube tunnel is displaced by 0.499 m from the neutral axis during the earthquake ($M_w=7.5$).

$$y_2 = 1 \cdot (\cos 45) \cdot \sin\left(2\pi \cdot \frac{3600}{(600 / \cos 45)}\right)$$

$$y_2 = 0.706 \text{ m}$$

This indicates that, the 3600th m. of the immersed tube tunnel is displaced by 0.706 m from the neutral axis during the design earthquake ($M_w=7.5$).

$$y_3 = 1 \cdot (\cos 45) \cdot \sin\left(2\pi \cdot \frac{3700}{(600 / \cos 45)}\right)$$

$$y_3 = 0.543 \text{ m}$$

This shows that, the 3700th m. of the immersed tube tunnel is displaced by 0.543 m from neutral axis during the design earthquake.

In order to calculate the corresponding distortion angles of θ_1 , θ_2 , and θ_3 , the following relationships are used.

$$\tan \theta_1 = \frac{y_2 - y_1}{x_2 - x_1} \quad (5.36)$$

$$\tan \theta_1 = 0.002 \rightarrow \theta_1 = 0.002$$

$$\tan \theta_3 = \frac{y_3 - y_2}{x_3 - x_2} \quad (5.37)$$

$$\tan \theta_3 = -0.0016 \rightarrow \theta_3 = -0.0016$$

The angular rotation between the two adjacent immersed tube units is equal to θ_2 . The opening value (the movement of the tube unit in the longitudinal direction) can be calculated by multiplying the tangent of θ_2 by the structure width.

$$\Delta_{opening} = \tan \theta_2 \cdot W \quad (5.39)$$

$$\theta_2 = \theta_3 + \theta_1 \quad (5.5.4)$$

$$\theta_2 = 0.002 + 0.0016 = 0.0036$$

$$\Delta_{opening} = \tan(0.0036) \cdot 39.8$$

$$\Delta_{opening} = 0.14 \text{ m}$$

The longitudinal movement between the 36th and 37th tube units of the immersed tube tunnel is found as 14 cm for the design ground motion. For instance, the axial and shear displacement of the tube units of the Osaka Port's Yumeshima Immersed Tube Tunnel had been investigated in a study, by using both experimental method and the numerical method during a seismic event. As a result of the study, it was found that the displacement (opening) of the tube unit changes between 0 to 300 mm in the longitudinal (axial) direction. Then, it was confirmed that these opening values are tolerable displacement values and they do not bring about any water leakage during an earthquake (Kiyomiya, et. al. 2004). Therefore, in order to confirm that the tunnel is safe against the water leakage and intolerable movements at the time of the designed seismic action, it should be checked that whether the found displacement (opening) values calculated for this IBITT are less than the acceptable limits. Also, using the max moment and shear values occurring due to the design earthquake ($M_w=7.5$) both in racking (transverse) and longitudinal direction, concrete crack width checks should be done to see if they are tolerable and cause no water leakage. As there is no standard procedure for this check for immersed tube tunnels in Turkey, similar procedure used in the Far East can be used (Egeli 1996).

CHAPTER 6

GROUND IMPROVEMENT ALONG THE TUNNEL ALIGNMENT

6.1. Ground Improvement

The soil along the tunnel route is very loose and does not enough capacity to carry the imposed loads due to the tunnel construction. In other words, soil may undergo large elastic settlements. In such a case, it is necessary to improve the technical properties of in situ-soil.

To improve the soil, several techniques are available at the present time. However, choosing of any ground improvement technique depends on the aim of the ground improvement and the soil type. For instance, since the rock layer has been found at about 250 m. depth near the Çiğli side, deep foundation technique types (bored piles socketed into bedrock, friction piles or fibrex piles, and pre-cast piles types friction piles), ground improvement methods are not applicable for treatment of the tunnel ground. It is known that precast or vibrex type friction displacement piles in Çiğli side and Mavişehir sides built in 1980's continue to settle substantially (Egeli and Pulat 2008) and hence they cannot be considered as reliable foundations in such very deep and very loose sub-soils. Other vibration techniques such as vibropacement (stone columns), vibro piles, vibro compaction, and vibro-concrete columns unsuitable for treatment of the tunnel route subsoil also. Because these methods are suitable to treat the soil, only up to max 35 m depth from the seabed level.

Grouting which is an alternative ground improvement method can be used for both rock and soil. Its principle is the injection of liquid materials under pressure into a soil or rock to change its engineering properties. The following properties can be improved by the grouting process:

1. Shear strength can be increased.
2. Compressibility, permeability, and liquefaction risk can be reduced.
3. Swelling and shrinking can be controlled.

4. Durability can be extended.

There are four types of grouting methods:

1. Chemical (Permeation) Grouting
2. Slurry (Intrusion) Grouting
3. Jet (Replacement) Grouting
4. Compaction (Displacement) Grouting

6.1.1 Grouting Types

1. Chemical Grouting; is done by the injection of a chemically permeable material that has low viscosity into sandy soil or rock under low pressure. This method is mostly used for the purpose of controlling water flow and producing sandstone like masses to carry the imposed loads. As this method is applied under low pressure, engineering properties of the soil do not change and only its mechanical properties can change, such as its permeability and porosity. The chemical grouting process is illustrated in Figures 6.1. and 6.2.

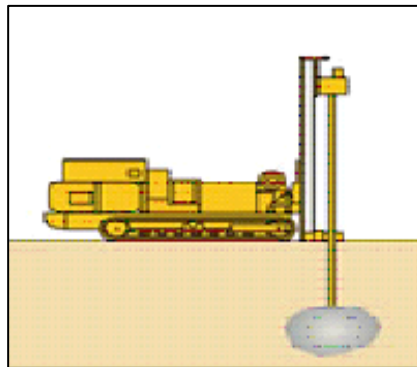
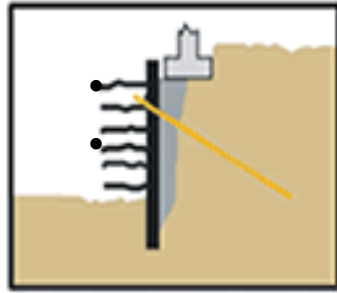
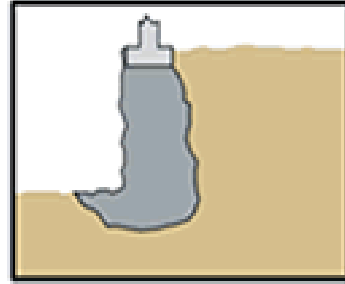


Figure 6.1. Chemical grouting process
(Source: Hayward Baker 2008)

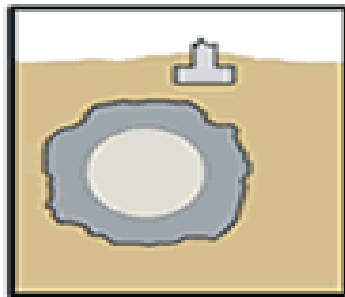
The chemical (permeation) grouting applications are shown below:



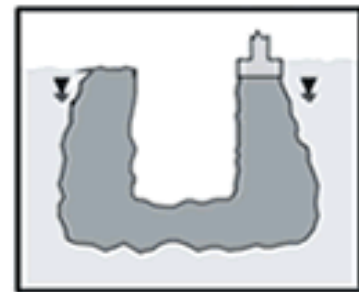
a) For lagging operation



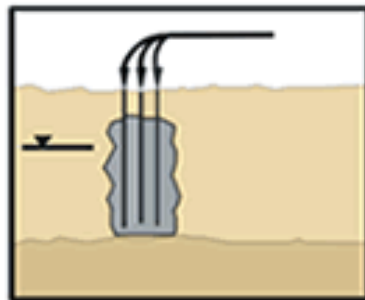
b) Support of footing



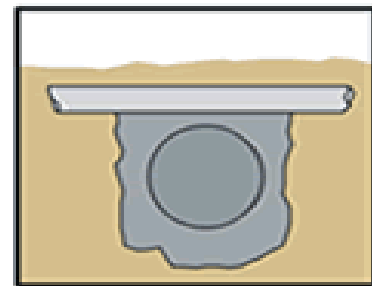
c) Grouted tunnel support



d) Pit excavation below water



d) Grouted cut-off wall



e) Grouted pipeline support

Figure 6.2. Chemical grouting applications

(Source: Hayward Baker 2008)

2. Slurry Grouting; (also called cement grouting) is done by intrusion of a low viscosity, flowable particulate grout into voids and cracks in a soil, under high pressure. This grouting is not possible for most of the tunnel-route soils, as $N^{(*)}$ (corrected)

values are less than 11. The application process of the slurry grouting process is illustrated in Figure 6.3.

$$N = \frac{D_{15}(\text{soil})}{D_{85}(\text{grout})}$$

where D is the grain size.

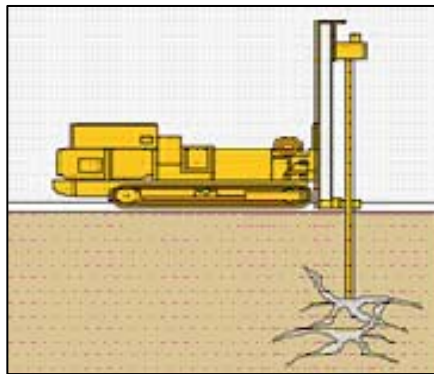


Figure 6.3. Slurry grouting process
(Source: Hayward Baker 2008)

Typical slurry (cement) grouting applications are:

- Rock foundation treatment of a dam site
- Rock cut-off curtains
- Pressure injected anchors
- Stabilization of gravels and shotcreted rock

3. Jet Grouting; is a versatile ground modification system used to create in-situ, cemented formations of soils, called soilcrete. To form soilcrete, the injection pipe is inserted into the soil at a desired depth. Then the soil is being subjected to a horizontal high-pressure air water jet, at the same time the soil is mixed with grout, so the engineering properties of the soil are improved. The most important advantage of this method is that it can be applied to all soil types. The jet grouting process was shown in Figure 6.4.

Jet grouting applications are:

- Control of underground fluids
- Excavation of unstable soil

Increase the bearing capacity of soil

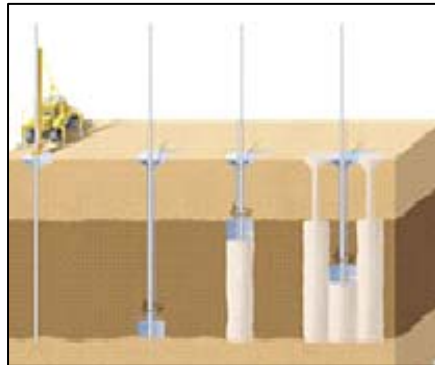


Figure 6.4. Jet grouting process
(Source: Hayward Baker 2008)

4. Compaction Grouting; is done by injection of a very viscous (low-mobility), aggregate grout under high pressure to displace and compact the surrounding soil. This method can be used in any type of soil and underwater, but mostly preferred in soils finer than the medium sands. One of the most important advantages is that, its maximum effect is obtained in the weakest soil zones. The compaction grouting process is shown in Figure 6.5.

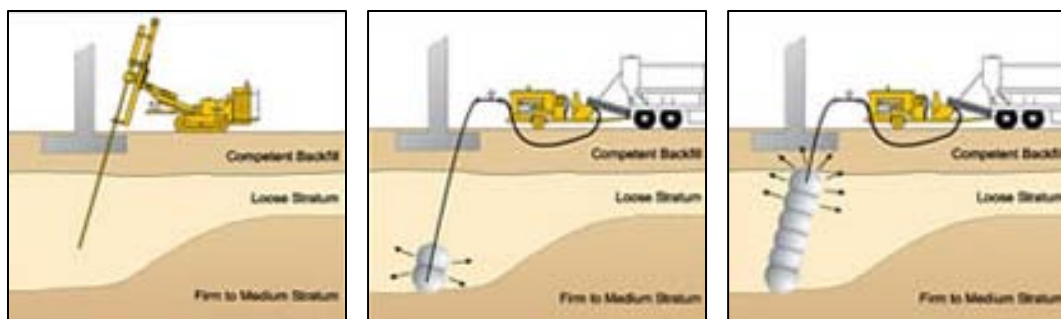


Figure 6.5. Compaction Grouting Process
(Source: Hayward Baker 2008)

Compaction grouting applications:

- Densification of soil before construction
- Prevention of settlement in tunneling through soft ground
- Provide underpinning of structures
- Strengthen the supporting ground
- Increase the bearing capacity of the founding soils

Decreasing the liquefaction risk of subsoils.

6.2. Encountered Soil Issues of the İzmir Bay

The İzmir Bay seabed consists of very loose to loose silty sands/sandy silts (as understood from the available 3 borehole data obtained from the DLH) with very low SPT-N penetration values. Especially, near the Çiğli side, the soil is like a deep swamp and the penetration values are less than 2. This is why, the soil does not have allowable bearing capacity to bear the loads transferred to it and causing very large and intolerable total and differential settlements, underneath the tunnel base. Moreover, the existing limited subsoil data also shows that the İzmir Bay soil along the IBITT route has high liquefaction risk, particularly near the Çiğli side. Consequently, it is required to apply a ground improvement process at the site along the tunnel alignment.

The reasons to make ground improvement are;

- Increase the bearing capacity
- Strengthen the shear strength of the ground
- Decreasing the liquefaction risk
- Decreasing the intolerable settlement

6.2.1 Which Method should be used?

The preferred method for the İzmir Bay is ‘compaction grouting’ type ground improvement method by virtue of being the most appropriate method, in order to treat the problems of the seabed soil of İzmir Bay. If four methods are compared, the reason to choose this method can be understood as below;

Chemical grouting treats the soils’ mechanical properties, such as permeability and porosity, but it has no effect on the engineering properties of a soil, because of

being applied under low pressure. However, the grouting is necessary to improve the shear strength and settlement properties of the tunnel seabed, as total settlements in excess of 2.5 cm (25 mm) underneath the tunnel (ie. at the tunnel foundation level) can't be tolerated.

Although the slurry method is applied under a high pressure, it is suitable for rocks and gravels, whose N -values are bigger than 11, but not for loose soils. Though jet grouting can be used for most soil types, it's actually not an injection method, but a kind of mixer technique. Jet grouting mostly used to prevent excessive settlements beneath the foundations of columns or to form an impermeable barrier against water leakage for tunnels. In addition, it is still a controversial subject that whether this method decreases the liquefaction risk of the soil. On top of that, the methods explained above are not appropriate for using underwater. However, the compaction grouting is especially used for large areas, including the underwater structures, by virtue of being a displacement method, it also compacts the soil by displacing it. Because this method leads to further compaction of the surrounding soil, the engineering properties of the soil are also improved. Moreover, it is preferred for liquefiable soils, in order to diminish this drawback.

Consequently, when all the ground improvement methods are compared, it can be understood that compaction grouting is the most proper one, in order to meet the needs of the seabed soils along the tunnel alignment. In addition, if it is investigated, it can be realized that compaction grouting is a most preferred improvement method for immersed tube tunnels in the world as well as in the Marmaray Project of our country. It should be noted that when doing compaction grouting type ground improvement, the seabed soil area to be treated should be 5 m larger on either side of tunnel base. (i.e $39.8\text{ m} + 2 \times 5 = 50\text{ m}$) due to the stress bulb extension at depth beneath the tunnel foundation level. This also helps to reduce further bearing capacity/shear failure problems at the edges of the tunnel base.

6.3. New Situation of the Seabed Soil after Ground Improvement

It is a good practice that, a 0.3 m thick sandlayer is placed under the tunnel to distribute the loads evenly. The region that the ground improvement will be done, is the depth between beneath the sand bed and the 50 m depth soil layer, where the min. SPT-N

value should exceed 15 in the first stage. Later for the second stage, this value will be risen to 35 from the beneath the sand bend to 0.75B (30 m) depth below the seabed (Egeli, et al. 1983).

6.3.1. Allowable Bearing Capacity of Soil after Ground Improvement

It was found that the min SPT_N value after the ground improvement should be 35 so that the tunnel can resist to the seismic design movement (See Chapter 5). Assuming that ground improvement has been made and the min N value rises to 35, between the depth 0-30 m and it rises to 15 between the depth 30-50 m beneath the foundation level, the new allowable bearing capacity of the soil is calculated as below:

a). Post ground improvement allowable bearing pressure, based on the ultimate capacity

$$da/D = 1 \quad R_w = 0.5 \quad R'_w = 0 \quad \text{from Figure 3.1}$$

The ultimate bearing capacity of the seabed soil after ground improvement is calculated by Eq 3.1:

$$q_{ult} = 0.004882 \cdot (3 \cdot 35^2 \cdot 130.544 \cdot 0 + 5 \cdot (100 + 35^2) \cdot 93.48 \cdot 0.5)$$

$$q_{ult} = 1511.72 \text{ t/m}^2$$

The allowable bearing capacity of the seabed soil after ground improvement is calculated by Eq 3.2:

$$q_a = \frac{1511.72}{3} = 503 \text{ t/m}^2$$

b) Post ground improvement allowable bearing pressure, based on max. tolerable settlement of 2.5 cm

$$P_{overburden} = 40 \text{ psi} = 28.12 \text{ t/m}^2 \quad (\text{it had been calculated at part 3.1.2})$$

Corrected N value is calculated by by Eq 3.3.a as below:

$$N = 35 \cdot \left(\frac{50}{40 + 10} \right) = 35$$

The allowable bearing capacity of the seabed soil after ground improvement is calculated by Eq 3.4:

$$q_a = 0.004882 \cdot (720 \cdot (35 - 3) \cdot \left(\frac{130.544 + 1}{2 \cdot 130.544} \right)^2 \cdot 0.5)$$

$$q_a = 14.27 \text{ t/m}^2$$

Since 14.27 t/m² is less than 503.27 t/m² the allowable bearing capacity of the seabed soil was taken as 14.27 t/m². This value is bigger than the additional (net) effective pressure applied on the seabed soil. Thus, it can be said that the soil has enough allowable bearing capacity after the ground improvement.

6.3.2. Liquefaction Potential of the Soil after Ground Improvement

The liquefaction potential of the seabed soil after ground improvement is examined by using two different criteria as below:

6.3.2.1 Liquefaction Analysis by using Depth and SPT Data

Relationship

As it is mentioned earlier of this chapter, after the recommended ground improvement, the new SPT_N value of the seabed soil will rise to 35 from the tunnel base to 0.75B (30 m depth). After this point, the SPT_N value will be 15 until 50 m meter depth beneath the tunnel base. From Figure 3.4., it can be seen that the liquefaction potential for this new situation of the seabed soil is low.

6.3.2.2. Liquefaction Analysis by using Simplified Procedure

The cyclic resistance ratio, $CSR = 0.278$ (See Chapter 3)

The corrected SPT_N value,

C_N, C_E, C_B, C_R, C_S values were found in Chapter 3

For $N = N_m = 35$, new $(N_1)_{60}$ value is calculated by Eq 3.10.

$$(N_1)_{60} = C_N \cdot C_E \cdot C_B \cdot C_R \cdot C_S \cdot N_m$$

$$(N_1)_{60} = 0.375 \cdot 1.0 \cdot 1.15 \cdot 1.0 \cdot 1.10 \cdot 35$$

$$(N_1)_{60} = 16.6$$

From Figure 3.4 the CRR value is,

For $(N_1)_{60} = 16.6$ and $M_w = 7.5 \rightarrow CRR = 1.6$

At last, factor of safety can be calculated by Eq 3.5 as below;

$$F.S. = \frac{CRR}{CSR} = \frac{1.6}{0.278} = 5.26$$

$F.S. = 5.26 > 1.25$, thus, the soil has not been under liquefaction risk.

Both first method and second method shows that, the liquefaction potential of the soil is diminished after the recommended ground improvement.

6.3.3. Static Analysis after Ground Improvement

Because the modulus of subgrade reaction value (k_s) is improved, thanks to the designed ground improvement, the settlement value of the soil is also diminished. Therefore, the new static analysis should be performed in Calculix, according to the

new ks value, in order to investigate whether the settlement of the soil can be tolerable or not after ground improvement. The vertical displacement of the tube is calculated as about 0.22 cm. The settlement value is well below the maximum tolerable 2.5 cm settlement of the foundation soil. Therefore, it can be said that the seabed soil upon which the IBITT will be placed will not have intolerable settlement. The analysis result in Calculix is shown in Figure 6.6.

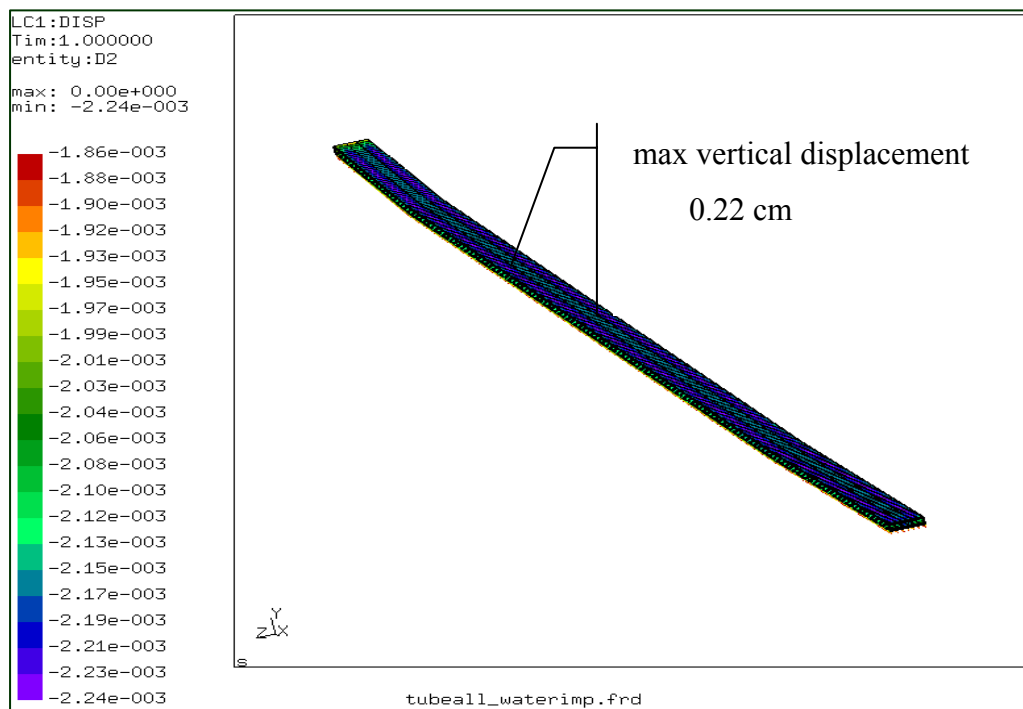


Figure 6.6. Maximum vertical displacement of the immersed tube unit after ground improvement

6.4. Analysis Results after Ground Improvement

As it is seen that thanks to recommended ground improvement:

- The allowable bearing capacity of soil is increased.
- The liquefaction risk of the soil is eliminated.
- Intolerable settlement is prevented.
- The soil has enough strength to resist the earthquake effect.

How the soil is treated after the ground improvement is shown in Table 6.1.

Table 6.1. The Situation of soil before and after ground improvement

	Before Ground Improvement N=4	After Ground Improvement N=35
The allowable bearing capacity (t/m ²)	0.44	14.27
The liquefaction potential	FS<1.25 High liquefaction risk	FS>1.25 Low liquefaction risk
The settlement value (cm)	6.59	0.22
max stress in longitudinal direction due to the earthquake effect (MPa)	21	19.6

CHAPTER 7

CONCLUSION

In this study, a preliminary design and analysis of an immersed tube tunnel proposed for the İzmir Bay is presented. First, the alignment where the tunnel can be constructed was determined. Based on this alignment, the total length of the tunnel has been determined, being 7580 m, among which 5560 m of this route is the immersed tube tunnel. The width of each tube unit is 39.8 m., the height is 10 m., and the length is between 100 m and 120 m. The results obtained at the end of this study have been summarized as below:

1. This study was based on the limited soil investigations done earlier and archived by the Devlet Limanlar ve Havayolları (DLH) İzmir Region. The test results shows that the seabed of the İzmir Bay generally consist of very loose silty sand/sandy silt layer, because the SPT-N values are less than 4 in the most parts of the seabed soils.

2. The subsoil does not have enough allowable bearing capacity to resist against the static loads placed upon it due to construction of the IBITT.

3. The liquefaction potential of the subsoil was also investigated. This examination was made by using both the interaction diagram between the SPT-N values v.s. the liquefaction risk and with respect to the procedure developed by Seed and Idriss in 1983. These investigations show that the İzmir Bay subsoil has high liquefaction potential along the tunnel alignment.

4. The total settlement of the soil during construction was investigated. It was found to be **6.59 cm, which** is above the acceptable serviceability displacement value of (2.5 cm).

5. In order to both increase the bearing capacity of the soil and reduce the liquefaction risk, ground improvement was recommended and it was determined that the most appropriate improvement type is compaction grouting, since this method provides the opportunity to change the engineering properties of the seabed soil.

6. The response of the structure during a predetermined design seismic event ($M_w=7.5$) was examined. Therefore, first the racking analysis was made to calculate the racking deformations of the tunnel, due to the seismic wave. This analysis was performed by using a simplified frame model and a soil-structure interaction approach in Calculix. Since the second approach gives more realistic results than the first approach, the latter results were taken into consideration. The total racking deformation was found 0.0004 m and the total shear stress was 3.37×10^6 N/m². Thus, it was understood that the structure is reliable against racking deformation during the design earthquake ($M_w=7.5$).

Then, the response of the structure during the same earthquake was investigated assuming that the earthquake wave affects the structure in the longitudinal direction applied at a 45-degree angle. The analysis was made by using both a simplified procedure and various numerical methods. Both analyses showed that the tunnel does not withstand against the design earthquake effect if the subsoil are not improved.

7. To eliminate these drawbacks, compaction grouting type of ground improvement method was recommended. Then, by assuming ground improvement was made and the min SPT_N value is increased to 35, all analyses were remade. As a result, it was found that if the soil is treated, the soil reaches enough allowable bearing capacity to resist the static loads imposed on it. The liquefaction risk of the seabed soil is decreased, the settlement values can be tolerated and the immersed tube tunnel has enough capacity to withstand the design seismic motion ($M_w=7.5$).

As a result of this study, it has been understood that in the prevailing circumstances and use of the limited S.I. data available from the DLH, construction of the immersed tube tunnel is technically possible and financially feasible. Because:

1. There is an opportunity to have a straight crossing of the tunnel alignment linearly.

2. The depth of the water is less than 20 m.

3. Taking the advantage of the natural buoyancy of water, the total load transferred to the soil can be reduced. Hence, very loose seabed subsoil is not loaded under excessive loads.

4. Since the soil is generally very loose silty sand, it is appropriate for the recommended ground improvement. However, it should be noted here that during

the feasibility report stage and later during the detailed design stage, more soil investigations are needed to be done. In addition, it should be noted here that the tunnel may be sunk to an additional 10m., if the currently used İzmir Port will be continued to be used and larger ship will enter the İzmir Bay area.

REFERENCES

- Akimoto, K., Y. Hashidate, H. Kitayama, and K. Kumagai. 2002. Immersed tunnels in Japan: Recent technological trends. *Underwater Technology, Proceedings of the 2002 International Symposium on* 81-86
- Anastasopoulos, I., N. Gerolymos, V. Drosos, T. Georgarakos, R. Kourkoulis, and G. Gazetas. 2007. Behaviour of deep immersed tunnel under combined normal fault rupture deformation and subsequent seismic shaking. *Bulletin of Earthquake Engineering* 6(2): 213.
- Akan, Aslı E., Ö. Özen. 2007. Bursa Yeşil Türbe'nin sonlu elemanlar yöntemiyle deprem analizi. *Deprem Sempozyumu Kocaeli 2007*. <http://kocaeli2007.kocaeli.edu.tr/> (accessed September 5, 2008).
- Baltzer, W., P. Hehengeber. 2003. The case for immersed tubes. *Tunnels and Tunneling International* 35(5):40-42.
- Bowles, Joseph E. 1988. *Foundation analysis and design*. Singapore: McGraw-Hill International Editions.
- Calculix 1.7* A Free Software Three-Dimensional Structural Finite Element Program. 2007.
- Das, Braja M. 1983. *Fundamentals of soil dynamics*. New York: Elsevier Science PublishingCo. Inc.
- Demiryollar, Limanlar ve Hava Meydanları İnşaatı Genel Müdürlüğü. 1985. İzmir Körfezi deniz sondajları arşivi. TC Ulaştırma Bakanlığı İzmir Bölge Müdürlüğü, İzmir.
- Egeli, I., E. Orhan, and I. Ruwaih. 1983. Settlement of a large tank on coastal deposits. *Symposium International on In-Situ Testing 2*: 67-70.
- Egeli, I. 1996. Western Harbour Crossing Immersed Tube Tunnel design and construction aspects internal report, MGSL. Hong Kong, China.
- Egeli, I. and H.F. Pulat. 2008. İzmir Mavişehir'deki su taşkınları için bir çözüm önerisi. IMO-İzmir Branch Publication: Bulten 138:15-19.
- Google Earth 4.2. 2008.
- Grantz, W.C., D.R. Curwell, H. Duddeck, Chr. J. Hakkaart, K. Hestner, N. Rasmussen, E. Serensen, T. Tamatso, and H. Wind. 1993. Catalog of immersed tube tunnels. *Tunneling and Underground Space Technology* 8(2):175-263.

Gouting Types from <http://www.haywardbaker.com> (accessed march 2008).

Hakkaart, Chr. J. A., A. Lancelotti, H. Ostlid, R. Marazza, K.A. Nyhus, and D.R. Culverwell.1993. *Tunneling and Underground Space Technology* 8(2):265-285.

Hashash, Y. M.A., W.S. Tseng, and A. Krimotat. 1998. Seismic soil-structure interaction analysis for immersed tube tunnels retrofit. *Geotechnical Special Publication* 2:1380-1391.

Hashash, Y.M.A. and D. Park. 2001. Non-linear one-dimensional seismic ground motion propagation in the Mississippi Embayment. *Engineering Geology* 62(1-3): 185-206.

Hashash, Y. M. A., J. J. Hook, B. Schmidt, and J. I. Yao. 2001. Seismic design and analysis of underground structures. *Tunneling and Underground Space Technology* 16: 247-293.

Huang, M.H., D.P. Thambiratnam, and N.J. Perera. 2005. Vibration characteristics of shallow suspension bridge with pre-tensioned cables. *Engineering Structures* 27: 1220–1233.

Husam, N., H. Nassif, N. Gucunski, S. Albhaisi, and P. Khoshkbari. 2005. Seismic Analysis of retaining walls, buried structures, embankments, and integral abutments FHWA-NJ-2005 no. 002:1-160. <http://www.cait.rutgers.edu> (accessed February 07, 2008).

Karayolları Genel Müdürlüğü. 2005. İzmir-Çeşme, İzmir-Aydın Otoyolu yıllık ortalama günlük trafik değerleri. TC Karayolları 2. Bölge Müdürlüğü, İzmir.

Kiyomiya, O., M. Nakamichi, H. Yokota, and S. Shiraishi. 2004. New type flexible joint for the Osaka Port Yumeshima Tunnel. *Oceans '04-MTTS/ IEEE Techno-Ocean '04* 4: 2086-2091.

Kouretzis, G.P., G.D. Bouckovalas, and C.J. Gantes. 2006. 3-D Shell analysis of cylindrical underground structures under seismic shear (S) wave action. *Soil Dynamics and Earthquake Engineering* 26:909-921.

Lee, K.L. and H.B. Seed.1967. Drained strength characteristics of sands. *Journal of the Soil Mechanics and Foundations Division (ASCE)* 93(SM6): 117-141.

Liao, S.S.C. and R.V. Whitman.1986. Overburden correction factors for SPT in sands, *Journal of Geotechnical Engineering (ASCE)* 112: 373-337.

Marmaray Project. <http://www.marmaray.com> (accessed June 3, 2006).

- Murowchick, Robert E. 2008. Bridging the GAP. *calliope* 18(9):25-27. <http://www.search.eb.com> (accessed June 3, 2008).
- Nelson., Stephen A. 2004. Earthquake hazard and risks. <http://www.tulane.edu> (accessed March 7, 2008).
- Newmark, N. M. 1968. Problems in wave propagation in soil and rock. *Proceedings of the Symposium on Wave Propagation and Dynamic Properties of Earth Materials*.
- Ostadan, F. and J. Penzien. 2001. Seismic design of cut-and-cover sections of the Bay Area Rapid Transit Extension to San Francisco Airport. *2nd US-Japan SSI Workshop, Tsukuba, Japan, March 6-8*. <http://www.pwri.go.jp> (accessed December 28, 2008).
- Owen, G. N. and R.E. Scholl. 1981. Earthquake engineering of large underground structures. Prepared for the Federal Highway Administration. FHWA/RD-80/195
- Penzein, J. 2000. Seismically induced racking of tunnel linings. *Earthquake Engineering and Structural Dynamics* 29:683-691
- Power, M., D. Rosidi, and J. Kaneshiro. 1998. Vol. III Strawman: Screening, evaluation, and retrofit design of tunnels. Report Draft. National Center for Earthquake Engineering Research, Buffalo, New York.
- SAP2000 Structural Analysis Program*, Computers and Structures Inc. 2004
- Seed, H. B. and I. M. Idriss. 1971. Simplified procedure for evaluating soil liquefaction potential. *Journal of the ASCE Soil Mechanics and Foundations Division* 97(SM9):1249-1273.
- Seed, H.B, I.M. Idriss, and I. Arango. 1983. Evaluation of liquefaction potential using field performance data. *Journal of Geotechnical Engineering, ASCE* 109: 1249-1273.
- Shamsabadi, A., H. Sedarat, and A. Kozak. 2001. Seismic soil-tunnel-structure interaction of the analysis and retrofit of the Posey-Webster Street tunnels. *2nd US-Japan SSI Workshop, Tsukuba, Japan, March 6-8*, <http://www.pwri.go.jp> (accessed December 28, 2008)
- Sivrikaya, O. and E. Toğrol. 2003. İnce daneli zeminlerde SPT sonuçlarının düzeltilmesi üzerine bir çalışma. *itüdergisi/d mühendislik* 2(6): 59-67
- St. John, C. M. and T. F. Zahrah. 1987. A seismic design of underground structures. *Tunnelling and Underground Space Technology* 2(2):165-197.
- Taiwan High Speed Rail Project Contract. 2003. C240 /WP/3.1. *Cut and cover tunnels: seismic design methodology*

- Taylor, P.R., H.I. Hisham, and D. Yang. 2005. Seismic retrofit of George Massey Tunnel. *Earthquake Engineering & Structural Dynamics* 34(4-5): 519-542
- Teng, Wayne C. 1962. *Foundation Design*. New Jersey:Prentice-Hall, Inc., Englewood Cliffs.
- Tezcan, Semih S. and Zuhul Özdemir. 2004. Liquefaction risk analysis and mapping techniques.İstanbul: EAV (Yüksek Öğrenim Eğitim ve Araştırma Vakfı) Yayınları
- Tezcan, S. 2007. Geotechnical design review İzmir Metro-Stage: I (Halkapınar-Üçyol) Underground Railway Project. *Notes on Special Lecture at DEU, Buca-İzmir*
- Tokimatsu, K., and Y.Yoshimi. 1983. Empirical correlation of soil liquefaction based on SPT-N value and fines content. *Soil and Foundations* 23(4): 56-74.
- Transit Cooperative Research Program and National Cooperative Highway Research Program. 2006. *Transportation Security:Making Transportation Tunnel Safe and Secure*. TCRP Report 86/ NCHRP Report 525: 12.
- Wang, Jaw-Nan. 1993. *Seismic Design of Tunnels, A Simple State-of-the-Art Design Approach*. New York: Parsons Brinckerhoff Inc.
- Watanabe, E. and T. Utsunomiya. 2003. Analysis and design of floating bridges. *Progress in Structural Engineering and Material* 5(3): 127-144